Processes in the Southern Ocean carbon cycle:

Dissolution of carbonate sediments and inter-annual variability of carbon fluxes

Dissertation

zur Erlangung des akademischen Grades eines
Doktors der Naturwissenschaften
– Dr. rer. nat –
am Fachbereich 2 (Biologie/Chemie) der Universität Bremen

Judith Hauck
Bremen, Mai 2012

Gutachter

Prof. Dr. Dieter A. Wolf-Gladrow
Prof. Dr. Birgit Schneider

"Das Klima der Kontinente und die Wärmeabnahme in der Luft [werden beeinflusst durch die Veränderungen], welche der Mensch auf der Oberfläche des Festlands durch Fällen der Wälder, durch die Veränderung in der Verteilung der Gewässer und durch die Entwicklung großer Dampf- und Gasmassen an den Mittelpunkten der Industrie hervorbringt."

Alexander von Humboldt (1844)

Central-Asien: Untersuchungen ueber die Gebirgsketten und die vergleichende Klimatologie, Berlin, Klemann

Vielen Dank an / Thanks to ...

Mario Hoppema
für die uneingeschränkte fachliche und organisatorische Unterstützung und die immer raschen und hilfreichen Kommentare zu den zahlreichen Versionen jedes Textes.

Christoph Völker
für die Einführung in die Kohlenstoffkreislauf- und Ökosystemmodellierung und die vielen fruchtbaren Diskussionen zu deren Grundlagen, Feinheiten und Schwächen.

Dieter Wolf-Gladrow
für die entscheidenden Gedankenanstöße und Weichenstellungen im richtigen Moment und die Bereitschaft, das erste Gutachten zu übernehmen.

Birgit Schneider und Kai Bischof
für die Bereitschaft, das zweite Gutachten, bzw. das Amt eines Prüfers zu übernehmen.

Claus-Dieter Hillenbrand, Gerhard Kuhn, und Dieter Gerdes
für die hervorragende fachliche Unterstützung und das Bereitstellen von Probenmaterial, Messgeräten, und/oder Daten.

Kevin Arrigo and Gert van Dijken
for providing data and very constructive comments.

Martin Losch
für die Beantwortung aller naiven Fragen und das Lösen so einiger technischer Probleme.

Gernot Nehrke
für zahlreiche wegweisende Diskussionen, insbesondere zu Beginn der Arbeit.

meine Kochgruppe in wechselnder Besetzung
für einen festen Programmpunkt am Tag inklusive Auffüllen der Akkus und so viel leckerem Essen.

meine Mitmodellierer / my fellow modelers
für's Dasein und den Austausch / for being there and helping out.

alle Biogeos, Pendlerfreunde und andere AWI-Bekanntschaften
für die gute Arbeitsatmosphäre, viel Kuchen, und auch mal ein Lächeln zwischendurch.

Contents

Danksagung **i**

Contents **iii**

1 Summary & Zusammenfassung **1**

2 Introduction **7**
2.1 Carbon dioxide - the principal knob on Earth's thermostat 8
2.2 The natural carbon cycle 11
2.2.1 The marine carbon cycle 11
2.3 The fate of anthropogenic CO_2 14
2.3.1 Carbon sink reactions 14
2.3.2 Ocean acidification 15
2.4 The Southern Ocean 16
2.4.1 The unknowns in the marine carbon cycle 19
2.4.2 Acidification 20
2.5 Outline of the thesis 21
2.6 List of publications and declaration of own contribution 24

3 Distribution and mineralogy of carbonate sediments on Antarctic shelves
J. Hauck, D. Gerdes, C.-D. Hillenbrand, M. Hoppema, G. Kuhn, G. Nehrke, C. Völker, D.A. Wolf-Gladrow, *Journal of Marine Systems, Vol. 90, Issue 1, 2012* **26**

4 Insignificant buffering capacity of Antarctic shelf carbonates
J. Hauck, K.R. Arrigo, M. Hoppema, G.L. van Dijken, C. Völker, D.A. Wolf-Gladrow, *in review at Global Biogeochemical Cycles* **39**
4.1 Introduction 41
4.2 Data and fitting procedure 44
4.3 Results and discussion 49
4.3.1 Evaluation of $CaCO_3$ maps 49
4.3.2 $CaCO_3$ reservoir 53
4.3.3 Buffering capacity of Antarctic shelf carbonates 54
4.4 Conclusions 56
References 56

5 Inter-annual variability of Southern Ocean organic and inorganic carbon fluxes
J. Hauck, C. Völker, T. Wang, M. Hoppema, M. Losch, D.A. Wolf-Gladrow, *to be submitted to Global Biogeochemical Cycles* **61**
5.1 Introduction . . . 63
5.2 Model . . . 65
5.3 Results: mean model state . . . 68
5.3.1 Southern Ocean circulation and sea-ice dynamics . . . 68
5.3.2 Phytoplankton growth limitation and distribution . . . 71
5.3.3 Contemporary carbonate system . . . 74
5.4 Inter-annual variability . . . 75
5.4.1 Response of Southern Ocean physics to SAM . . . 77
5.4.2 Response of nutrients and biological production to SAM . . . 77
5.4.3 Response of carbon fluxes to SAM . . . 80
5.5 Concluding remarks . . . 83
References . . . 84
Supplementary Information: Model equations . . . 91

6 Synthesis **108**
6.1 Current and future changes in the Southern Ocean carbon cycle . . . 109
6.2 Dissolution of carbonate sediments . . . 109
6.3 Inter-annual variability of carbon fluxes . . . 114
6.4 Conclusion . . . 118

References **120**

Eidesstattliche Erklärung **iv**

Chapter 1

Summary & Zusammenfassung

Summary

The Southern Ocean carbon cycle is and will be undergoing various changes in a high-CO_2 world. This thesis analyzes two key processes: dissolution of carbonate sediments on Antarctic shelves and inter-annual variability of upper ocean carbon fluxes.

In the first part of the thesis, the main question is whether dissolution of carbonate sediments from Antarctic shelves can be a negative feedback or *buffer* to ocean acidification. Most crucial to know is the amount of carbonates in Antarctic shelf sediments and whether they are in the form of the better soluble aragonite, as expected from the abundance of aragonitic pteropods, or in the form of calcite. More than 200 sediment samples were analyzed with respect to their carbonate content and mineralogy; in addition data was compiled from the literature. Aragonite was absent in all samples; nearly all preserved $CaCO_3$ was in the form of low-Magnesium calcite. Patterns in the $CaCO_3$ distribution could be related to primary production in the overlying water column and to water depth. The relationship between $CaCO_3$ and primary production can be described by an optimum function: Initially, $CaCO_3$ increases in the sediments with increasing primary production due to the coupling of organic matter and $CaCO_3$ production by organisms. This relationship is valid for autotrophic and heterotrophic calcifiers as the latter depend on the food supply by primary producers. Past the optimum level, $CaCO_3$ decreases in the sediments with further increasing primary production due to metabolic-CO_2 production that subsequently dissolves $CaCO_3$. Applying this relationship, $CaCO_3$ on the Antarctic shelves could be predicted using satellite-derived primary production data and water depth. Accordingly, data gaps could be filled and a chart of $CaCO_3$ on the shelves all around the Antarctic was produced. Based on this map, the inventory of $CaCO_3$ on all Antarctic shelves was calculated to be 4 Pg $CaCO_3$ or 0.5 Pg C and is of the same order of magnitude as the annual CO_2 uptake of the Southern Ocean. This suggests that $CaCO_3$ from the sediments will dissolve without releasing a significant alkalinity signal and will not delay acidification.

The second process study addresses the inter-annual variability of carbon fluxes in the Southern Ocean by means of a three dimensional general circulation and ecosystem model (MITgcm and REcoM-2). The Southern Annular Mode (SAM) drives most of the

atmospheric variability in the Southern Hemisphere and thereby affects ocean circulation and biogeochemical cycles. Observed patterns of temperature and chlorophyll variability as a response to the SAM could be reproduced. Stronger upwelling and entrainment of carbon and nutrient-rich deep water occurs during the high-index polarity of the SAM. On the one hand, this leads to an increase of the dissolved inorganic carbon of the surface layer, suggesting that more natural CO_2 outgassing would take place. On the other hand, the increased nutrient availability leads to an increase of total chlorophyll, and primary and export production. As iron is brought up to the surface, diatoms thrive and outcompete small phytoplankton. South of the Polar Front, the drawdown of CO_2 by increased export production has a larger effect on the surface carbon inventory than the outgassing of CO_2, underlining the important role of the biological carbon pump for the inter-annual varying carbon fluxes. North of the Polar Front, the positive phase of the SAM is associated with a reduction of primary and export production. In total this leads to an additional natural CO_2 outgassing of 0.09 Pg C yr^{-1} per unit of standardized SAM index south of 30°S in line with previous studies.

The positive trend in the SAM is projected to continue in a warming climate, so that these processes will play an important role in the future Southern Ocean. The inter-annual variability of natural carbon fluxes is overlain by the trend of anthropogenic carbon uptake. As a result, the contemporary CO_2 uptake currently increases each year, even if the increase might not be as strong as expected from the growth rate of atmospheric CO_2 alone. Acidification will proceed and will not be delayed by dissolution of shallow carbonate sediments.

Zusammenfassung

Der Kohlenstoffkreislauf im Südpolarmeer ist durch den Anstieg von CO_2 in der Atmosphäre von zahlreichen Veränderungen betroffen. In der vorliegenden Dissertation werden zwei wichtige Prozesse untersucht. Erstens, die Auflösung von Karbonatsedimenten auf dem antarktischen Schelf und zweitens die interannuelle Variabilität von Kohlenstoffflüssen im oberen Ozean.

Der erste Teil beschäftigt sich mit der Frage, ob die Auflösung von Karbonatsedimenten auf dem antarktischen Schelf die Ozeanversauerung dämpfen oder, anders ausgedrückt, 'puffern' kann. Hierzu ist es entscheidend, die Menge an Karbonat in antarktischen Schelfsedimenten zu kennen, und zu wissen, ob diese in der Form des leichter löslichen Aragonit oder als Kalzit vorliegen. Aragonit wird von Flügelschnecken produziert, die im Südpolarmeer weit verbreitet sind. Mehr als 200 Sedimentproben wurden auf ihren Karbonatgehalt und ihre mineralogische Zusammensetzung analysiert. Des Weiteren wurde der Datensatz durch Daten aus der Literatur ergänzt. Aragonit wurde in den Sedimentproben nicht gefunden; fast die gesamte Karbonatfraktion war in der Form von Niedrig-Magnesium-Kalzit. Die vorgefundenen Muster der $CaCO_3$-Verteilung konnten mit der Primärproduktion in der Wassersäule sowie der Wassertiefe in Zusammenhang gebracht werden. Die Beziehung zwischen $CaCO_3$ und Primärproduktion kann mit Hilfe einer Glockenkurve beschrieben werden: Anfangs nimmt der $CaCO_3$-Gehalt der Sedimente mit steigender Primärproduktion zu, weil Produktion von Kalziumkarbonat an die Produktion von organischem Material gekoppelt ist. Diese Beziehung hat für autotrophe und heterotrophe Kalzifizierer Bestand, da letztere von der Nahrungszufuhr durch Primärproduzenten abhängen. Wenn das Optimum überschritten wurde, nimmt der Karbonatgehalt der Sedimente mit weiter steigender Primärproduktion ab. Dies liegt an der Produktion von metabolischem CO_2 in den Sedimenten, das anschließend Kalziumkarbonat auflösen kann. Wenn man diese Beziehung zusammen mit von Satellitenmessungen abgeleiteten Schätzungen der Primärproduktion und Daten der Wassertiefe anwendet, kann man den $CaCO_3$-Gehalt in antarktischen Schelfsedimenten ableiten. Auf diese Weise konnten Datenlücken gefüllt und eine Karte der $CaCO_3$-Verteilung auf den zirkumantarktischen Schelfen hergestellt werden. Basierend auf dieser Karte konnte das

$CaCO_3$-Inventar auf dem gesamten antarktischen Schelf berechnet werden. Es beträgt ca. 4 Pg $CaCO_3$ bzw. 0,5 Pg C und liegt damit in der gleichen Größenordnung wie die jährliche CO_2-Aufnahme des Südpolarmeers. Diese Abschätzung legt nahe, dass sich die Karbonatsedimente auflösen werden, ohne dass ein signifikantes Alkalinitätssignal freigesetzt oder die Ozeanversauerung aufgehalten werden wird.

Die zweite Studie untersucht die interannuelle Variabilität von Kohlenstoffflüssen mit Hilfe eines dreidimensionalen Ozeanzirkulations- und Ökosystemmodells (MITgcm und REcoM-2). Die Antarktische Oszillation (AAO auch bekannt als SAM für Southern Annular Mode) ist für den Großteil der atmosphärischen Variabilität in der Südhemisphäre verantwortlich und beeinflusst dadurch die Ozeanzirkulation und biogeochemische Kreisläufe. Beobachtete Muster in der Variabilität von Temperatur und Chlorophyll als Reaktion auf die AAO konnten mit dem Modell reproduziert werden. Während der positiven Phase der AAO findet verstärkter Aufwärtstransport und Aufnahme von Kohlenstoff- und Nährstoff-reichem Tiefenwasser in die Oberflächenschicht statt. Einerseits führt das zu einem Anstieg des Kohlenstoffgehalts in seiner anorganischen gelösten Form in der Oberflächenschicht und suggeriert, dass mehr sogenanntes natürliches CO_2 ausgasen kann. Andererseits führt die gestiegene Nährstoffkonzentration zu einem Anstieg des Chlorophyllgehalts, der Primär- und in der Folge auch der Exportproduktion. Durch die Zufuhr von Eisen können sich Diatomeen vermehrt ausbreiten und gegen kleines Phytoplankton durchsetzen. Südlich von der Polarfront hat die CO_2-Zehrung durch steigende Exportproduktion einen größeren Einfluß auf das Inventar an gelöstem anorganischem Kohlenstoff als das Ausgasen von CO_2. Dies unterstreicht den wichtigen Beitrag der biologischen Pumpe zur interannuellen Variabilität der Kohlenstoffflüsse. Nördlich von der Polarfront ist die positive Phase des SAM mit einem Rückgang der Primär- und Exportproduktion assoziiert. Über das gesamte Südpolarmeer integriert resultiert ein zusätzliches Ausgasen von 0.09 Pg C yr^{-1} an natürlichem CO_2 pro Einheit des normalisierten SAM Index, in Übereinstimmung mit vorangegangenen Studien.

Der positive Trend des SAM wird voraussichtlich in einem sich erwärmenden Klima anhalten, so dass diese Prozesse im Südpolarmeer in der Zukunft eine wichtige Rolle spielen werden. Die interannuelle Variabilität von natürlichen Kohlenstoffflüssen wird überlagert von der steigenden Aufnahme von anthropogenem Kohlenstoff. Insgesamt nimmt die heutige CO_2-Aufnahme durch den Ozean jedes Jahr zu, auch wenn dieser Anstieg nicht so stark sein mag, wie man es von der Wachstumsrate der atmosphärischen CO_2-Konzentration allein erwarten würde. Die Versauerung der Ozeane wird voranschreiten und wird nicht durch Auflösung von in flachen Wassertiefen abgelagerten Karbonatsedimenten aufgehalten werden.

Chapter 2

Introduction

2.1 Carbon Dioxide - the Principal Knob on Earth's Thermostat

Greenhouse Effect The sun is the Earth's principal energy supplier. An average square meter of the Earth's outer atmosphere receives 342 Joules per second. To explain the preservation of thermal equilibrium, that is, a stable long-term average temperature, the incoming radiation must be balanced by outgoing radiant energy. This is attained by reflection of short-wave radiation and by long-wave (infrared) absorption and emission by the Earth's surface and atmospheric constituents.

About 30% of the solar radiation that the planet receives is reflected back into space, 20% is absorbed in the atmosphere and the remaining 50% reaches the Earth's surface (Figure 2.1). The Earth's surface and atmosphere, warmed by the absorption of solar energy, emit thermal radiation proportional to the fourth power of its temperature according to the Stefan-Boltzmann law. But the actual thermal infrared radiation that leaves the outer atmosphere at certain wave lengths is reduced compared to the theoretical value as given by the Planck function (see e.g., *Pierrehumbert*, 2011). This is due to absorption of infrared radiation by gases in the atmosphere. The so-called greenhouse gases act as an insulator for the Earth, reducing the loss of heat to the outer space. The insulating role of the atmosphere and the importance of the balance between short and long-wave radiation was first postulated by Joseph Fourier in 1827, although he did not recognize the role of greenhouse gases in the energy balance (*Fourier*, 1827; *Archer and Pierrehumbert*, 2011). As a result of the reduced outgoing long-wave radiation, the Earth's temperature is higher than that of a black body with the same size and energy supply but no greenhouse gases, at thermal equilibrium (Planck function). The natural greenhouse effect raises the actual average surface temperature on Earth from -18°C to roughly +15°C (*Pierrehumbert*, 2011).

In 1861, John Tyndall discovered the importance of the trace gases CO_2 and water vapor for the opaqueness of the atmosphere to infrared radiation (*Tyndall*, 1861). Nevertheless, it it took another 150 years to show that CO_2 is the most important greenhouse gas in Earth's atmosphere (*Lacis et al.*, 2010). The direct contribution of CO_2 to the greenhouse effect is about 20%, whereas water vapor and clouds trap more infrared radiation and account for 75% of the greenhouse effect. It is the non-condensing CO_2, though, that constitutes the key radiative forcing to sustain an atmospheric temperature that can hold a large amount of water vapor. Without CO_2, all water vapor would condense and precipitate, spiraling the planet into a *Snowball Earth* climate state. Rising CO_2 in the atmosphere intensifies the water vapor feedback cycle as warmer air can hold more water vapor - and quadruples the CO_2-induced greenhouse effect (*Pierrehumbert et al.*, 2007;

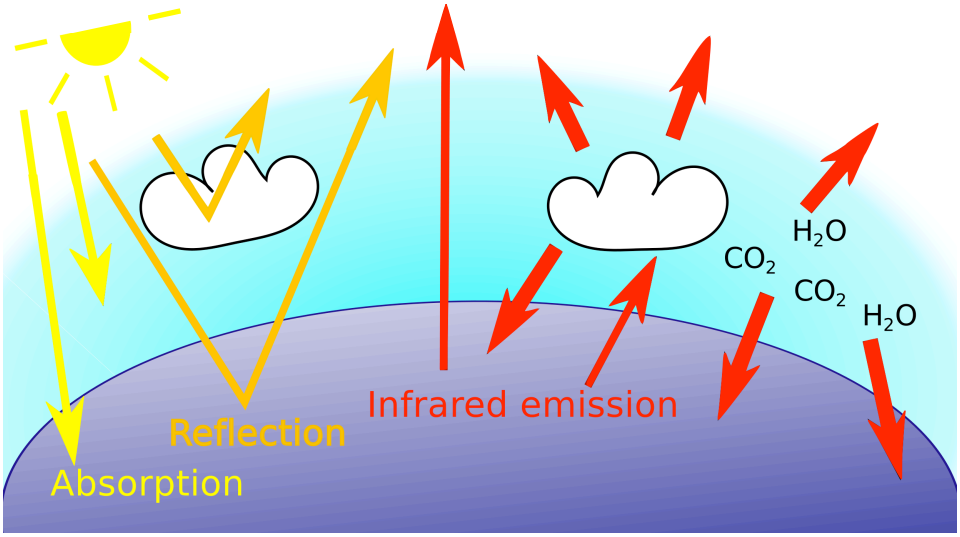

Figure 2.1: A simplified scheme of the greenhouse effect. Short-wave radiation is partly absorbed in the atmosphere, partly reflected back into space and the rest is absorbed by the Earth's surface. The warmed surface and atmosphere emit infrared radiation. The atmosphere is mostly opaque to IR radiation: Clouds and greenhouse gases, such as CO_2 and water vapor, absorb IR radiation and re-emit it into all directions.

Pierrehumbert, 2011; *Dessler and Sherwood*, 2009; *Lacis et al.*, 2010).

Weathering Thermostat The global temperature on our planet has been relatively stable over geological time scales. This is intriguing, especially when considering the early Earth, an era when the solar irradiation was less energetic than today. The *faint young sun paradox* is the conundrum of equable temperature on Earth at varying solar radiation intensities. A negative feedback (or self-stabilizing) system was proposed to enhance the greenhouse effect at low temperature and to down-regulate the greenhouse effect at rising temperature (*Walker et al.*, 1981; *Broecker and Sanyal*, 1998).

To be precise, it is the equilibrium between volcanic and hydrothermal degassing of CO_2 (metamorphism) and the reaction of CO_2 with siliceous minerals (weathering) that is sensitive to temperature changes and can trigger a strengthening or weakening of the greenhouse effect (Figure 2.2). The equilibrium is summed up by the Urey reaction:

$$CaSiO_3 + CO_2(g) \underset{metamorphism}{\overset{weathering}{\rightleftharpoons}} CaCO_3 + SiO_2 \tag{2.1}$$

The reaction of siliceous minerals with atmospheric CO_2 constitutes a sink for CO_2. The intermediate reaction products, bicarbonate ions and silicic acid, are transported into the ocean where organisms use them to build calcareous and silicic shells. After the death of the organisms, the biominerals sink and accumulate on the sea floor. They will ultimately

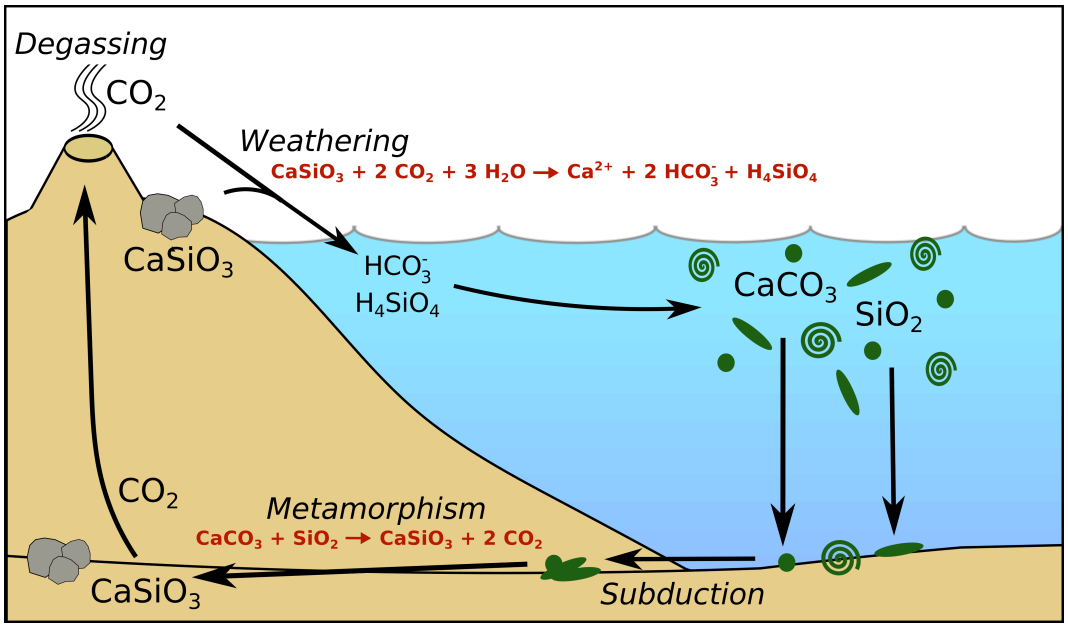

Figure 2.2: Idealized scheme of the weathering thermostat. On time scales of hundreds of thousands of years, the equilibrium between weathering (CO_2 consumption) and metamorphism (CO_2 production) is sustained.

be transformed back into CO_2 and igneous rocks when being exposed to high pressure and temperature in subduction zones (metamorphism). Once in gaseous form, CO_2 can escape from the solid earth by volcanic and hydrothermal degassing.

Metamorphism and volcanic degassing of CO_2 are independent of atmospheric temperature. The weathering reaction, in contrast, is indirectly accelerated by higher atmospheric temperature due to the reaction's dependence on water availability (see Figure 2.2). A temperature perturbation therefore leads to a change in the weathering reaction rate. At high temperatures, the water cycle is intensified, leading to more weathering. Consequently, more CO_2 is removed from the atmosphere. Cooling, in contrast, leads to less precipitation, less weathering and therefore higher atmospheric CO_2. This is a negative feedback, stabilizing the Earth's temperature (*Walker et al.*, 1981). The CO_2 thermostat prevents the Earth from spiraling into extremely warm or extremely cold climate states after a small temperature perturbation. At the time of the *faint young sun*, the temperature and consequently also the weathering rate was lower than today and allowed CO_2 to accumulate in the atmosphere. Therefore, the direct greenhouse effect of CO_2 and the water vapor feedback were stronger than today and this explains the high and equable temperature in the Earth's infancy.

2.2 The Natural Carbon Cycle

Until the mid 18^{th} century, the concentration of CO_2 in the atmosphere had been relatively constant at 260 to 280 ppm for 10,000 years, mirroring a stable natural carbon cycle (*Siegenthaler et al.*, 2005). Carbon rotates between four reservoirs: atmosphere, ocean, land and the solid earth. The solid earth constitutes the largest inventory for carbon with more than 90 million Pg C deposited in the Earth's crust including deep marine sediments and fossil fuels. This carbon is exchanged with the atmosphere on time-scales of hundreds of thousands to millions of years (*Sundquist*, 1993). In preindustrial times, the atmosphere contained roughly 600 Pg C. The atmospheric carbon is rapidly exchanged with the terrestrial biosphere and the surface ocean (*Sundquist*, 1993). On land, plants take up CO_2 to convert it to biomass during photosynthesis. Later on, this biomass is decomposed by respiration of plants, organisms and soils, and CO_2 is released back into the atmosphere. The carbon standing stocks on land amounted to 2,300 Pg C before industrialization (*IPCC*, 2007). The ocean contains 38,000 Pg C, which is about fifty times the amount of carbon in the atmosphere, and about twenty times more than the reservoirs on land. Consequently, the ocean figures prominently in the global carbon cycle. It has a large impact on the atmospheric CO_2 concentration, for example in glacial–interglacial cycles. It is widely accepted that CO_2 drawn down from the atmosphere during glacial times was stored in the ocean (e.g., review by *Sigman et al.*, 2010, and references therein).

2.2.1 The Marine Carbon Cycle

The atmosphere and the surface ocean exchange carbon in the form of gaseous CO_2. The equilibrium between the CO_2 content in the air and in the seawater is set by Henry's Law:

$$[CO_2(aq)] = K_0 \cdot pCO_2 \tag{2.2}$$

where $[CO_2(aq)]$ is the concentration of aqueous CO_2, pCO_2 is the partial pressure of CO_2 in the air and K_0 is the solubility coefficient, which depends on temperature and salinity. In contrast to other gases such as N_2 or O_2, dissolved CO_2 reacts with water to form (true) carbonic acid (H_2CO_3), which dissociates into bicarbonate (HCO_3^-), and carbonate (CO_3^{2-}) ions:

$$CO_2(aq) + H_2O \rightleftharpoons H_2CO_3 \rightleftharpoons HCO_3^- + H^+ \rightleftharpoons CO_3^{2-} + 2\,H^+ \tag{2.3}$$

An equilibrium comes into place and about 1% of the carbon that was taken up as gaseous CO_2 remains in the form of $CO_2(aq)$. As a result, more inorganic carbon is dissolved in

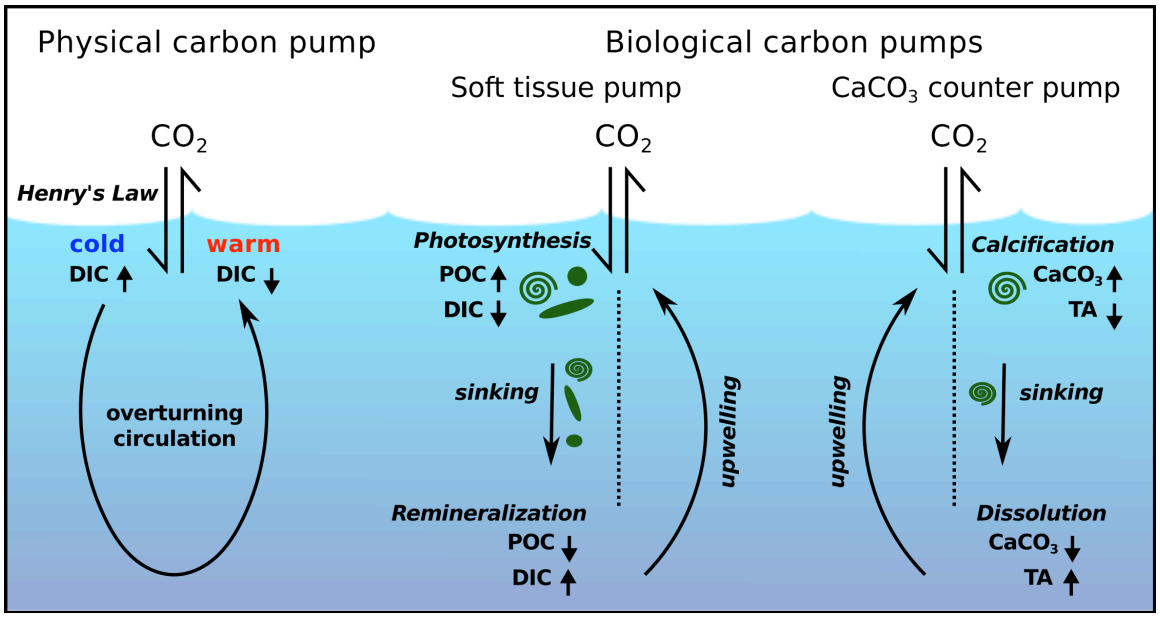

Figure 2.3: Simplified illustration of the physical and biological carbon pumps that transfer carbon from the surface to the deep ocean. See text for further explanation. Adapted from *Heinze et al.* (1991). POC: particulate organic carbon, DIC: dissolved inorganic carbon, TA: total alkalinity.

the ocean than expected from the solubility of an inert gas. The sum of dissolved CO_2, true carbonic acid, bicarbonate and carbonate ions is known as dissolved inorganic carbon (DIC).

The concept of total alkalinity (TA) provides a measure of the excess of proton acceptors over proton donors (*Dickson et al.*, 2007; *Dickson*, 1981). When a weak acid, such as CO_2, is added to seawater, the proton acceptors can partially neutralize the acid. Therefore alkalinity is also referred to as the buffer capacity of seawater. Carbonate and bicarbonate ions are the main contributors to alkalinity in seawater:

$$\begin{aligned} \mathrm{TA} \; = & [\mathrm{HCO_3^-}] + 2\,[\mathrm{CO_3^{2-}}] + [\mathrm{B(OH)_4^-}] + [\mathrm{OH^-}] + [\mathrm{HPO_4^{2-}}] \\ & + 2\,[\mathrm{PO_4^{3-}}] + [\mathrm{H_3SiO_4^-}] + [\mathrm{NH_3}] + [\mathrm{HS^-}] \\ & - [\mathrm{H^+}]_\mathrm{F} - [\mathrm{HSO_4^-}] - [\mathrm{HF}] - [\mathrm{H_3PO_4}] \end{aligned} \tag{2.4}$$

Carbon pumps The exchange of carbon between the surface and the interior of the ocean (Figure 2.3) is mediated by the physical and biological carbon pumps (*Volk and Hoffert*, 1985). They are responsible for the gradient from low DIC at the surface to high DIC in the deep ocean.

The physical (or solubility) pump denotes the process of carbon transport that is associated with deep vertical mixing. At high latitudes, surface water is cooled and

becomes more salty when brine is rejected during sea-ice formation. The high density of these water parcels leads to the sinking of cold water masses, primarily in the North Atlantic and around Antarctica. As CO_2 is more soluble at low temperatures, these cold and dense water masses are rich in carbon and carry it into the deep ocean. It is brought back to the surface in upwelling regions at lower latitudes where the water warms up and releases some of its CO_2 according to the thermodynamic equilibrium (Henry's Law, Eq. 2.2).

The biological carbon pump encompasses two processes. One is the soft tissue (or organic carbon) pump, which is driven by phytoplankton that converts DIC into organic matter (or particulate organic carbon, POC) by photosynthesis. Phytoplankton has a short turnover time, making marine carbon fixation much more efficient than carbon fixation by plants on land. Although phytoplankton biomass constitutes only 0.1% of global primary producer biomass, it is responsible for half of the global net primary production (*Field et al.*, 1998; *Falkowski*, 2003). The largest fraction of primary production is remineralized within the euphotic zone, while a small part is exported from the surface to the ocean's interior and removed from the atmosphere for hundreds to thousands of years (the residence time of water in the ocean). Upwelling of deep water brings the remineralized carbon back to the surface to complete the cycle.

The other process contributing to the biological carbon pump is the carbonate counter pump, which describes the production and sinking of $CaCO_3$ by calcifying organisms, and which, as a by-product, releases CO_2 into the water:

$$Ca^{2+} + 2\ HCO_3^- \rightarrow\ CaCO_3 + CO_2 + H_2O \tag{2.5}$$

Depending on the carbonate equilibria and the CO_2 saturation state of the seawater, this CO_2 can be discharged into the atmosphere. Assuming a steady state of the $CaCO_3$ cycle, the $CaCO_3$ production must be equal or larger than its export from the surface layer; this constrains the export $CaCO_3$ flux to at least 1.6 Pg C year^{-1} (*Berelson et al.*, 2007). The export is partitioned into dissolution in the water column and at the sea floor, and burial into the sediments. $CaCO_3$ dissolution releases alkalinity, to some extent directly in shallow depth layers and the remainder in the deep ocean. Up to 60% of the dissolution might occur in the upper 2000 m due to different processes, such as dissolution in microenvironments (e.g., bacterial organic matter oxidation in sinking particles) or dissolution of more soluble Mg-calcite or aragonite (*Millero*, 2007). Model studies suggest that dissolution of aragonite plays a major role (*Jansen et al.*, 2002; *Gangstø et al.*, 2008), whereas dissolution in sinking particles (*Jansen et al.*, 2002) and in copepod guts (*Jansen and Wolf-Gladrow*, 2001) contribute scarcely to shallow dissolution. The latter

was confirmed in experiments (*Langer et al.*, 2007). About 0.4 Pg C year^{-1} reach the deep ocean of which only about a quarter is buried in the sediments (*Berelson et al.*, 2007; *Millero*, 2007). The $CaCO_3$ buried in the sediments constitutes an important component of global ocean sediments. Its preservation can serve as a proxy for past climate conditions, with higher preservation indicating sediments from glacial times (*Farrell and Prell*, 1989).

While the soft tissue pump tends to decrease pCO_2 in the surface ocean, the carbonate counter pump has the opposite effect. In sum, the biological carbon pumps still lower surface pCO_2. That is accredited to the fact that about 16 times more organic carbon is exported from the surface layer than $CaCO_3$ (*Sarmiento et al.*, 2002). This measure of the relative strengths of the biological carbon pumps is known as the rain ratio (POC export : $CaCO_3$ export). Switching off all biological production in the ocean would double atmospheric CO_2 according to a model study (*Maier-Reimer et al.*, 1996). This emphasizes the role of the biological carbon pumps in controlling atmospheric CO_2 levels.

2.3 The Fate of Anthropogenic CO_2

Today, humans disturb the natural carbon cycle by land use change and by burning of fossil fuels from naturally sequestered geological reservoirs. Between 1850 and 2006, about 490 Pg C were released to the atmosphere (*Canadell et al.*, 2007). The concentration of CO_2 in the atmosphere has increased to 391.8 ppm in 2011 (equivalent to 830 Pg C), which is a 40% increase relative to the preindustrial level of 280 ppm.

The CO_2 thermostat (section 2.1) acts on time scales of hundreds of thousands of years. It will reduce atmospheric CO_2 concentrations only beyond human time scales. Nevertheless, only about 50% of the annually emitted CO_2 remains in the atmosphere. Land and ocean each take up 25 to 30% of the CO_2 release and thereby dampen the rapid rise in atmospheric CO_2 (*Canadell et al.*, 2007).

2.3.1 Carbon Sink Reactions

The terrestrial biosphere currently acts as a sink for atmospheric CO_2 of about the same magnitude as the ocean (*Canadell et al.*, 2007). Within a few centuries, the accumulated CO_2 release alone will potentially be two to three times larger than the total terrestrial carbon reservoir including biosphere and soils. The biosphere will be inundated by CO_2 and will not be able to act as a significant CO_2 sink anymore, possibly as early as 2050 (*Cox et al.*, 2000). The ocean, in contrast, has a much larger carbon reservoir and will continue to sequester CO_2. Increasing partial pressure of CO_2 in the atmosphere leads to a strengthening of the solubility pump, which is the primary mechanism for uptake of

anthropogenic carbon (*IPCC*, 2007). Further, the ocean has the capacity to take up far more CO_2 due to seawater buffering and $CaCO_3$ neutralization.

Seawater Buffering According to Le Chatelier's principle, a chemical equilibrium that is disturbed by a change in concentration, temperature, volume or partial pressure, will respond by a shift in the equilibrium to counteract the disturbance. This is also valid for the carbonate system (Eq. 2.3) and has the effect that anthropogenic CO_2 added to this system is buffered due to the reaction with CO_3^{2-} ions:

$$CO_2(aq) + CO_3^{2-} + H_2O \rightleftharpoons 2\ HCO_3^- \tag{2.6}$$

The amount of CO_2 that can be buffered depends on the buffering capacity of the carbonate system, or, in other words, on how much CO_2 has been taken up and been buffered already. This adjustment of the carbonate equilibria is an active process nowadays; it will, however, take several hundred to a thousand years, as determined by the time scale of ocean circulation, to reach a new equilibrium. In the end, chemical buffering of CO_2 is the quantitatively biggest sink for CO_2, sequestering 60 to 80% of the CO_2 emissions (*Archer et al.*, 1997; 2009).

$CaCO_3$ Neutralization Ocean carbonate chemistry is buffered by $CaCO_3$ depositions on the sea floor and on land. Direct neutralization of CO_2 by dissolution of $CaCO_3$, primarily in the deep ocean, is an important negative feedback on time scales of about five to ten thousand years (*Archer et al.*, 1997; 2009):

$$CO_2 + CaCO_3 + H_2O \rightarrow 2\ HCO_3^- + Ca^{2+} \tag{2.7}$$

The release of alkalinity restores the CO_2-buffering capacity of the seawater and hence the ocean's potential to take up more CO_2 from the atmosphere (Eq. 2.6).

2.3.2 Ocean Acidification

On time scales of decades to centuries, the increase of CO_2 in the atmosphere has manifold consequences, including global warming, melting of ice-caps and glaciers, sea-level rise, and changes in precipitation patterns (*IPCC*, 2007). One direct effect of the oceanic CO_2 uptake is a shift in the carbonate equilibria and a decline in pH (a negative logarithmic measure of the acidity). As CO_2 reacts with seawater (Eq. 2.3), H^+ ions are released, making the seawater more acidic. This process has recently been referred to as *ocean acidification* when it concerns added CO_2 through anthropogenic activities (*Caldeira and*

Wickett, 2003). Since preindustrial times, global mean surface pH has decreased by about 0.1 units, from 8.2 to 8.1, which is equivalent to a 30% increase in H^+ ion concentration (*IPCC*, 2007).

The shift in carbonate equilibria leads to a reduction in carbonate ions (Eq. 2.6) and consequently to a decline in $CaCO_3$ saturation states. This has an effect on the two main $CaCO_3$ polymorphs, namely calcite and aragonite. They differ in their crystal structure as calcite crystals are rhombohedral while the structure of aragonite is orthorhombic. As a consequence, the two polymorphs have different solubilities, with calcite being the more stable phase. The saturation states of calcite (Ω_C) and aragonite (Ω_A) are defined as the product of Ca^{2+} and CO_3^{2-} ion concentrations, divided by the stoichiometric solubility product K^*_{sp} for calcite or aragonite, respectively (*Zeebe and Wolf-Gladrow*, 2001; *Mucci*, 1983):

$$\Omega_C = \frac{[Ca^{2+}][CO_3^{2-}]}{K^*_{sp\,C}}, \qquad \Omega_A = \frac{[Ca^{2+}][CO_3^{2-}]}{K^*_{sp\,A}} \tag{2.8}$$

A saturation state > 1 indicates oversaturation and a saturation state < 1 denotes undersaturation. Nowadays, the saturation state is largest at the surface and decreases towards the sea floor, primarily due to the pressure dependence of K^*_{sp}. The water depth at which Ω equals 1 represents the saturation level (or saturation horizon). The calcium ion concentration varies little in the open ocean, hence the saturation state is typically controlled by the CO_3^{2-} ion concentration. It is less costly for calcifying organisms to produce $CaCO_3$ at high saturation states. Below the saturation level $CaCO_3$ can dissolve (unless it is protected by organic layers). The decline in CO_3^{2-} ion concentration, which implies a reduction of the calcite and aragonite saturation states, therefore has an impact on calcifying organisms. Most $CaCO_3$ producers investigated so far show reduced calcification as a response to ocean acidification (e.g., review by *Fabry et al.*, 2008), however, exceptions from this rule exist (for example, *Beaufort et al.*, 2011).

The shift of the calcite and aragonite saturation horizons will expose carbonate sediments to undersaturated bottom water, which will cause their dissolution. According to Eq. 2.7 this releases alkalinity and can thereby counteract acidification. The shift of the saturation horizon will go on until a new equilibrium between the deep sea and atmospheric carbon cycle compartments is reached.

2.4 The Southern Ocean

The Southern Ocean is a crucial player in the global climate system. It contains the strongest ocean flow, namely the Antarctic Circumpolar Current (ACC), which connects the Atlantic, Pacific and Indian Ocean basins. The ACC is driven by westerly winds and

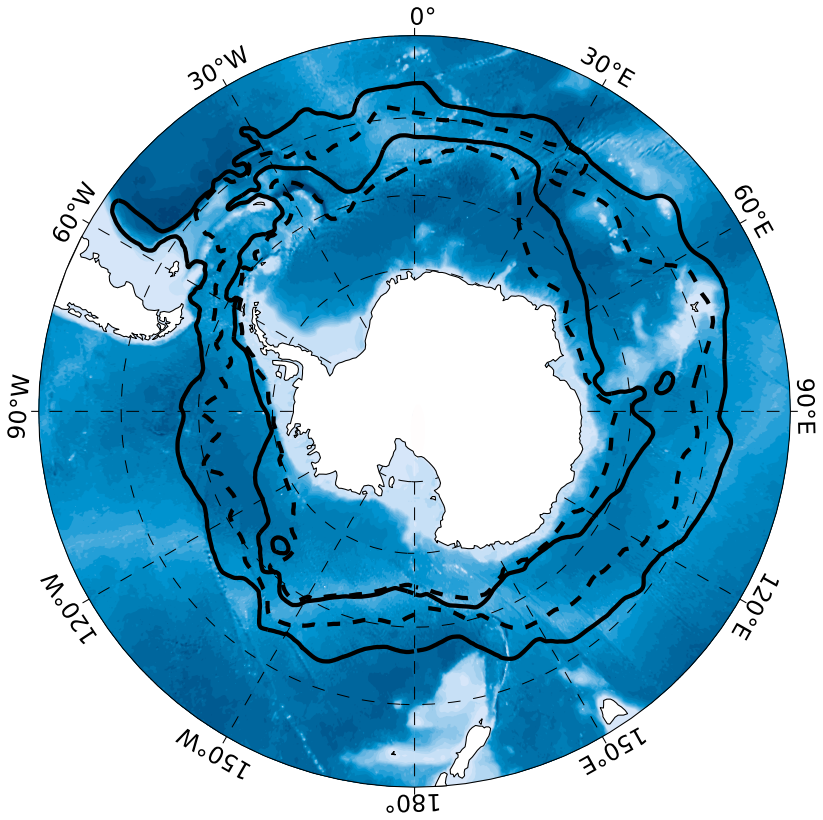

Figure 2.4: Map of the Southern Ocean with overlaid fronts, from north to south: Subantarctic Front (SAF, solid line), Polar Front (PF, dashed line), Southern Antarctic Circumpolar Current Front (SACCF, solid line), southern boundary of the Antarctic Circumpolar Current (dashed line) according to *Orsi et al.* (1995).

transports about 130 to 140 Sv (*Whitworth*, 1983; *Whitworth and Peterson*, 1985). It receives about 70% of the total wind energy going into the ocean (*Wunsch*, 1998). As the ocean's interior circulation is primarily sustained by the wind (*Wunsch*, 2002; *Lozier*, 2010), this highlights the importance of the Southern Ocean with regard to ocean mixing. Traditionally, the flow of the ACC was thought to be concentrated in jets at three major fronts: the Subantarctic Front (SAF), the Polar Front (PF) and the southern ACC front (SACCF) (e.g., *Orsi et al.*, 1995). The fronts are circumpolar and extend from the surface to the sea floor (Figure 2.4). More recently, the ACC was described as a multiple jet structure, dividing the three traditional jets into a large number of intermittent filaments (*Sokolov and Rintoul*, 2007; 2009).

Variability in the wind-driven ACC is closely connected to variability in the subpolar westerlies. The Southern Annular Mode (SAM) is a pattern that can explain much of the internal variability of the atmospheric circulation in the Southern Hemisphere. The SAM index is a measure of the sea level pressure anomaly between the subpolar low and

subtropical high pressure systems. In years when the SAM index is positive, the pressure gradient is stronger than usual, leading to a displacement of the atmospheric jet stream towards the pole and intensified westerly winds south of 45°S. A trend towards a positive SAM has been observed in the last decades (*Marshall*, 2003). The ACC's response to the perturbed wind forcing is an initial poleward shift and stronger northward Ekman transport at the surface (*Hall and Visbeck*, 2002; *Böning et al.*, 2008). This implies increased upwelling of carbon and nutrient-rich water, impacting biogeochemical cycles (*Lenton and Matear*, 2007). Observations and eddy-resolving models, however, suggest that with a lag of a few years, transport and overturning could be balanced by stronger eddy activity (for instance *Screen et al.*, 2009; *Böning et al.*, 2008).

South of the ACC, two principal cyclonic gyres exist that are characterized by upwelling in their center: the Weddell Gyre and the Ross Gyre. A few more cyclonic circulation systems appear to be present, that are smaller in extent, such as the one in the Australian-Antarctic basin (*Aoki et al.*, 2010). The northern boundary of the Weddell and Ross Gyres is set by the ACC, where Circumpolar Deep Water (CDW) is the predominant water mass. When the gyres branch off from the ACC, CDW mixes with Antarctic Surface Water (AASW) and other surface waters in the eastern limbs and forms modified Circumpolar Deep Water (mCDW). The southern limbs of the gyres follow the coast of the Antarctic continent and join the coastal current, a westward flowing circumpolar current driven by Polar Easterlies. In the regions where no cyclonic gyre is formed between the ACC and the Antarctic continent (e.g., the Bellingshausen Sea and Amundsen Sea) the southern boundary of the ACC comes close to the shelf break (*Orsi et al.*, 1995), with regular intrusions of CDW onto the shelf.

In the subsurface of the Weddell Gyre, another modified form of CDW exists, namely Central Intermediate Water (CIW, see Figure 2.5). It is characterized by a depletion of oxygen, enrichment of nutrients and a maximum in DIC resulting from shallow remineralization of export production (*Whitworth and Nowlin*, 1987; *Hoppema et al.*, 1997; *Hoppema*, 2004a). CIW leaves the Weddell Gyre to the north, carrying DIC to abyssal depths and thereby contributing significantly to the sequestration of natural carbon (*Hoppema*, 2004a).

In the AASW, DIC is being changed due to three competing processes. On the one hand, the upwelling of mCDW carries high natural carbon and nutrient concentrations into the surface layer. On the other hand, biological activity draws down natural carbon and nutrient inventories. In addition, anthropogenic carbon is taken up as a result of high partial pressure of CO_2 in the atmosphere. The surface water is subducted north of the Polar Front and contributes to Antarctic Intermediate Water (AAIW, Figure 2.5).

Heat loss to the atmosphere and brine rejection during sea-ice formation produce

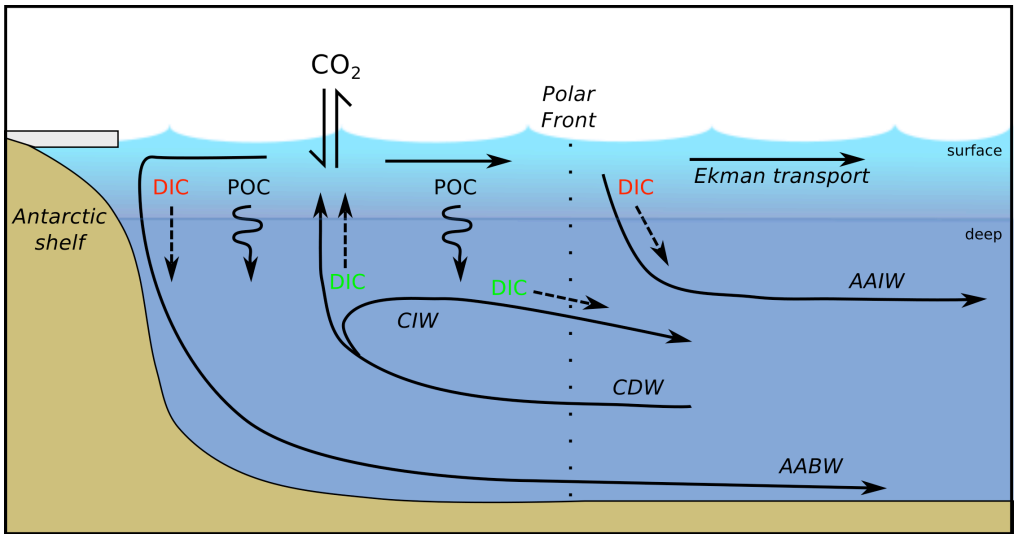

Figure 2.5: Idealized scheme of the Southern Ocean circulation and carbon fluxes. Dashed arrows denote transport of natural (green) and anthropogenic (red) carbon due to advection and the solubility pump. Wiggled arrows indicate carbon fluxes by virtue of the biological carbon pump. POC: particulate organic carbon, DIC: dissolved inorganic carbon, AAIW: Antarctic Intermediate Water, CIW: Central Intermediate Water, CDW: Circumpolar Deep Water, AABW: Antarctic Bottom Water.

dense shelf water masses, which move down the continental slope into the abyssal sea (Figure 2.5). The newly formed water mass is generally known as Antarctic Bottom Water (AABW), with regional variants, e.g., Weddell Sea Deep Water (WSDW). Bottom water formation occurs in few shelf regions of the Southern Ocean, including the western Weddell Sea, Ross Sea, and off Adélie Land (e.g., *Huhn et al.*, 2008; *Foldvik*, 2004; *Rintoul*, 1998; *Gordon et al.*, 2009). Along with the sinking water parcels, anthropogenic carbon is conveyed to the abyssal world oceans and sequestered for the time scale of the ocean's overturning circulation (as described in section 2.3).

2.4.1 The Unknowns in the Marine Carbon Cycle

Prior to industrialization, the Southern Ocean was most likely a source of CO_2 to the atmosphere (e.g., *Hoppema*, 2004b; *Mikaloff Fletcher et al.*, 2007). Upwelling of old water masses, which have accumulated remineralized carbon, lead to oversaturation of the surface waters with respect to CO_2. Together with an inefficient biological carbon pump, limited by iron, light, and grazing, this resulted in outgassing of CO_2 into the atmosphere.

With a significantly higher level of CO_2 in the atmosphere, due to anthropogenic activity, the same amount of upwelled carbon-rich deep water now causes undersaturation of surface waters with respect to CO_2. The Southern Ocean has not only become a net sink for CO_2 (e.g., *Gruber et al.*, 2009; *Takahashi et al.*, 2009), but also the primary

conduit by which 40% of all anthropogenic CO_2 enters the ocean (*Khatiwala et al.*, 2009). Nonetheless, unresolved questions remain regarding the Southern Ocean CO_2 uptake. Different models and data analyses, which converge to similar total CO_2 fluxes, show large differences in the spatial distribution within the Southern Ocean (*Gruber et al.*, 2009). The ocean inversion method (*Gruber et al.*, 2009) in the Southern Ocean suggests it to be a consistent sink for CO_2 south of 44°S. The pCO_2-based estimate, in contrast, shows strong uptake of CO_2 between 44°S and 58°S, and outgassing south of 58°S (*Gruber et al.*, 2009; *Takahashi et al.*, 2009). A regional model of the Ross Sea suggests the Antarctic shelves to be a strong CO_2 sink (*Arrigo et al.*, 2008), in line with observations of soaring carbon in the coastal Weddell Sea (*Hauck et al.*, 2010).

It is vehemently debated whether the Southern Ocean CO_2 sink has recently saturated and stagnates in spite of ever increasing atmospheric CO_2 levels (*Le Quéré et al.*, 2007; *Zickfeld et al.*, 2008; *Law et al.*, 2008; *Le Quéré et al.*, 2008). In their model study, *Le Quéré et al.* (2007) find a reduced sink relative to the trend in atmospheric CO_2, which they ascribe to shifting wind patterns (positive trend in SAM). They argue that stronger winds in the last decades cause more upwelling and entrainment of carbon-rich deep waters and subsequent outgassing of natural CO_2. They suggest that this trend will go on in the future. It is, however, also plausible that this trend reverses in the future (*Zickfeld et al.*, 2008): Once the surface ocean has become richer in carbon than the deep ocean, higher wind speeds would accelerate the uptake of anthropogenic carbon. Another issue raised is that augmented eddy fluxes at elevated wind speed could balance intensified northward Ekman transport and co-occurring carbon fluxes. This suggests that upwelling and transport in the ACC is almost unresponsive to recent changes in wind stress (*Böning et al.*, 2008).

2.4.2 Acidification

Acidification is strongest in high latitudes predominantly because of the cold temperatures (*Orr et al.*, 2005). CO_2 is more soluble in cold water, and therefore surface background and anthropogenic carbon concentrations are highest in the polar regions. Furthermore, the temperature dependence of the carbonate equilibria generates lowest surface CO_3^{2-} concentrations in the high latitudes. Within the Southern Ocean, anthropogenic carbon uptake and ensuing acidification is strongest on the shelf (*Hauck et al.*, 2010; *Arrigo et al.*, 2008). Here, the surface acidification signal penetrates down to water depths of about 1000 m. It is under debate when the Southern Ocean will be completely undersaturated with respect to aragonite (*Orr et al.*, 2005; *González-Dávila et al.*, 2011; *Hauck et al.*, 2010; *van Heuven et al.*, 2011). Wintertime undersaturation might start to occur within the next decades (*McNeil and Matear*, 2008) and calcite undersaturation will follow several

decades later (*Orr et al.*, 2005; *McNeil and Matear*, 2008).

Carbonate producers, which are supposed to be among the organisms that will be first and strongest affected by acidification, are an integral part of the planktonic and benthic Southern Ocean ecosytems. Calcifying phytoplankton, coccolithophores, appear in the Subantarctic Zone and the Polar Frontal Zone, but hardly south of the Polar Front (*Balch et al.*, 2011). Heterotrophic calcifiers, foraminifera and pteropods, occur in all zones and are the dominant calcifiers in the Antarctic Zone. Aragonitic pteropods (in the Southern Ocean mainly *Limacina helicina*) can contribute to more than half of the inorganic carbon flux according to sediment trap studies in the Ross Sea (*Accornero et al.*, 2003; *Collier et al.*, 2000). There are, however, still major gaps in the understanding of the distribution of *L. helicina* and their life cycle (*Hunt et al.*, 2008; *Bednaršek et al.*, 2011). The calcitic *Neogloboquadrina pachyderma* is the dominant foraminiferan species in polar regions (*Fraile et al.*, 2008) and can inhabit sea ice in large quantities (e.g., *Lipps and Krebs*, 1974). Recently, *Moy et al.* (2009) reported a 35% decline in Southern Ocean calcification since the Industrial Revolution based on shell weights of the foraminifera *Globigerina bulloides* in sediment traps and Holocene sediments.

2.5 Outline of the Thesis

Setting the scene – The Southern Ocean in a high-CO_2 world The Southern Ocean carbon cycle is and will be experiencing a number of changes as a result of human CO_2 emissions. Different processes are co-occurring, making its future role difficult to predict. The direct effect of increasing atmospheric CO_2 concentrations is a strengthening of the oceanic CO_2 sink and ensuing acidification.

Soaring atmospheric carbon leads to a change of climate. The future ocean will be warmer; it is, however, elusive whether a warmer climate will lead to more or less ocean mixing and ventilation. The prevailing understanding until a few years ago was that a warmer climate would lead to a more stratified ocean due to the warming of the surface layer and an intensified hydrological cycle with more freshwater input to the surface ocean (*Sarmiento et al.*, 1998; *Caldeira and Duffy*, 2000). Since then, the view on the role of winds for ocean mixing and ventilation was reassessed and winds are considered to be the driving force for the global overturning circulation (*Wunsch*, 1998; 2002; *Lozier*, 2010). Concurrently, a reinforcement of westerly winds has been observed accompanying a positive trend in the Southern Annular Mode (*Hurrell and Van Loon*, 1994; *Thompson and Solomon*, 2002; *Marshall*, 2003), which is predicted to continue in the future (*Shindell and Schmidt*, 2004; *Thompson et al.*, 2011). At the current state of knowledge, less stratification is to be expected in a warmer Southern Ocean, in line with observations

of more sluggish circulation during the last glacial (*Russell et al.*, 2006; *Toggweiler and Russell*, 2008).

More mixing causes higher levels of nutrient input into the surface layer, but it could also induce light limitation for phytoplankton production. Deep mixing allows for anthropogenic carbon to be transported into the deep sea and more anthropogenic carbon can be taken up at the surface. On the other hand, the entrained deep water is charged with carbon, which might reduce the CO_2 uptake capability from the atmosphere.

There are a number of possible biogeochemical and ecological feedback mechanisms that add even more complexity to the system: Dissolution of shallow carbonate sediments could possibly be a negative feedback to acidification, especially from the more soluble aragonite fraction. In addition, disappearance or reduction of carbonate producers could be a negative feedback to acidification (*Orr et al.*, 2005). Strengthening of westerly winds could enhance carbon export due to the added nutrients from the deep ocean or reduce primary production due to light limitation (*Lovenduski and Gruber*, 2005). Community shifts could enhance carbon export when chain-forming or highly silicified species are favored (*Tortell et al.*, 2008). A change in the Si:C ratio of diatoms due to altered iron supply could equally have an effect on the sinking of particulate organic carbon.

This thesis aims to address two of these key aspects of current and possible future changes in the Southern Ocean carbon cycle: The dissolution of shallow carbonate sediments and the inter-annual variability of upper ocean carbon fluxes in a high-CO_2 world.

Buffering capacity of Antarctic shelf carbonates The first process study is on the interaction between Southern Ocean acidification and shallow carbonate sediments (chapter 3 and 4). The central question is whether dissolution of carbonate sediments from Antarctic shelves can release a sufficiently large alkalinity signal to counteract acidification in the Southern Ocean and if so, on which regional and temporal scale. It is well-known that deep-sea carbonates will be a significant negative feedback to CO_2 on time scales of several thousand years (section 2.3). The Antarctic shelves undergo rapid acidification and will be the first region where carbonate sediments will be in contact with a carbonate undersaturated water column. Carbonate sediments will start to dissolve. Do the sediments bear sufficient carbonate to accumulate alkalinity when (slow) dissolution kinetics and (rapid) mixing with adjacent water masses are considered? How much aragonite is preserved in the sediments that could provide initial buffering against acidification?

This study presents the first compilation of $CaCO_3$ measurements on Antarctic shelves (chapter 3). It describes the distribution and mineralogy of $CaCO_3$ in the surface sediments and disentangles relevant environmental impacts, such as water depth, primary

production, ocean circulation, width of the shelf and sea-ice extent. A first qualitative assessment is made about the feedback capacity of shelf carbonates against acidification.

The feedback or buffering capacity of carbonate sediments from Antarctic shelves is quantified in chapter 4. The $CaCO_3$ data is interpolated using parameterizations based on environmental impacts as pinpointed in chapter 3. Maps of $CaCO_3$ concentrations in the surface sediments all around the Antarctic continent are produced. Based on these maps, the $CaCO_3$ inventory on Antarctic shelves and its buffer capacity is quantified.

Inter-annual variability in the Southern Ocean carbon cycle As a second aspect of the Southern Ocean carbon cycle, the inter-annual variability of the upper ocean carbon fluxes is addressed. The oceans take up about a quarter of the annual anthropogenic CO_2 emissions and the Southern Ocean is the main gateway for transport of anthropogenic carbon into the ocean's interior. The amount of CO_2 taken up every year, however, is highly variable in space and time and is poorly quantified (*Takahashi et al.*, 2009; *Gruber et al.*, 2009). Atmospheric climate modes generate variability in ocean circulation, mixing processes and biogeochemical cycles (e.g., *Lenton and Matear*, 2007).

A modeling approach is applied to study the inter-annual variability of carbon fluxes in the Southern Ocean between 1948 and 2010 as a response to the Southern Annular Mode (chapter 5). To understand the impact of the Southern Annular Mode on sea-air CO_2 exchange, the changes in entrained DIC, northward transport, outgassing of natural CO_2, and drawdown of CO_2 by increased primary and export production have to be considered. Although the importance of stronger upwelling and entrainment was discussed in previous studies (*Lenton and Matear*, 2007; *Lovenduski et al.*, 2007; *Le Quéré et al.*, 2007), it has hardly been quantified (*Dufour*, 2011). A three dimensional circulation and ecosystem model provides the framework to simultaneously quantify all changing carbon fluxes. The spatial patterns of variability following a positive SAM event are investigated and a surface DIC budget during the positive phase of the SAM is calculated. A better understanding of the upper ocean carbon fluxes during the high-index polarity of the SAM will help to better predict the future CO_2 uptake capacity as the trend towards a more positive SAM is expected to continue.

The synthesis (chapter 6) provides a summary and overall discussion of the results with respect to how the Southern Ocean carbon cycle might change in a high-CO_2 world.

2.6 List of publications and declaration of own contribution

Publication I: J. Hauck, D. Gerdes, C.-D. Hillenbrand, M. Hoppema, G. Kuhn, G. Nehrke, C. Völker, D. A. Wolf-Gladrow (2012): Distribution and mineralogy of carbonate sediments on Antarctic shelves. *Journal of Marine Systems, 90(1), pp. 77-87*

Ich habe die Proben im Labor bearbeitet und die Ergebnisse ausgewertet. D. Gerdes, C.-D. Hillenbrand und G. Kuhn haben Daten und/oder Probenmaterial beigesteuert. Das Manuskript habe ich in Zusammenarbeit mit den Koautoren verfasst.
I have analyzed the samples in the laboratory and analyzed the results. D. Gerdes, C.-D. Hillenbrand und G. Kuhn have contributed data and/or sample material. I have written the manuscript in cooperation with the coauthors.

Publication II: J. Hauck, K. R. Arrigo, M. Hoppema, G. L. van Dijken, C. Völker, D. A. Wolf-Gladrow: Insignificant buffering capacity of Antarctic shelf carbonates. *In review at Global Biogeochemical Cycles*

Ich habe die Daten analysiert und das Manuskript in Zusammenarbeit mit den Koautoren verfasst.
I have analyzed the data and and written the manuscript in cooperation with the coauthors.

Publication III: J. Hauck, C. Völker, T. Wang, M. Hoppema, M. Losch, D. A. Wolf-Gladrow: Inter-annual variability of Southern Ocean organic and inorganic carbon fluxes. *To be submitted to Global Biogeochemical Cycles in June 2012*

Ich habe die Modellexperimente zusammen mit C. Völker geplant und selbst ausgeführt. Ich habe die Ergebnisse ausgewertet. Ich habe das Manuskript in Zusammenarbeit mit den Koautoren verfasst.
I have planned the model experiments together with C. Völker and conducted them independently. I have analyzed the results. I have written the manuscript in cooperation with the coauthors.

Chapter 3

Distribution and mineralogy of carbonate sediments on Antarctic shelves

Journal of Marine Systems 90 (2012) 77–87

Contents lists available at SciVerse ScienceDirect

Journal of Marine Systems

journal homepage: www.elsevier.com/locate/jmarsys

Distribution and mineralogy of carbonate sediments on Antarctic shelves

Judith Hauck [a,*], Dieter Gerdes [a], Claus-Dieter Hillenbrand [b], Mario Hoppema [a], Gerhard Kuhn [a], Gernot Nehrke [a], Christoph Völker [a], Dieter A. Wolf-Gladrow [a]

[a] Alfred Wegener Institute for Polar and Marine Research, Postfach 12 01 61, 27515 Bremerhaven, Germany
[b] British Antarctic Survey, High Cross, Madingley Road, Cambridge CB3 0ET, United Kingdom

ARTICLE INFO

Article history:
Received 10 January 2011
Received in revised form 26 August 2011
Accepted 7 September 2011
Available online 21 September 2011

Keywords:
Southern Ocean
Feedback
Ocean acidification
Macrozoobenthos
Carbon cycle

ABSTRACT

We analyzed 214 new core-top samples for their $CaCO_3$ content from shelves all around Antarctica in order to understand their distribution and contribution to the marine carbon cycle. The distribution of sedimentary $CaCO_3$ on the Antarctic shelves is connected to environmental parameters where we considered water depth, width of the shelf, sea-ice coverage and primary production. While $CaCO_3$ contents of surface sediments are usually low, high (>15%) $CaCO_3$ contents occur at shallow water depths (150–200 m) on the narrow shelves of the eastern Weddell Sea and at a depth range of 600–900 m on the broader and deeper shelves of the Amundsen, Bellingshausen and western Weddell Seas. Regions with high primary production, such as the Ross Sea and the western Antarctic Peninsula region, have generally low $CaCO_3$ contents in the surface sediments.

The predominant mineral phase of $CaCO_3$ on the Antarctic shelves is low-magnesium calcite. With respect to ocean acidification, our findings suggest that dissolution of carbonates in Antarctic shelf sediments may be an important negative feedback only after the onset of calcite undersaturation on the Antarctic shelves.

Macrozoobenthic $CaCO_3$ standing stocks do not increase the $CaCO_3$ budget significantly as they are two orders of magnitude lower than the budget of the sediments.

This first circumpolar compilation of Antarctic shelf carbonate data does not claim to be complete. Future studies are encouraged and needed to fill data gaps especially in the under-sampled southwest Pacific and Indian Ocean sectors of the Southern Ocean.

1. Introduction

Human emissions of CO_2 lead to ocean acidification (OA): as the oceans take up CO_2 from the atmosphere, carbonate equilibria in the oceans shift toward lower pH and lower carbonate ion concentration. As a result, undersaturation with respect to carbonate minerals can occur, leading to dissolution of carbonates in marine sediments. The dissolution reaction releases carbonate ions and subsequently tends to increase pH. This mechanism is known as buffering, and it will occur on centennial time scales on the abyssal sea floor (Archer et al., 1997). Within this century, it will be significant and observable at those places where carbon chemistry will change significantly and seafloor sediments bear sufficient carbonate.

OA, which is measurable by change in pH, will be strongest in high latitudes (McNeil and Matear, 2008; Orr et al., 2005) due to the temperature dependence of carbonate equilibria and solubility. Within the polar regions, OA is intensified on the shallow shelves (Arrigo et al., 2008b; Hauck et al., 2010). Antarctic shelves will undergo large changes in pH and calcite and aragonite saturation horizons in the near future. The GLODAP (Key et al., 2004) and CARINA (Key et al., 2010) projects have compiled extensive global biogeochemical data sets which give a broad picture of recent carbon inventories and ongoing acidification.

In contrast, it is not clear how abundant carbonate sediments are on the Antarctic shelves. The Antarctic shelf is unique compared to other continental shelves. It is deeper, has a rugged topography and often a landward-sloping profile, in particular in West Antarctica (Anderson, 1999). The overdeepening of the Antarctic shelf is mainly attributed to long-term glacial erosion, and to a minor degree to the isostatic depression of the bed by the Antarctic ice sheet. The area of the entire Antarctic shelf (depth<1000 m) is 4.4×10^6 km^2 (based on Timmermann et al. (2010)) and it has a mean water depth of approximately 500 m (Anderson, 1999).

It has been common knowledge that extensive carbonate oozes appear only in shallow low-latitude sediments (e.g. Archer and Maier-Reimer, 1994; Milliman, 1994; Seiter et al., 2004). However, a first data compilation including the Southern Ocean (Seiter et al., 2004) showed that also sediments from the Southern Ocean may have moderate to high carbonate contents. In the global data set of Seiter et al. (2004), though, samples from polar areas are still underrepresented, and it is unknown, how abundant carbonates really are

* Corresponding author.
E-mail addresses: judith.hauck@awi.de (J. Hauck), dieter.gerdes@awi.de (D. Gerdes), hilc@bas.ac.uk (C.-D. Hillenbrand), mario.hoppema@awi.de (M. Hoppema), gerhard.kuhn@awi.de (G. Kuhn), gernot.nehrke@awi.de (G. Nehrke), christoph.voelker@awi.de (C. Völker), dieter.wolf-gladrow@awi.de (D.A. Wolf-Gladrow).

0924-7963/$ – see front matter © 2011 Elsevier B.V. All rights reserved.
doi:10.1016/j.jmarsys.2011.09.005

in Antarctic shelf sediments, and which main factors control their distribution. In the past, circum-Antarctic and regional carbonate distributions were mainly inferred from distributions of calcareous and agglutinated foraminifera in surface sediments (e.g. Anderson, 1975; Kellogg and Kellogg, 1987; McCoy, 1991) rather than from bulk $CaCO_3$ contents.

Calcium carbonate is produced by marine organisms in the form of two main polymorphs, calcite and aragonite. Its solubility increases with pressure and with decreasing temperature. The depth levels below which aragonite or calcite are undersaturated are denominated aragonite and calcite saturation horizons. The saturation states for calcite (Ω_C) and aragonite (Ω_A) are defined as

$$\Omega_C = \frac{\left[Ca^{2+}\right]\left[CO_3^{2-}\right]}{K^*_{spC}} \quad (1)$$

$$\Omega_A = \frac{\left[Ca^{2+}\right]\left[CO_3^{2-}\right]}{K^*_{spA}} \quad (2)$$

where K^*_{sp} is the stoichiometric solubility product (Mucci, 1983; Zeebe and Wolf-Gladrow, 2001). By definition, Ω is >1 above and <1 below the saturation horizon. Aragonite is the more soluble phase, hence its saturation horizon is shallower than that of calcite. An additional factor that controls the solubility of calcite is the amount of magnesium incorporated into calcite, with high-Mg calcite being more soluble than pure calcite (Mucci and Morse, 1984).

A variety of planktonic and benthic organisms produce $CaCO_3$ in the Southern Ocean (SO), for example pteropods (aragonite), foraminifera (calcite and high- and low-Mg calcite), bryozoans (calcite in Antarctica), echinoderms (high-Mg calcite), bivalves (calcitic and aragonitic species) and brachiopods (low-Mg calcite) (Blackmon and Todd, 1959; Kuklinski and Taylor, 2009; Milliman, 1994; Weber et al., 1969).

One calcitic foraminifera species, *Neogloboquadrina pachyderma (sin.)*, is omnipresent and the dominant planktonic foraminifera species in the Southern Ocean (e.g. Bergami et al., 2009; Donner and Wefer, 1994; Swadling et al., 2010). Extremely high amounts of *N. pachyderma* appear in sea ice (Dieckmann et al., 1991; Lipps and Krebs, 1974; Spindler and Dieckmann, 1986). *N. pachyderma* in sea ice can be 70 times more abundant per volume than in the underlying sea water. The second largest planktonic carbonate producers are pteropods and the dominant species south of the Polar Front is the aragonitic species *Limacina helicina* (Hunt et al., 2008). The distribution of *L. helicina* based on meso- and macrozooplankton analyses is not well understood and appears to be very patchy (Boysen-Ennen and Piatkowski, 1988; Hunt et al., 2008; Swadling et al., 2010). Accornero et al. (2003) and Collier et al. (2000) found *L. helicina* to be the main contributor to carbonate fluxes from sediment trap studies in the Ross Sea, with minor contributions of *N. pachyderma*. Other sediment trap studies on the eastern Weddell Sea shelf (Isla et al., 2009) and in the Bransfield Strait (Donner and Wefer, 1994) observed *N. pachyderma* to be the dominant foraminifera in their sediment traps, but do not report on whether pteropods occurred.

Benthic foraminifera are much more diverse than planktonic foraminifera. Mikhalevich (2004) found Antarctic shelf species to be circum-Antarctic, but highly patchy. Representative species include agglutinated, high-Mg calcitic and low-Mg calcitic species in equal shares (Blackmon and Todd, 1959). Bryozoans and echinoderms are crucial parts of the Antarctic macrobenthos (Brey and Gerdes, 1998; Gutt, 2007; Hayward, 1995; Smith, 2007). Together with sponges, bryozoans are the most significant occupiers of the seafloor and their remains may comprise the majority of the coarse bottom sediment (Barnes and Clarke, 1998; Bullivant, 1961; Hayward, 1995). Echinoderms can dominate the community standing stocks, especially at water depths >500 m (Brey and Gerdes, 1998; Brey et al., 1999). The aragonitic bivalve *Laternula elliptica* is widespread in the Antarctic nearshore waters (Ahn and Shim, 1998) and is generally preserved in the sediments as it is one of the most common macrofossils of Antarctic Quaternary and Tertiary sediments (Tada et al., 2006). Other common calcareous macroorganisms in the Southern Ocean are the aragonitic bivalve *Yoldia eightsi* and calcitic gastropods and brachiopods (McClintock et al., 2009).

In this study we investigate the distribution of $CaCO_3$ in surface sediments from Antarctic shelves as well as its mineralogy in order to contribute to the understanding of the fate of biologically produced carbonate. In addition to the analysis of core-top sediments, we estimate the macrozoobenthic $CaCO_3$ standing stocks. The knowledge about $CaCO_3$ distribution and mineralogy leads to a qualitative statement about the buffering capacity of carbonates in surface sediments from Antarctic shelves and forms a basis for future quantification of carbonate dissolution effects.

2. Methods

2.1. Sample material

214 core-top samples from the core repositories at the British Antarctic Survey (BAS), the British Ocean Sediment Core Research Facility (BOSCORF), the Antarctic Marine Geology Research Facility (AMGRF, Florida State University, USA), from recent Polarstern cruises (ANT-XXVI/3 and ANT-XXIII/9) and from Jubany station (Potter Cove) were analyzed. The samples cover the eastern and western Antarctic Peninsula, the Bellingshausen and Amundsen Seas, the Ross Sea and small parts of the southwest Pacific and Indian shelf sectors of the Southern Ocean. All samples were taken from the surface sediments, mostly from 0–1 cm core depth, but a few samples were taken from 1–2, 2–3 or 3–4 cm depth. Wherever possible, we took the samples from box and multiple cores, because surface sediments in gravity and vibrocores are sometimes disturbed or partially lost.

2.1.1. Additional $CaCO_3$ data

In addition to the 214 samples that were measured for the first time in this study, we compiled literature data to cover a representative area in terms of geographical coverage and water depth, resulting in a total of 390 data points. Data from the shelves in the Weddell Sea were taken from Melles et al. (1991) and additional published data from the Antarctic Peninsula, the Bellingshausen and Amundsen Seas were included (Hillenbrand et al., 2003, 2010). Data from the George V shelf in East Antarctica were supplied by Post et al. (2011). Furthermore, Antarctic shelf data were extracted and quality controlled from the global data compilation by Seiter et al. (2004). Only data where the water depth is at most 1000 m were used. The location of the samples is depicted in Fig. 1.

This study makes use of previously sampled sediment cores and literature data. The regional and bathymetric distribution of our data is therefore not random, but induced by the availability of data and samples. Data from easily accessible areas as the Antarctic Peninsula are frequent, whereas other more remote areas and very shallow depth regions are underrepresented. Data from shallower than 200 m are available from the Bellingshausen Sea (n = 1), Ross Sea (n = 1), eastern Weddell Sea (n = 3), western Antarctic Peninsula (n = 9), southwestern Pacific and Indian shelf sectors of the Southern Ocean (n = 5), but not from the Amundsen Sea, eastern Antarctic Peninsula and western Weddell Sea. Hence, only 5% of the total 390 data points are from water depths shallower than 200 m. The shallow depth regions contribute only a small percentage to the total area of the Antarctic shelves. Furthermore, these shallows are not easily accessible, because the bathymetry is poorly known and therefore research vessels rarely sample sediments in these areas.

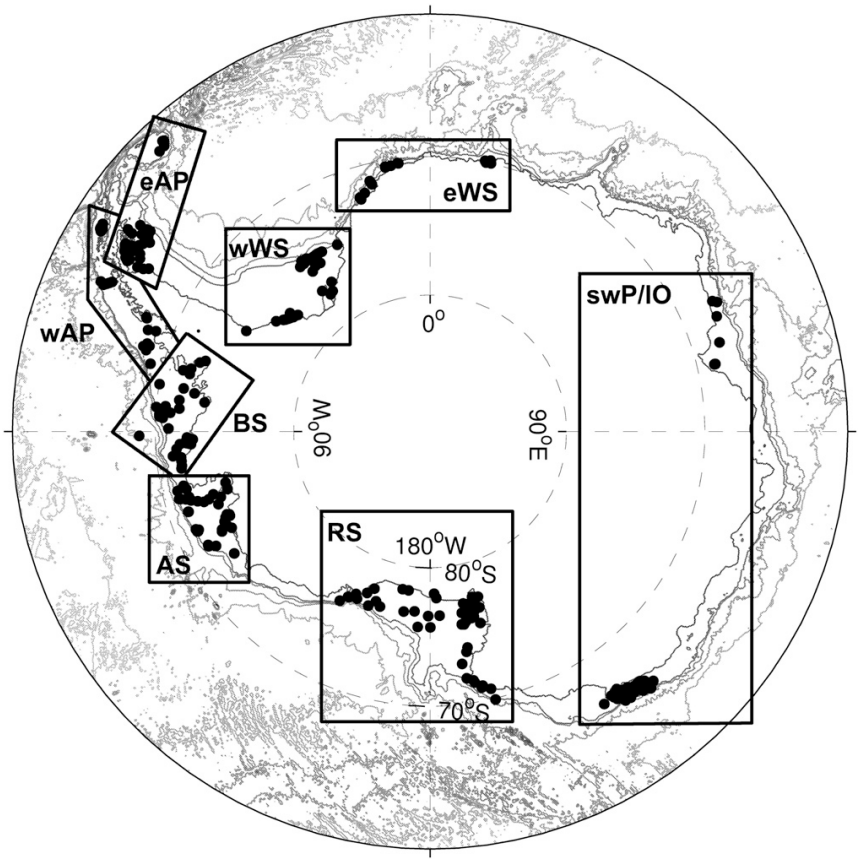

Fig. 1. Position of all core-top data (new and literature data). Isolines are from the topography of Timmermann et al. (2010) and lines are drawn every 1000 m. Different shelf regions are indicated by boxes. AS: Amundsen Sea; BS: Bellingshausen Sea; eAP: eastern Antarctic Peninsula; eWS: eastern Weddell Sea; RS: Ross Sea; swP/IO: southwest Pacific/Indian Ocean; wAP: western Antarctic Peninsula; wWS: western Weddell Sea.

The $CaCO_3$ data and all metadata such as position, sample depth, core type and data origin of all individual samples are listed in a data table in Pangaea (doi:10.1594/PANGAEA.757933).

2.2. Chemical analyses

All geochemical analyses were carried out on samples that were freeze-dried and ground to homogeneous powders. The mineralogical phase identification was done by means of X-ray diffraction (XRD) on all samples. In a second step, total carbon (TC) and total organic carbon (TOC) were determined.

Large calcareous particles, such as fragments of bryozoans or entire bivalves were excluded, i.e., taken out of the sample before grinding and measurement of TC and TOC. These particles do contribute to the sedimentary $CaCO_3$ inventory, but from a small core-top sample it is difficult to decide, whether these particles are representative for the region and how abundant they are over a larger area. Therefore, our $CaCO_3$ data give a lower boundary of $CaCO_3$ contents. The distribution of carbonate forming macrozoobenthos and their contribution to carbonate budgets is discussed in Sections 2.4 and 3.3.

2.2.1. Phase identification

The bulk sediment was analyzed using a Philips PW diffraction analyzer with a cobalt anode (CoKα radiation, 40 kV, 40 mA). A range of 3–100° 2θ was scanned with a step scan speed of 0.02° 2θ per second. The diffractograms were evaluated with the program "X'Pert HighScore Plus" (Version 2.2c, PANalytical B.V., Almelo, The Netherlands) without internal standard. The position of the calcite peak was corrected for the offset of the quartz peak position from its theoretical value (Tucker, 1996). The Bragg equation was used to convert the 2θ angle into lattice spacing (d). The relationship of Goldsmith et al. (1961) was employed to relate the peak shift of the d_{104} peak with the Mg content in the calcite of the specific sample as recommended by Milliman (1994) and Tucker (1996). Samples with more than 2% $CaCO_3$ (doi:10.1594/PANGAEA.757933) were used for the analysis of the carbonate mineralogy.

2.2.2. $CaCO_3$ quantification

The percentage of calcium carbonate (in wt. %) in the bulk sample was determined on the basis of total inorganic carbon (TIC) which is obtained from TC and TOC measurements. TC was measured on subsamples of 10 to 20 mg using a combustion analyzer (Vario EL III, Elementar Analysensysteme GmbH, Germany) and TOC by a carbon–sulfur determinator (LECO CS-125, LECO Instrumente GmbH, Germany). Samples for TOC measurements (30 to 50 mg) were treated with three drops of ethanol and 0.5 ml HCL (37%) and heated for two hours at 250 °C to remove TIC. A salt correction was applied to TC and TOC raw data, hence $CaCO_3$ contents are reported per mass of salt-free dry sediment. Relative analytical precision expressed as the standard deviation obtained under repeatability conditions is 2% for TC and 0.5% for TOC. The $CaCO_3$ percentage was converted to g $CaCO_3$ m^{-2} following the procedure described in detail in Archer (1996). This protocol calculates

an average porosity (ϕ) for the top 10 cm of the sediment based on the percentage of $CaCO_3$. Calculated porosities range between 0.751 and 0.863 with a mean of 0.857. We use an average grain density (ρ) of 2.5 g cm^{-3} and consider the top 10 cm (d) of the sediment in which we assume the $CaCO_3$ content to be constant. The top 10 cm of the sediment reflect the bioturbated layer in which dissolution can take place. The $CaCO_3$ content in the 10 cm surface layer is then given as:

$$CaCO_3\left(g\ m^{-2}\right) = \frac{CaCO_3(\%)}{100}\cdot\rho\cdot(1-\phi)\cdot d\cdot f \quad (3)$$

where f is the conversion factor from g cm^{-2} to g m^{-2}.

2.3. GLODAP and CARINA data

The GLODAP and CARINA data bases were used to estimate bottom water saturation states of calcite and aragonite on the Antarctic shelves. These data bases provide global, extensive quality controlled and internally consistent full water column data of carbon and carbon-relevant variables (Key et al., 2004, 2010). The data were filtered to find stations adjacent to the Antarctic continent with water depths shallower than 1500 m. An offset in water depth of 300 m compared to the bathymetry by Timmermann et al. (2010) was accepted. This procedure assured that only bottom data were considered, but also that data were not discarded due to uncertainties in water depth. As discussed for the sediment samples (Section 2.1), also the GLODAP and CARINA data sets consist mainly of non-shelf data. After the filtering procedure, 67 data points remained. These data cover the western Antarctic Peninsula, Ross Sea, western Weddell Sea and the southwest Pacific and Indian shelf sectors of the Southern Ocean, include data from 1989 to 2003 and allow a valid estimate for Ω_C and Ω_A during the period when most of the sediment cores were taken. Dissolved inorganic carbon (DIC) and total alkalinity (A_T) as well as potential temperature, salinity, pressure, phosphate and silicate data were used from GLODAP/CARINA to calculate Ω_C and Ω_A with the program CO2SYS (Lewis and Wallace, 1998). The carbonic acid dissociation constants from Mehrbach et al. (1973) refit by Dickson and Millero (1987) and the KSO_4 dissociation constant by Dickson (1990) were used.

Potential temperature and salinity were utilized to group the data into different water masses (see Table 2). The following water masses were considered: Circumpolar Deep Water (CDW) which is transported around the continent with the Antarctic Circumpolar Current (ACC). This water mass is mixed with Antarctic Surface Water (AASW) south of the ACC to form modified Circumpolar Deep Water (mCDW). In certain regions (mainly Weddell and Ross Sea), the release of heat and salt during sea-ice formation on the shelf produces High-Salinity Shelf Water (HSSW) and Ice Shelf Water (ISW). These water masses can sink to depth and mix with surrounding mCDW producing Antarctic Bottom Water (AABW).

Table 1
List of acronyms.

Acronym	Full name
AABW	Antarctic Bottom Water
AASW	Antarctic Surface Water
ACC	Antarctic Circumpolar Current
AS	Amundsen Sea
A_T	Total alkalinity
BS	Bellingshausen Sea
CDW	Circumpolar Deep Water
DIC	Dissolved inorganic carbon
eAP	Eastern Antarctic Peninsula
eWS	Eastern Weddell Sea
HSSW	High-Salinity Shelf Water
ISW	Ice-Shelf Water
mCDW	Modified Circumpolar Deep Water
RS	Ross Sea
SO	Southern Ocean
swP/IO	Southwestern Pacific and Indian Ocean
TC	Total carbon
TIC	Total inorganic carbon
TOC	Total organic carbon
XRD	X-ray diffraction
wAP	Western Antarctic Peninsula
wWS	Western Weddell Sea

Table 2
Main water masses occurring in the Antarctic shelf and slope region.

Water mass [a]	θ [b] (°C)	Salinity	Reference
AABW	−1.7 to 0	34.64 to 34.73	Gordon (1974); Carmack (1977)
AASW	−1.7 to 0.5	<34.4	Grosfeld et al. (2001); Orsi et al., (1995)
CDW [c]	>0		Orsi et al. (1993, 1995)
HSSW	−1.9 to −1.7	>34.65	Grosfeld et al. (2001)
ISW	<−1.9		Grosfeld et al. (2001)

[a] AABW: Antarctic Bottom Water, AASW: Antarctic Surface Water, HSSW: High-Salinity Shelf Water, ISW: Ice-Shelf Water, CDW: Circumpolar Deep Water.
[b] Potential temperature.
[c] Modified Circumpolar Deep Water (mCDW) is defined as being colder and less saline than CDW (Whitworth et al., 1998).

2.4. Macrozoobenthos data

Macrozoobenthic wet mass data were analyzed to estimate the contribution of macrozoobenthic carbonate producers to the carbonate budget in surface sediments from the Antarctic shelves. The dataset consists of 243 stations on the eastern and western Antarctic Peninsula and the eastern and western Weddell Sea shelf and slope. Only data where the water depth is <1000 m were used (218 stations). Samples were collected with giant box corers, multiple box corers and Van Veen grabs between 1985 and 2007. These samples were sieved over 500 μm meshsize screens and abundance and wet mass were determined for 35 major taxonomic groups. For the present study, only taxonomic groups which are known to produce $CaCO_3$ were considered: hydrozoa, bryozoa, brachiopoda, polyplacophora, bivalvia, gastropoda, scaphopoda, echinoidea, holothuroidea, asteroidea, ophiuroidea and crinoidea.

The wet mass was converted to $CaCO_3$ by conversion factors from Brey et al. (2010). For bivalvia and gastropoda, $CaCO_3$ was calculated by converting from wet mass with shell to wet mass without shell. The shell mass was considered equivalent to $CaCO_3$ mass and was taken as $CaCO_3$ standing stock for bivalvia and gastropoda. For all other groups, wet mass was converted to dry mass and ash-free dry mass. We use the ash mass, i.e., the difference between dry mass and ash-free dry mass, as a proxy for $CaCO_3$. This is a valid estimate as only groups with calcareous endo- and exoskeletons were considered. No conversion factor was available for polyplacophora, therefore this group was discarded. The wet mass contribution of polyplacophora to the total wet mass at all stations is 0.2%. The $CaCO_3$ content per dry mass for echinoderms as calculated with conversion factors by Brey et al. (2010) is comparable to the $CaCO_3$ contents of echinoderms as determined by Lebrato et al. (2010) except for holothuroidea. Lebrato et al. (2010) measured only one holothuroidean species with a $CaCO_3$ content of 3.46% per dry mass. In contrast, Brey et al. (2010) considered data of 51 species where the ash content ranged from <10 to >80% of the dry weight (mean: 44.5%). In Antarctica, holothuroidea are very diverse and many are heavily calcified (Gutt, 1988). The $CaCO_3$ standing stocks are given in g $CaCO_3$ m^{-2}, where the volume considered depends on the penetration depth of the sampling device into the sediment. The penetration depth varied with the sediment type and was between 10 and 40 cm. These data are available in Pangaea (doi:10.1594/PANGAEA.757933).

3. Results and discussion

3.1. Geographical and bathymetric $CaCO_3$ distribution

The sediment samples can be grouped into different regions: the western Antarctic Peninsula (wAP) including Marguerite Bay; the eastern Antarctic Peninsula (eAP) including the South Orkney Islands; the Bellingshausen Sea (BS); the Amundsen Sea (AS); the eastern Weddell Sea (eWS), the western Weddell Sea (wWS) and the Ross Sea (RS). Samples from the southwestern Pacific and Indian shelf sectors of the Southern Ocean (swP/IO) are rare and thus were not further split into different regions.

The regions show distinct patterns of carbonate preservation in the sediments (Fig. 2). In the western and eastern Antarctic Peninsula regions, $CaCO_3$ is hardly preserved in the sediments with mean values of 1.3% $CaCO_3$ (444 g $CaCO_3$ m^{-2}, n = 45) and 1.0% (340 g $CaCO_3$ m^{-2}, n = 72), respectively, and $CaCO_3$ contents consistently lower than 10%. A similar situation is found in the Ross Sea with a mean $CaCO_3$ content of 2.0% (714 g $CaCO_3$ m^{-2}, n = 52) and all $CaCO_3$ contents < 10%. Higher $CaCO_3$ contents were found in the Amundsen Sea (mean: 5.1%, 2053 g $CaCO_3$ m^{-2}, n = 44), eastern Weddell Sea (mean: 6.8%, 3138 g $CaCO_3$ m^{-2}, n = 24), western Weddell Sea (mean: 4.3%, 2153 g $CaCO_3$ m^{-2}, n = 42), and especially in the Bellingshausen Sea (mean 8.0%, 3546 g $CaCO_3$ m^{-2}, n = 40). The swP/IO region is not well captured by our data set because of low sample coverage; 58 of the 71 samples are from the George V shelf and 13 from Prydz Bay. The mean $CaCO_3$ content of these samples is 2.0% (719 g $CaCO_3$ m^{-2}).

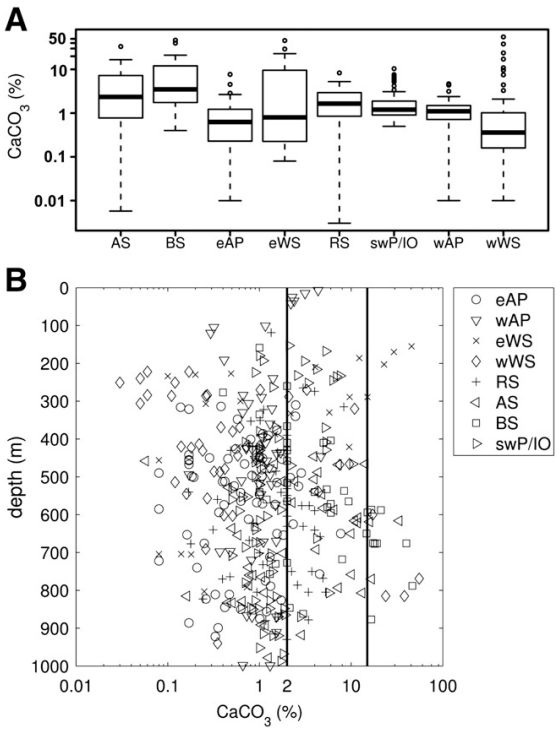

Fig. 2. (A) Boxplots of sedimentary $CaCO_3$ content (%) in the different Antarctic shelf regions. The box shows the upper and lower quartiles of the data, i.e., 50% of the data are within the box and the line through the box indicates the median. The whiskers extend to the most extreme data points if they are not more than 1.5 times the interquartile range from the box. The dots show data points outside this range. AS: Amundsen Sea (n = 44); BS: Bellingshausen Sea (n = 40); eAP: eastern Antarctic Peninsula (n = 72); eWS: eastern Weddell Sea (n = 24); RS: Ross Sea (n = 52); swP/IO: southwest Pacific/Indian Ocean (n = 71); wAP: western Antarctic Peninsula (n = 45); wWS: western Weddell Sea (n = 42), (B) Sedimentary $CaCO_3$ content (%) versus water depth on the Antarctic shelves. Different shelf regions are indicated by different symbols. Bold lines indicate 2 and 15% $CaCO_3$, respectively.

The $CaCO_3$ content varies with depth (Fig. 2b), and shows maxima with $CaCO_3$ contents >15% around 150–200 m and between 600 and 900 m. However, variances at single depths are quite large. These two depth intervals reflect two different mechanisms of carbonate preservation. On the parts of the shelf shallower than 200 m, carbonates are preserved, where they were produced and possibly concentrated by currents (winnowing). These carbonates include the entire range of carbonates produced by planktonic and benthic organisms. In the depth interval between 600 and 900 m, carbonates are exclusively accumulated at the outer shelf or near the shelf break. These are locations where carbonates are accumulated by currents and also terrigeneous sand contents are high. On the outer shelf in the BS, for example, sand and calcitic foraminifera are enriched by winnowing of silt and clay (Hillenbrand et al., 2003, 2010).

The different shelf regions can be grouped according to which $CaCO_3$ preservation mechanism applies to them. In the regions with broad and deep shelves, i.e., in the Bellingshausen and Amundsen Seas and in the wWS (Figs. 2b and 3), carbonates are found to be deposited on the outer shelf (note that no data are available from depths shallower than 200 m in the wWS and in the AS and only one data point in the BS). This corresponds to calcareous foraminifera distributions which were found in high concentrations only on the outer shelf of the Amundsen and western Weddell Seas (Anderson, 1975; Hillenbrand et al., 2003, 2010; Kellogg and Kellogg, 1987).

In the eWS, which is characterized by narrow, shallower shelves, $CaCO_3$ accumulates only at the shallow depth interval. High carbonate concentrations in the eWS are mainly produced by benthic communities, such as bryozoan colonies and molluscs (Gingele et al., 1997). While in our dataset hardly any sample from the George V shelf contains >10% $CaCO_3$, Domack (1988) reported carbonate contents of 10–30% with barnacles, bryozoans, and ostracods dominating the sand and gravel fractions of surface sediments. Post et al. (2010) observed bryozoans and foraminifera, with rare abundances of bivalves, gastropods, ostracods, as well as aragonitic hydrocorals on the continental slope. The 13 samples from Prydz Bay are consistently below 2% $CaCO_3$.

In the Ross Sea, carbonate concentrations are generally low, independent of water depth (Fig. 2). This is surprising in the light of reports of high densities of aragonitic pteropods in the water column (Hunt et al., 2008) and sediment traps (Accornero et al., 2003). A total number of 52 sediment samples from the Ross Sea were analyzed, however, the shallow banks in the western Ross Sea are represented by only two samples. Domack et al. (1999) reported $CaCO_3$ contents of >10% for two cores from one of these shallow banks. Despite the high number of data points in the RS, the mean carbonate deposition might be underestimated due to the fact that these banks are undersampled and often contain winnowed bioclastic carbonates (Anderson, 1999). Likewise, the eastern and western Antarctic Peninsula regions are very poor in $CaCO_3$ independent of water depth.

Different factors control the deposition and preservation of carbonates in the surface sediments. Important is the flux of organic matter to the ocean floor (related to primary production) and its respiration/remineralization in the sediments, transport of carbonate material by currents and calcium carbonate saturation states of the water mass above the sediment. These factors are discussed below with respect to the distribution of our $CaCO_3$ data.

3.1.1. Primary production

The Ross Sea and the western Antarctic Peninsula are regions known for very high primary production within the Southern Ocean (Arrigo et al., 2008a; Smith and Gordon, 1997). The mean chlorophyll a concentrations from in situ data are four and five times higher in the western Antarctic Peninsula region and Ross Sea, respectively, than in the remaining SO (Arrigo et al., 2008b). The BS, AS, wWS and large parts of the George V shelf are covered by sea ice for most of the year, limiting

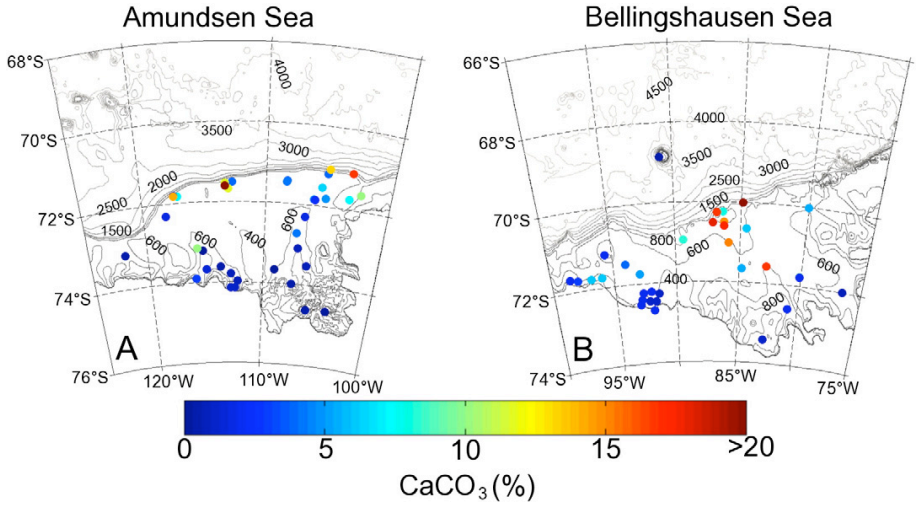

Fig. 3. Sedimentary $CaCO_3$ content (%) (A) on the Amundsen Sea shelf and (B) on the Bellingshausen Sea shelf. Isolines are from the topography of Timmermann et al. (2010), lines are drawn every 200 m between 0 and 1000 m and every 500 m at water depths >1000 m.

the phytoplankton growing season and total production, which likely leads to a reduction of the export production. Respiration in the sediments of the RS and wAP with their high primary production rates is expected to be orders of magnitude higher than in the other shelf regions and alters carbonate chemistry. High export production feeds a benthic community which includes carbonate producers (Cattaneo-Vietti et al., 1999, 2000; Dayton et al., 1982; Smith, 2007), but this carbonate is dissolved after the death of the organisms and thus not preserved in the sediments. Accordingly, in regions with low primary productivity and export production, there is a small benthic community with few calcareous organisms. Carbonate contents thus reflect the concentration of planktonic foraminifera. These are especially abundant in sea ice. Spindler and Dieckmann (1986), Dieckmann et al. (1991) and Thomas et al. (1998) report large abundances of *N. pachyderma* in sea ice of the Weddell and Amundsen Seas. This disparity in primary productivity may be the dominant factor in $CaCO_3$ distribution (Hillenbrand et al., 2003).

3.1.2. Currents

Current velocities are not available for the entire study region. There are indications for a strong current in the BS close to the shelf edge, associated with the southern boundary of the ACC with velocities of up to 28 cm s^{-1} (Read et al., 1995). This current probably winnows silt and clay and favors an enrichment of calcitic particles in the sand fraction. Carbonates are mainly represented by *N. pachyderma* (Hillenbrand et al., 2003, 2010). Winnowing by strong currents on the outer shelf and continental slope was suggested to facilitate carbonate accumulation by other studies (Gingele et al., 1997; Melles and Kuhn, 1993).

3.1.3. Calcium carbonate saturation state of water masses

The overlying water mass is another factor controlling carbonate chemistry besides respiration. If the water is undersaturated with respect to one of the carbonate minerals, this mineral will dissolve. The Antarctic shelves with water depths down to 1000 m are today still supersaturated with respect to calcite. This is demonstrated using joint data products from GLODAP and CARINA (see Section 2.3). Bottom water calcite and aragonite saturation states for all stations with water depths down to 1500 m adjacent to the Antarctic continent are shown in Figs. 4, 5a and b. A regression through the data points provides an estimate of the aragonite saturation horizon of about 1100 m (Fig. 5b). However, single data points indicate that the water is undersaturated with respect to aragonite at even shallower depths at particular locations, even though the data do not take into account sedimentary respiration. Thus, dissolution of aragonite by CO_2-rich water masses might play a role on certain locations of the Antarctic shelves already, especially where ACC water masses protrude onto the shelf (see Section 3.2). In contrast, dissolution of calcite due to undersaturated water masses can be ruled out for the recent past.

All these factors affect the distribution of $CaCO_3$ in core-top sediments, and they also interact. Primary production appears to be the dominant factor, determining whether significant proportions of $CaCO_3$ (>2%) can be preserved in the sediments. In addition, carbonate production, width of shelf, sea-ice coverage and calcite saturation state of the overlying seawater impact $CaCO_3$ distribution. The calcite saturation state of the overlying water mass will only play a role when it falls below a threshold. This critical value is dependent on the region and all contributing factors. While a defined calcite saturation state of the bottom water might lead to undersaturation in pore waters in the high-productivity regions, wAP and RS, it might not have any effect in the BS or any other low-productivity region.

Further physical and biological processes play a role in the disintegration of $CaCO_3$ within the sediment (e.g., Nelson, 1988; Smith and Nelson, 2003). Early sea-floor processes include abrasion, bioturbation and bioerosion. The latter involves microbial organisms, that burrow, bore and excavate the carbonate substrate (Smith and Nelson, 2003). Further petrographic work could shed light on the impact of microbially mediated dissolution. This is beyond the scope of our study, which is trying to disentangle environmental impacts on $CaCO_3$ distribution and mineralogy.

Although we observe general patterns of carbonate distribution, these patterns do not imply that the entire shallow shelf of the eastern Weddell Sea, for example, is covered by biogenic carbonates. The distribution of $CaCO_3$ is highly patchy, as subsets of samples taken very close to each other in the Lazarev Sea (eWS) demonstrate (Fig. 6, data from Gingele et al. (1997)). The patchiness is not well understood, but we assume it is triggered by small-scale topographic features, e.g., differences in substratum for benthic communities or variations of currents.

3.2. Mineralogy

The X-ray diffractograms of the samples with more than 2% $CaCO_3$ (52 out of 189 samples available for X-ray diffraction) showed only one carbonate component to be present and this was calcite throughout all samples. Only in one sample, a calcite and a weak aragonite

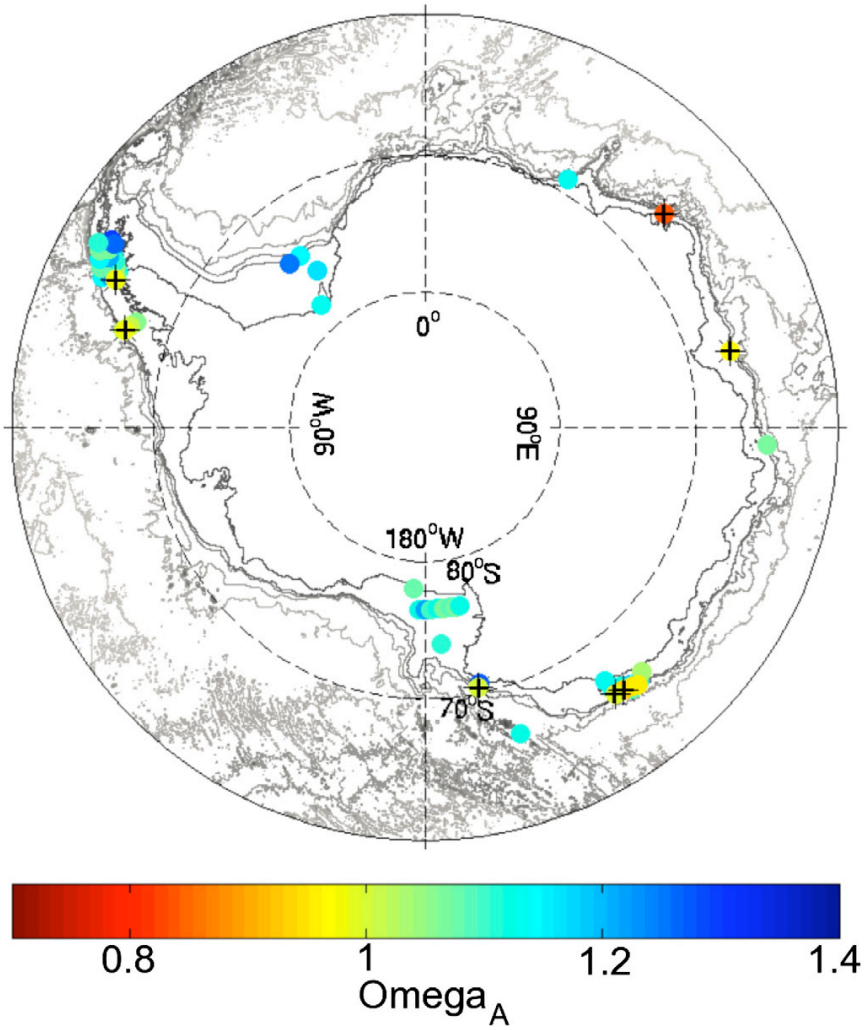

Fig. 4. Bottom water Ω_A on the Antarctic shelves from GLODAP and CARINA data. Occurrence of undersaturation at depths shallower than 1100 m is marked with a black cross. Isolines are from the topography of Timmermann et al. (2010) and lines are drawn every 1000 m.

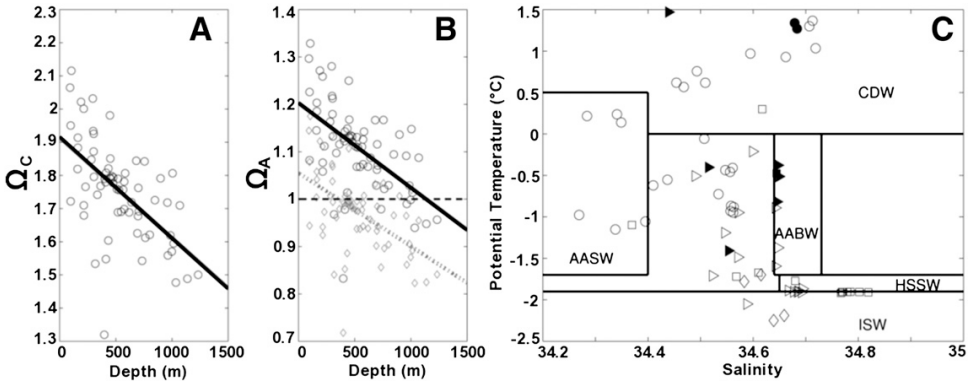

Fig. 5. Bottom water saturation states (a) Ω_C and (b) Ω_A on the Antarctic shelves and slope from GLODAP and CARINA data. Calcite is supersaturated at all depths. A linear regression through Ω_A reveals a mean saturation horizon of about 1100 m with certain areas being undersaturated at even shallower depths. The gray diamonds and dotted regression line were calculated assuming a DIC increase of 20 μmol kg^{-1} within the first cm of the sediment related to oxic remineralization of organic matter. (c) T/S-diagram of Antarctic shelf data from the GLODAP and CARINA data sets. Filled markers indicate $\Omega_A < 1$. Different markers indicate different regions: Ross Sea (squares), western Antarctic Peninsula (circles), western Weddell Sea (diamonds), southwest Pacific and Indian shelf sectors of the Southern Ocean (triangles). The properties of the main water masses are indicated by boxes. Modified Circumpolar Deep Water is not indicated, but is defined as being colder and less saline than Circumpolar Deep Water. See text, Tables 1 and 2 for further explanation and abbreviations.

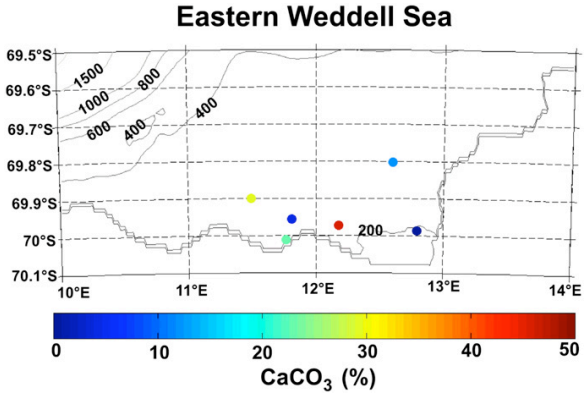

Fig. 6. Sedimentary $CaCO_3$ content (%) on the eastern Weddell Sea shelf with data from Gingele et al. (1997).

peak were detected. Low-Mg calcite is dominating throughout the samples, whereas high-Mg calcite was detected in 8% of the samples with a range of 9.9 to 13.9 mol% $MgCO_3$.

Given that aragonitic pteropods and bivalves (see also Section 3.3) are common in their respective habitats in the SO, it is astonishing that no aragonite was found.

As discussed above, aragonite undersaturation in the overlying water may be a reason at certain locations, but cannot explain the general absence of aragonite. In Fig. 4, locations with $\Omega_A<1$ are highlighted. These occur on the wAP shelf and in the swP/IO region. The occurrences of aragonite undersaturation on the George V shelf and close to the Ross Sea can be explained by the relation between Ω_A and depth (Fig. 5b). Here, aragonite undersaturation is found at water depths between 963 and 1233 m which fall in the range of the saturation horizon. The data points below 1000 m water depth show the characteristics of Antarctic Bottom Water (Fig. 5c). Solely the one point at 963 m water depth is less saline.

Aragonite undersaturation appears at water depths of 413 and 734 m on the wAP shelf, at 317 m water depth in Prydz Bay and at 398 m water depth at 48°E. The link between these locations is their exposure to Circumpolar Deep Water (CDW, see Fig. 5c). The southern boundary of the ACC comes close to the shelf break in these areas (Orsi et al., 1995). CDW can penetrate onto the shelf either directly or further altered as modified Circumpolar Deep Water (mCDW). Salinity and potential temperature reveal that the seawater at locations with $\Omega_A<1$ is CDW (wAP and Prydz Bay locations) or modified Circumpolar Deep Water (at 48°E). The ACC transports these warm and CO_2-rich water masses around the Antarctic continent. In the large cyclonical gyres, i.e. the Weddell, Ross and Kerguelen Gyres, the ACC cannot penetrate near to the shelf. This is consistent with the finding of $\Omega_A>1$ in the Ross and Weddell Seas and the Kerguelen Gyre (Fig. 4). The large gyres impede the exposure of the shelf to naturally more acidic water masses (CDW). There is also a cyclonic gyre in the Prydz Bay region. Although there is only one data point available in Prydz Bay, which indicates aragonite undersaturation, we hypothesize that in the small gyre CDW is less modified and therefore more acidic than in the large gyres.

Ice Shelf Water, High-Salinity Shelf Water and Antarctic Surface Water are not undersaturated with respect to aragonite (Fig. 5c). This is in contrast to the conclusion of Anderson (1975) that relates the absence of calcareous foraminifera in the southwestern Weddell Sea to the predominance of Ice Shelf Water. We hypothesize that the low numbers of calcareous, but also arenaceous foraminifera are caused by the low primary productivity in this area which cannot sustain a rich benthic community.

High respiration rates in the sediment-water interface can further reduce Ω_A. CO_2 is produced in Southern Ocean shelf sediments due to respiration and can be assessed assuming that 1 mol CO_2 is produced for 1 mol O_2 respired at constant alkalinity as a first approximation. Oxygen consumption is highly variable in the Antarctic shelf and slope sediments with oxygen penetration depths reaching from 1.2 cm up to several meters (Sachs et al., 2009). If we assume an increase in DIC in the sediment by 20 μmol kg^{-1}, this would bring the actual aragonite saturation horizon to about 400 m depth (Fig. 5b). An increase of 20 μmol kg^{-1} DIC is a conservative estimate, a 100–200 μmol kg^{-1} DIC increase is conceivable in high productivity areas based on the oxygen profiles by Sachs et al. (2009).

Given the observation that carbonate accumulations occur either shallower than 200 m or deeper than 600 m, aragonite could only be preserved at very shallow depths, i.e., at narrow shelves with limited sea-ice cover and limited primary productivity where CO_2-rich water masses do not impinge onto the shelf. The review of Hunt et al. (2008) identified the Antarctic Peninsula, Weddell Sea, Lazarev Sea and a coastal region between 30 and 90°E as regions with low *L. helicina* densities. South Georgia and the Ross Sea are regions of high *L. helicina* densities. Additionally a continuous plankton recorder transect between 60 and 160°E longitude and between 50°S and the Antarctic continent exhibited high abundances of *Limacina spp.*. This is in accordance with the finding of large numbers of pteropods by E. Domack (pers. communication) at very shallow depths on the George V shelf. A. Post (pers. communication) found traces of pteropods at two stations at water depths of 233 and 520 m on the George V shelf.

As discussed in Section 2, shallow depth intervals are undersampled for several reasons. From the samples available for X-ray diffraction analysis only 10 samples were available from this important depth interval. Nine of those were from the wAP and one from the RS, which all fall into the domain of very high primary productivity and poor $CaCO_3$ preservation. We would expect to find pteropods to be preserved in regions with high pteropod densities, average primary productivity and seasonal sea-ice cover on rather narrow, shallow shelves where the ACC does not penetrate onto the shelf. This reduces possible accumulation sites for pteropods to few locations on the shallow swP/IO shelf, especially the Kerguelen Gyre. More samples along the coast would be needed to prove or disprove this hypothesis.

The aragonitic bivalve *L. elliptica* is reported to be preserved in sediments as a macrofossil (Tada et al., 2006). As stated in Section 2, large calcareous particles were disregarded for the bulk sediment analysis. If this bivalve is preserved as a whole and not ground into a smaller size fraction by natural processes, it will be completely missed by the bulk $CaCO_3$ and XRD analysis. Therefore, the contribution of macrozoobenthos to carbonate distribution is assessed in the following section.

3.3. Macrozoobenthic carbonate abundance

Since the contribution of the macrozoobenthic community is not included in the core-top analyses, we present an estimate of the carbonate abundance due to this group of organisms from our analysis of box corers and grab samples. Mean macrozoobenthic carbonate standing stocks are presented in Fig. 7. The largest $CaCO_3$ standing stock from macrozoobenthic communities is found in the eastern Weddell Sea with 24.5 g $CaCO_3$ m^{-2}. This is in line with the report of coarse calcareous debris in the Lazarev Sea (eWS) by, e.g., Gingele et al. (1997). The main contributors are: bivalvia (38%), asteroidea (15%), bryozoa (14%), and ophiuroidea (12%).

In the western Antarctic Peninsula region macrozoobenthic $CaCO_3$ contribution (mean: 10.4 g $CaCO_3$ m^{-2}) is very patchy. The macrozoobenthic $CaCO_3$ contribution in the wAP region is concentrated around the tip of the wAP, especially in the Bransfield Strait. The wAP south of 64°S alone has a mean $CaCO_3$ standing stock of 1.6 g $CaCO_3$ m^{-2}. At the tip of the Antarctic Peninsula, benthic communities thrive under the high primary productivity and export

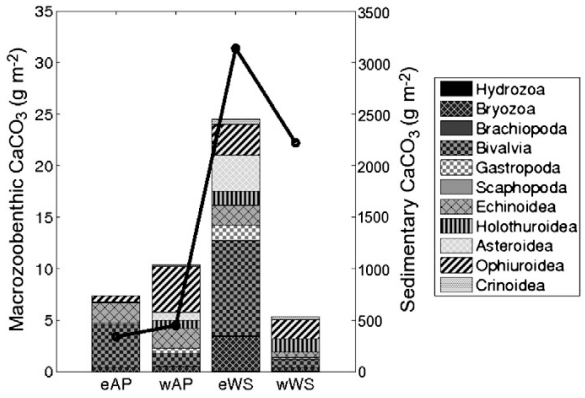

Fig. 7. Mean carbonate contribution in g m^{-2} for the west and east Antarctic Peninsulas (wAP and eAP) and western and eastern Weddell Sea (wWS and eWS) regions. Bars show the contribution by macrozoobenthos (left scale) and circles depict sedimentary $CaCO_3$ (right scale).

flux. Most $CaCO_3$ is produced by ophiuroidea (43%), echinoidea (19%), and bivalvia (13%) in the wAP region.

The eastern Antarctic Peninsula, which is represented in this data set mainly by data from the Larsen shelf and the South Orkney Islands, and the western Weddell Sea regions show lower $CaCO_3$ contributions (7.4 and 5.4 g $CaCO_3$ m^{-2}, respectively). This is at least partly related to trophic limitations caused by extensive sea-ice cover. $CaCO_3$ is mainly produced by bivalvia (56%) and echinoidea (27%) in the eAP region and by ophiuroidea (35%), holothuroidea (24%) and bivalvia (15%) in the wWS region.

In general, the most important taxonomic groups that contribute to macrozoobenthic $CaCO_3$ standing stocks on the Antarctic shelves are bivalvia (32%), ophiuroidea (20%), asteroidea (12%), echinoidea (11%) and bryozoa (11%). Holothuroidea and gastropoda play a minor role and brachiopoda, scaphopoda, crinoidea and aragonitic hydrozoans contribute less than 2% each. The mean standing stock of $CaCO_3$ by macrozoobenthic organisms (15.6 ± 45.4 g $CaCO_3$ m^{-2}) and its range (0.001–585 g $CaCO_3$ m^{-2}) on the Southern Ocean shelves is comparable to the numbers found by Lebrato et al. (2010), who only considered echinodermata. The high degree of variability that was found for the carbonate contents of the sediments (Section 3.1) characterizes also the distribution of calcareous macrozoobenthos on the Antarctic shelves, although numbers are generally two orders of magnitude lower for macrozoobenthos. This high degree of variability is caused by several factors. Mühlenhardt-Siegel (1989) named sediment structure as the most important parameter determining Antarctic zoobenthos assemblages. Gerdes et al. (1992) reported that a high portion of soft-bottom sediment and strong water currents caused the absence of bryozoans in the Filchner Depression area. Additional factors are productivity of the water column and disturbance by iceberg grounding (Mühlenhardt-Siegel, 1988). The influence of iceberg scouring was investigated in Gerdes et al. (2003, 2008). Iceberg scouring wipes out benthic communities, thereby reducing the total abundance of macrozoobenthos and $CaCO_3$ standing stocks. During recolonization, motile fauna such as echinoderms dominate the earliest succession stage, followed by sessile pioneers such as bryozoans. The disturbance by icebergs may also partly explain the low $CaCO_3$ standing stocks in the eAP and wWS region.

Within the phylum of echinodermata, ophiuroidea (39%) provide most $CaCO_3$, followed by asteroidea (22%). We observe that echinoidea make up 22% which is significantly more than the 9% found by Lebrato et al. (2010) and more than holothuroidea (13%). Crinoidea account for 4% of the echinodermata $CaCO_3$ standing stock.

Bivalves produce 32% of macrozoobenthic $CaCO_3$ standing stocks, but, although aragonitic species occur, it is unknown to us which percentage of bivalves is aragonitic. However, as macrozoobenthic $CaCO_3$ inventories appear to be two orders of magnitude lower than sedimentary carbonates, aragonite is definitely only an insignificant part of the total $CaCO_3$. Echinoderms are responsible for half of macrozoobenthic $CaCO_3$ standing stocks and produce high-Mg calcite (Weber et al., 1969). Thus their skeletons will probably be the first to dissolve, before calcitic bryozoan and bivalve skeletons as well as calcitic foraminifera will be affected.

4. Summary

We presented the first circum-Antarctic data set of carbonate content and mineralogy. Up to today, there was no systematic sampling effort to study $CaCO_3$ production and preservation on Antarctic shelves. Large areas, especially in the southwest Pacific and Indian Ocean sectors of the Antarctic shelves are still largely undersampled. Future research in these regions is essential to achieve a process-based understanding of the fate of $CaCO_3$ in the sediments and the Southern Ocean $CaCO_3$ cycle in general.

Over the next decades, Antarctic Surface Water might become the most acidic water mass in the Southern Ocean (Hauck et al., 2010) as the surface ocean accumulates most CO_2 from the atmosphere; the CO_2 increase in the deeper layers is much smaller due to mixing with waters poor in anthropogenic CO_2. Once the saturation horizon for calcite will become as shallow to reach the Antarctic shelves, locally present carbonate-rich sediments will dissolve. The capacity to buffer future acidification is small in high-productivity regions, such as the western Antarctic Peninsula and the Ross Sea but higher in the Bellingshausen, Amundsen and Weddell Seas. The buffering effect cannot be quantified yet, but this will be attempted in a modeling approach.

The water masses most corrosive to $CaCO_3$ are Antarctic Bottom Water and Circumpolar Deep Water. Today, the cyclonic gyres, the Weddell, Ross and Kerguelen Gyres, keep the corrosive Circumpolar Deep Water away from the shelf in the respective regions. Undersaturation with respect to aragonite at depths shallower than 1100 m is found only outside these gyres. The corrosiveness of pore water depends on the combination of carbonate saturation state of the bottom water and the amount of CO_2 released by respiration.

Dissolution of aragonite is not a mechanism which can buffer ocean acidification in the Southern Ocean, as aragonite is not a prominent constituent of surface sediments on the Antarctic shelves.

Comparison of the contributions of sedimentary carbonate and macrozoobenthic carbonate (>500 μm) in the regions, from which data from both analyses is available (compare Fig. 7), emphasized the sedimentary carbonate to be quantitatively more important in the marine carbon cycle. Sedimentary carbonate contents are two orders of magnitude higher than macrozoobenthic carbonate contents. Hence, neglecting large debris in the determination of sedimentary $CaCO_3$ content does not lead to a significant underestimation of the total $CaCO_3$ content. In the eastern Antarctic Peninsula (eAP) region, macrozoobenthic contribution and sedimentary carbonate contents are low. In the western Antarctic Peninsula (wAP) region the macrozoobenthic carbonate standing stock is very patchy, whereas the sedimentary $CaCO_3$ is uniformly distributed, but low compared to the other regions. In the eastern Weddell Sea (eWS), both the $CaCO_3$ percentages in sediments and calcareous macrozoobenthos abundance are very high on their respective scales. Here, strong production and preservation favor high $CaCO_3$ contents. Considering only the eAP, wAP and eWS regions, there appears to be a relation between macrozoobenthic stocks and sedimentary carbonate contents. The western Weddell Sea is different. The macrozoobenthic carbonate abundance is the smallest within the study area, but the sedimentary part is comparable to the one in the eastern Weddell Sea. This underlines that in the regions with broad shelves, major sea-ice cover and limited primary production, benthic $CaCO_3$ production has a minor influence

on sedimentary $CaCO_3$ contents (compare Section 3.1). Calcium carbonate is mainly produced by planktonic organisms, presumably to a large extent by *N. pachyderma* living in the water column and in the sea ice.

Although we have no macrozoobenthos data from the Ross Sea, Bellingshausen Sea, Amundsen Sea, southwest Pacific and Indian Ocean, the classification we found in Section 3.1 indicates that a situation similar to that in the wWS applies to the Bellingshausen and Amundsen Seas. We expect macrozoobenthic $CaCO_3$ stocks similar to the wAP in the Ross Sea and similar to the eWS in the Kerguelen Gyre. This classification is based on environmental conditions such as sea-ice cover, primary production, width of the shelf and water mass distribution. There was not enough data available to make statements about the entire southwest Pacific and Indian Ocean region.

Acknowledgments

This paper is a contribution to the German project Biological Impacts of Ocean ACIDification (BIOACID), funded by the Federal Ministry of Education and Research (BMBF, FKZ 03F0608B). This research used samples provided by the Antarctic Marine Geology Research Facility (AMGRF) at Florida State University. The AMGRF is sponsored by the U.S. National Science Foundation. The British Ocean Sediment Core Research Facility (BOSCORF) is thanked for supplying sediment samples. We are grateful to Patrick Monien for bringing sediment samples from near Jubany station, King George Island.

References

Accornero, A., Manno, C., Esposito, F., Gambi, M.C., 2003. The vertical flux of particulate matter in the polynya of Terra Nova Bay. Part II. Biological components. Antarctic Science 15, 175–188.

Ahn, I.Y., Shim, J.H., 1998. Summer metabolism of the Antarctic clam, *Laternula elliptica* (King and Broderip) in Maxwell Bay, King George Island and its implications. Journal of Experimental Marine Biology and Ecology 224, 253–264.

Anderson, J.B., 1975. Factors controlling $CaCO_3$ dissolution in Weddell Sea from foraminiferal distribution patterns. Marine Geology 19, 315–332.

Anderson, J.B., 1999. Antarctic Marine Geology. Cambridge University Press.

Archer, D., 1996. An atlas of the distribution of calcium carbonate in sediments of the deep-sea. Global Biogeochemical Cycles 10, 159–174.

Archer, D., Maier-Reimer, E., 1994. Effect of deep-sea sedimentary calcite preservation on atmospheric CO_2 concentration. Nature 367, 260–263.

Archer, D., Kheshgi, H., Maier-Reimer, E., 1997. Multiple timescales for neutralization of fossil fuel CO_2. Geophysical Research Letters 24, 405–408.

Arrigo, K.R., van Dijken, G., Long, M., 2008a. Coastal Southern Ocean: a strong anthropogenic CO_2 sink. Geophysical Research Letters 35, L21602. doi:10.1029/2008GL035624.

Arrigo, K.R., van Dijken, G.L., Bushinsky, S., 2008b. Primary production in the Southern Ocean, 1997–2006. Journal of Geophysical Research-Oceans 113, C08004. doi:10.1029/2007JC004551.

Barnes, D.K.A., Clarke, A., 1998. The ecology of an assemblage dominant: the encrusting bryozoan *Fenestrulina rugula*. Invertebrate Biology 117, 331–340.

Bergami, C., Capotondi, L., Langone, L., Giglio, F., Ravaioli, M., 2009. Distribution of living planktonic foraminifera in the Ross Sea and the Pacific sector of the Southern Ocean (Antarctica). Marine Micropaleontology 73, 37–48.

Blackmon, P., Todd, R., 1959. Mineralogy of some foraminifera as related to their classification and ecology. Journal of Paleontology 33, 1–15.

Boysen-Ennen, E., Piatkowski, U., 1988. Mesozooplankton and macrozooplankton communities in the Weddell Sea, Antarctica. Polar Biology 9, 17–35.

Brey, T., Gerdes, D., 1998. High Antarctic macrobenthic community production. Journal of Experimental Marine Biology and Ecology 231, 191–200.

Brey, T., Gerdes, D., Gutt, J., Mackensen, A., Starmans, A., 1999. Growth and age of the Antarctic bryozoan *Cellaria incula* on the Weddell Sea shelf. Antarctic Science 11, 408–414.

Brey, T., Müller-Wiegmann, C., Zittier, Z.M.C., Hagen, W., 2010. Body composition in aquatic organisms—a global data bank of relationships between mass, elemental composition and energy content. Journal of Sea Research 64, 334–340.

Bullivant, J., 1961. Photographs of the Antarctic bottom fauna. Polar Record 10, 505–508.

Carmack, E., 1977. Water characteristics of the Southern Ocean south of the polar front. In: Angel, M. (Ed.), A Voyage of Discovery. Pergamon, Tarrytown, N.Y., pp. 15–41.

Cattaneo-Vietti, R., Chiantore, M., Misic, C., Povero, P., Fabiano, M., 1999. The role of pelagic–benthic coupling in structuring littoral benthic communities at Terra Nova Bay (Ross Sea) and in the Straits of Magellan. Scientia Marina 63, 113–121.

Cattaneo-Vietti, R., Chiantore, M., Schiaparelli, S., Albertelli, G., 2000. Shallow- and deep-water mollusc distribution at Terra Nova Bay (Ross Sea, Antarctica). Polar Biology 23, 173–182.

Collier, R., Dymond, J., Honjo, S., Manganini, S., Francois, R., Dunbar, R., 2000. The vertical flux of biogenic and lithogenic material in the Ross Sea: moored sediment trap observations 1996–1998. Deep-Sea Research Part II—Topical Studies in Oceanography 47, 3491–3520.

Dayton, P., Newmann, W., Oliver, J., 1982. The vertical zonation of the deep-sea Antarctic acorn barnacle, *Bathylasma corolliforme* (Hoek): experimental transplants form the shelf into shallow water. Journal of Biogeography 9, 95–109.

Dickson, A.G., 1990. Standard potential of the reaction $AgCl(s) + 1/2H_2(g) = Ag(s) + HCl(aq)$ and the standard acidity constant of the ion HSO_4^- in synthetic seawater from 273.15 K to 318.15 K. The Journal of Chemical Thermodynamics 22, 113–127.

Dickson, A.G., Millero, F.J., 1987. A comparison of the equilibrium constants for the dissociation of carbonic acid in seawater media. Deep-Sea Research Part A—Oceanographic Research Papers 34, 1733–1743.

Dieckmann, G.S., Spindler, M., Lange, M.A., Ackley, S.F., Eicken, H., 1991. Antarctic sea ice—a habitat for the foraminifer *Neogloboquadrina pachyderma*. Journal of Foraminiferal Research 21, 182–189.

Domack, E., 1988. Biogenic facies in the Antarctic glacimarine environment: basis for a polar glacimarine summary. Palaeogeography, Palaeoclimatology, Palaeoecology 63, 357–372.

Domack, E., Taviani, M., Rodriguez, A., 1999. Recent sediment remolding on a deep shelf, Ross Sea: implications for radiocarbon dating of Antarctic marine sediments. Quarternary Science Reviews 18, 1445–1451.

Donner, B., Wefer, G., 1994. Flux and stable-isotope composition of *Neogloboquadrina pachyderma* and other planktonic foraminifers in the Southern Ocean (Atlantic sector). Deep-Sea Research Part I—Oceanographic Research Papers 41, 1733–1743.

Gerdes, D., Klages, M., Arntz, W., Herman, R., Galéron, J., Hain, S., 1992. Quantitative investigations on macrobenthos communities of the southeastern Weddell Sea shelf based on multibox corer samples. Polar Biology 12, 291–301.

Gerdes, D., Hilbig, B., Montiel, A., 2003. Impact of iceberg scouring on macrobenthic communities in the high-Antarctic Weddell Sea. Polar Biology 26, 295–301.

Gerdes, D., Isla, E., Knust, R., Mintenbeck, K., Rossi, S., 2008. Response of Antarctic benthic communities to disturbance: first results from the artificial Benthic Disturbance Experiment on the eastern Weddell Sea Shelf, Antarctica. Polar Biology 31, 1469–1480.

Gingele, F.X., Kuhn, G., Maus, B., Melles, M., Schone, T., 1997. Holocene ice retreat from the Lazarev Sea Shelf, East Antarctica. Continental Shelf Research 17, 137–163.

Goldsmith, J., Graf, D., Heard, H., 1961. Lattice constants of the calcium–magnesium carbonates. American Mineralogist 46, 453–457.

Gordon, A., 1974. Varieties and variability of Antarctic Bottom Water. Processus de Formation des Eaux Océanique Profondes en Particulier en Méditerrannée Occidentale. Centre Nationale de la Recherche Scientifique, Paris, pp. 33–47.

Grosfeld, K., Schröder, M., Fahrbach, E., Gerdes, R., Mackensen, A., 2001. How iceberg calving and grounding change the circulation and hydrography in the Filchner Ice Shelf-Ocean System. Journal of Geophysical Research-Oceans 106, 9039–9055.

Gutt, J., 1988. Zur Verbreitung und Ökologie der Seegurken (Holothuroidea, Echinodermata) im Weddellmeer (Antarktis). Berichte zur Polarforschung 41, 92.

Gutt, J., 2007. Antarctic macro-zoobenthic communities: a review and an ecological classification. Antarctic Science 19, 165–182.

Hauck, J., Hoppema, M., Bellerby, R.G.J., Völker, C., Wolf-Gladrow, D., 2010. Data-based estimation of anthropogenic carbon and acidification in the Weddell Sea on a decadal timescale. Journal of Geophysical Research-Oceans 115, C03004. doi:10.1029/2009JC005479.

Hayward, P., 1995. Antarctic cheilostomatous bryozoa. Oxford University Press.

Hillenbrand, C.D., Grobe, H., Diekmann, B., Kuhn, G., Fütterer, D.K., 2003. Distribution of clay minerals and proxies for productivity in surface sediments of the Bellingshausen and Amundsen seas (West Antarctica)—relation to modern environmental conditions. Marine Geology 193, 253–271.

Hillenbrand, C.D., Larter, R.D., Dowdeswell, J.A., Ehrmann, W., Cofaigh, C.O., Benetti, S., Graham, A.G.C., Grobe, H., 2010. The sedimentary legacy of a palaeo-ice stream on the shelf of the southern Bellingshausen Sea: clues to West Antarctic glacial history during the Late Quaternary. Quaternary Science Reviews 29, 2741–2763.

Hunt, B.P.V., Pakhomov, E.A., Hosie, G.W., Siegel, V., Ward, P., Bernard, K., 2008. Pteropods in Southern Ocean ecosystems. Progress in Oceanography 78, 193–221.

Isla, E., Gerdes, D., Palanques, A., Gili, J.M., Arntz, W.E., König-Langlo, G., 2009. Downward particle fluxes, wind and a phytoplankton bloom over a polar continental shelf: a stormy impulse for the biological pump. Marine Geology 259, 59–72.

Kellogg, D.E., Kellogg, T.B., 1987. Microfossil distributions in modern Amundsen Sea sediments. Marine Micropaleontology 12, 203–222.

Key, R.M., Kozyr, A., Sabine, C.L., Lee, K., Wanninkhof, R., Bullister, J.L., Feely, R.A., Millero, F.J., Mordy, C., Peng, T.H., 2004. A global ocean carbon climatology: results from Global Data Analysis Project (GLODAP). Global Biogeochemical Cycles 18, GB4031. doi:10.1029/2004GB002247.

Key, R.M., Tanhua, T., Olsen, A., Hoppema, M., Jutterstroem, S., Schirnick, C., van Heuven, S., Kozyr, A., Lin, X., Velo, A., Wallace, D., Mintrop, L., 2010. The CARINA data synthesis project: introduction and overview. Earth System Science Data 2, 105–121.

Kuklinski, P., Taylor, P., 2009. Mineralogy of Arctic bryozoan skeletons in a global context. Facies 55, 489–500.

Lebrato, M., Iglesias-Rodriguez, D., Feely, R.A., Greeley, D., Jones, D.O.B., Suarez-Bosche, N., Lampitt, R.S., Cartes, J.E., Green, D.R.H., Alker, B., 2010. Global contribution of echinoderms to the marine carbon cycle: $CaCO_3$ budget and benthic compartments. Ecological Monographs 80, 441–467.

Lewis, E., Wallace, D., 1998. CO2SYS-program developed for the CO_2 system calculations. Carbon Dioxide Information Analysis Center. Report ORNL/CDIAC-105.

Lipps, J., Krebs, W., 1974. Planktonic foraminifera associated with Antarctic sea ice. Journal of Foraminiferal Research 4, 80–85.

McClintock, J.B., Angus, R.A., McDonald, M.R., Amsler, C.D., Catledge, S.A., Vohra, Y.K., 2009. Rapid dissolution of shells of weakly calcified Antarctic benthic macroorganisms indicates high vulnerability to ocean acidification. Antarctic Science 21, 449–456.
McCoy, F., 1991. Southern Ocean sediments: circum-Antarctic to 30°S. In: Hayes, D. (Ed.), Marine Geological and Geophysical Atlas of the Circum-Antarctic to 30°S. American Geophysical Union, Washington D.C., pp. 37–46.
McNeil, B.I., Matear, R.J., 2008. Southern Ocean acidification: a tipping point at 450-ppm atmospheric CO_2. Proceedings of the National Academy of Sciences of the United States of America 105, 18860–18864.
Mehrbach, C., Culberson, C., Hawley, J., Pytkowicz, R., 1973. Measurement of the apparent dissociation constants of carbonic acid in seawater at atmospheric pressure. Limnology and Oceanography 18, 897–907.
Melles, M., Kuhn, G., 1993. Subbottom profiling and sedimentological studies in the southern Weddell Sea, Antarctica—evidence for large-scale erosional depositional processes. Deep-Sea Research Part I—Oceanographic Research Papers 40, 739–760.
Melles, M., Kuhn, G., Fütterer, D., Meischner, D., 1991. Paläoglaziologie und Paläozeanographie im Spätquartär am Kontinentalrand des südlichen Weddellmeeres, Antarktis (Late quaternary paleoglaciology and paleoceanography at the continental margin of the southern Weddell Sea, Antarctica). Berichte zur Polar- und Meeresforschung 81, 190.
Mikhalevich, V.I., 2004. The general aspects of the distribution of Antarctic foraminifera. Micropaleontology 50, 179–194.
Milliman, J., 1994. Recent Sedimentary Carbonates 1: Marine Carbonates. Springer-Verlag.
Mucci, A., 1983. The solubility of calcite and aragonite in seawater at various salinities, temperatures, and one atmosphere total pressure. American Journal of Science 283, 780–799.
Mucci, A., Morse, J.W., 1984. The solubility of calcite in seawater solutions of various magnesium concentration, $I_t = 0.697$ m at 25 °C and one atmosphere total pressure. Geochimica et Cosmochimica Acta 48, 815–822.
Mühlenhardt-Siegel, U., 1988. Some results on quantitative investigations of macrozoobenthos in the Scotia Arc (Antarctica). Polar Biology 8, 241–248.
Mühlenhardt-Siegel, U., 1989. Quantitative investigations of Antarctic zoobenthos communities in winter (May/June) 1986 with special reference to the sediment structure. Archiv für Fischereiwissenschaft 39, 123–141.
Nelson, C. (Ed.), 1988. Non-tropical shelf sediments—modern and ancient: Sedimentary Geology, Vol. 60, pp. 1–367.
Orr, J.C., Fabry, V.J., Aumont, O., Bopp, L., Doney, S.C., Feely, R.A., Gnanadesikan, A., Gruber, N., Ishida, A., Joos, F., Key, R.M., Lindsay, K., Maier-Reimer, E., Matear, R., Monfray, P., Mouchet, A., Najjar, R.G., Plattner, G.K., Rodgers, K.B., Sabine, C.L., Sarmiento, J.L., Schlitzer, R., Slater, R.D., Totterdell, I.J., Weirig, M.F., Yamanaka, Y., Yool, A., 2005. Anthropogenic ocean acidification over the twenty-first century and its impact on calcifying organisms. Nature 437, 681–686.
Orsi, A.H., Nowlin, W.D., Whitworth, T., 1993. On the circulation and stratification of the Weddell Gyre. Deep-Sea Research Part I—Oceanographic Research Papers 40, 169–203.
Orsi, A.H., Whitworth, T., Nowlin, W.D., 1995. On the meridional extent and fronts of the Antarctic Circumpolar Current. Deep-Sea Research Part I—Oceanographic Research Papers 42, 641–673.
Post, A.L., O'Brien, P.E., Beaman, R.J., Riddle, M.J., De Santis, L., 2010. Physical controls on deep water coral communities on the George V Land slope, East Antarctica. Antarctic Science 22, 371–378.
Post, A.L., Beaman, R.J., O'Brien, P.E., Eléaume, M., Riddle, M.J., 2011. Community structure and benthic habitats across the George V Shelf, East Antarctica: trends through space and time. Deep Sea Research II 58, 105–118. doi:10.1016/j.dsr2.2010.05.020.
Read, J.F., Pollard, R.T., Morrison, A.I., Symon, C., 1995. On the southerly extent of the Antarctic Circumpolar Current in the southeast Pacific. Deep-Sea Research Part II—Topical Studies in Oceanography 42, 933–954.
Sachs, O., Sauter, E.J., Schlüter, M., van der Loeff, M.M.R., Jerosch, K., Holby, O., 2009. Benthic organic carbon flux and oxygen penetration reflect different plankton provinces in the Southern Ocean. Deep-Sea Research Part I—Oceanographic Research Papers 56, 1319–1335.
Seiter, K., Hensen, C., Schroter, E., Zabel, M., 2004. Organic carbon content in surface sediments—defining regional provinces. Deep-Sea Research Part I—Oceanographic Research Papers 51, 2001–2026.
Smith, A.M., 2007. Age, growth and carbonate production by erect rigid bryozoans in Antarctica. Palaeogeography, Palaeoclimatology, Palaeoecology 256, 86–98.
Smith, W.O., Gordon, L.I., 1997. Hyperproductivity of the Ross Sea (Antarctica) polynya during austral spring. Geophysical Research Letters 24, 233–236.
Smith, A.M., Nelson, C.S., 2003. Effects of early sea-floor processes on the taphonomy of temperate shelf skeletal carbonate deposits. Earth-Science Reviews 63, 1–31.
Spindler, M., Dieckmann, G.S., 1986. Distribution and abundance of the planktic foraminifer *Neogloboquadrina pachyderma* in sea ice of the Weddell Sea (Antarctica). Polar Biology 5, 185–191.
Swadling, K.M., Kawaguchi, S., Hosie, G.W., 2010. Antarctic mesozooplankton community structure during BROKE-West (30°E–80°E), January–February 2006. Deep-Sea Research Part II—Topical Studies in Oceanography 57, 887–904.
Tada, Y., Wada, H., Miura, H., 2006. Seasonal stable oxygen isotope cycles in an Antarctic bivalve shell (*Laternula elliptica*): a quantitative archive of ice melt runoff. Antarctic Science 18, 111–115.
Thomas, D., Lara, R., Haas, C., Schnack-Schiel, S., Dieckmann, G., Kattner, G., Nöthig, E., Mizdalski, E., 1998. Biological soup within decaying summer sea ice in the Amundsen Sea, Antarctica. In: Lizotte, M., Arrigo, K. (Eds.), Antarctic Sea Ice Biological Processes, Interactions and Variability. American Geophysical Union, Washington D.C., pp. 161–171.
Timmermann, R., Le Brocq, A., Deen, T., Domack, E., Dutrieux, P., Galton-Fenzi, B., Hellmer, H., Humbert, A., Jansen, D., Jenkins, A., Lambrecht, A., Makinson, K., Niederjasper, F., Nitsche, F., Nøst, O.A., Smedsrud, L.H., Smith, W.H.F., 2010. A consistent data set of Antarctic ice sheet topography, cavity geometry, and global bathymetry. Earth System Science Data 2, 261–273.
Tucker, M., 1996. Methoden der Sedimentologie. Ferdinand Enke Verlag.
Weber, J., Greer, R., Voight, B., White, E., Roy, R., 1969. Unusual strength properties of echinoderm calcite related to structure. Journal of Ultrastructure Research 26, 355–366.
Whitworth III, T., Orsi, A., Kim, S., Nowlin Jr., W., Locarnini, R., 1998. Water masses and mixing near the Antarctic slope front. In: Jacobs, S., Weiss, R. (Eds.), Ocean, Ice and Atmosphere: Interactions at the Antarctic Continental Margin. American Geophysical Union, Washington D.C., pp. 1–27.
Zeebe, R., Wolf-Gladrow, D., 2001. CO_2 in seawater: equilibrium, kinetics, isotopes. Number 65 in Elsevier Oceanography Series. Elsevier, p. 346.

Chapter 4

Insignificant buffering capacity of Antarctic shelf carbonates

Insignificant buffering capacity of Antarctic shelf carbonates

Judith Hauck[1], K. R. Arrigo[2], M. Hoppema[1], G. L. van Dijken[2], C. Völker[1], and D. A. Wolf-Gladrow[1]

[1] Alfred Wegener Institute for Polar and Marine Research, Postfach 12 01 61, 27515 Bremerhaven, Germany
[2] Department of Environmental Earth System Science, Stanford University, Stanford, California, USA

In review at Global Biogeochemical Cycles

Abstract We combined data sets of measured sedimentary $CaCO_3$ and satellite-derived pelagic primary production to parameterize the relation between $CaCO_3$ content on the Antarctic shelves and primary production in the overlying water column. $CaCO_3$ content predicted in this way was in good agreement with the measured data. The parameterization was then used to chart $CaCO_3$ content on the Antarctic shelves all around the Antarctic, using the satellite-derived primary production. The total inventory of $CaCO_3$ in the bioturbated layer of Antarctic shelf sediments was estimated to be 0.5 Pg C. This quantity is comparable to the total CO_2 uptake by the Southern Ocean in only one to a few years (dependent on the uptake estimate and area considered), indicating that the dissolution of these carbonates will neither delay ocean acidification in this area nor augment the Southern Ocean CO_2 uptake capacity.

4.1 Introduction

The atmospheric CO_2 content has been increasing since the beginning of the Industrial Revolution. In the decade between 2000 and 2009, the atmospheric CO_2 increase averaged 1.9 ppm per year due to anthropogenic perturbations of the carbon cycle (*Friedlingstein et al.*, 2010; *GCP*, 2010). In that decade, on average 8.8±1.2 Pg C year^{-1} were emitted by burning of fossil fuels, cement production and land use change. The carbon inventory in the atmosphere, however, increased by only 4.1±0.1 Pg C year^{-1}. The remaining 4.7 Pg C year^{-1} were taken up by the land and oceans in about equal amounts (*Friedlingstein et al.*, 2010; *GCP*, 2010). Hence, the terrestrial and marine carbon sinks decelerate atmospheric CO_2 increase and thus slow down anthropogenic climate change.

The increase of inorganic carbon in the oceans reduces pH (a process recently referred to as ocean acidification) and carbonate saturation states (Ω). Once the seawater is undersaturated with respect to calcium carbonate ($\Omega < 1$), carbonate sediments will start to dissolve, thereby releasing carbonate ions. This does not only counteract acidification, but also enhances the capability of the ocean to act as a CO_2 sink. High latitudes are most sensitive to changes in carbon inventories and might be the first regions to experience undersaturation with respect to calcium carbonate (*Orr et al.*, 2005; *McNeil and Matear*, 2008; *Yamamoto-Kawai et al.*, 2009; *Steinacher et al.*, 2009). Within the polar regions, the shallow shelves undergo the largest changes in pH (*Hauck et al.*, 2010; *Arrigo et al.*, 2008a). The saturation horizons in the Southern Ocean do not only shift upwards from the deep ocean; changes in the saturation state are largest at the surface and combined with already low surface saturation states, undersaturation might occur at the surface before the entire underlying water column is undersaturated (*Hauck et al.*, 2010). Calcareous sediments on the Antarctic shelves might thus provide an initial buffering of ocean acidification, where we refer to buffering by sedimentary carbonates as a negative feedback to acidification of any magnitude. In our definition, buffering does not necessarily mean that pH is maintained at a constant level, yet, if significant, it would delay or temper acidification as compared to a scenario where no $CaCO_3$ is available for dissolution. Whether or not there is a significant buffer effect is the subject of this study.

Aragonite is the most soluble form of calcium carbonate, and thus the first candidate for buffering. A circum-Antarctic data compilation revealed that aragonite is an insignificant constituent of Antarctic shelf sediments (*Hauck et al.*, 2012) despite the reports of high pteropod (pelagic mollusks that produce aragonite shells) densities in the water column (*Hunt et al.*, 2008; *Accornero et al.*, 2003). Almost all samples considered consisted of low-Mg calcites. As the distribution on a sub-regional scale was patchy and there were data gaps, especially in the southwest Pacific and Indian Ocean sectors of the Antarctic

shelves, it is not possible to simply interpolate the $CaCO_3$ data spatially to obtain a circum-Antarctic estimate. A method to predict $CaCO_3$ content based on environmental conditions in the areas with data gaps is crucial to estimate the total inventory of $CaCO_3$ on Antarctic shelves.

$CaCO_3$ is one of the main sedimentary substances, besides lithogenic material, opal and organic matter. The actual composition of sediments is the result of a complex interplay of various processes. Three main processes determine whether a substance can be found in the sediments. First, there needs to be a source of the material in the water column, i.e., production of the biogenic materials, or another source for lithogenic material, such as atmospheric dust deposition; second, dissolution or decomposition processes during the sinking through the water column determine how much of the material rains to the sea floor. Third, early diagenetic processes on the sea floor and in the sediment alter its composition and determine the burial in the sediment (*Martin and Sayles*, 2003).

The dissolution or decomposition of the biogenic materials on their way through the water column can be described as a function of the amount of material at the surface (e.g., *Martin et al.*, 1987; *Yamanaka and Tajika*, 1996). Hence, production in the euphotic zone controls the source terms at the surface and the loss terms in the water column. It is the balance between production at the surface and decay or dissolution at the sea floor that determines how much of the biogenic substances is found in the sediments. Oxic remineralization of organic matter is omnipresent in marine sediments and releases CO_2 (*Martin and Sayles*, 2003). This leads to metabolic-CO_2 driven dissolution of $CaCO_3$, as first mentioned by *Berger* (1970). The relative amounts of $CaCO_3$ and organic matter are further affected by the amount of lithogenic and siliceous material to the sea floor and by bottom currents and winnowing.

We base our analysis on the assumption that $CaCO_3$ production in the euphotic zone and metabolic dissolution of $CaCO_3$ in the sediments are the main processes determining how much $CaCO_3$ is present in the sediments (*Martin and Sayles*, 2003); this is of course a simplification of processes in the real world. $CaCO_3$ production and metabolic dissolution are by definition related to PP as none of them would exist without organic matter production or deposition. We hypothesize that increasing PP leads to more $CaCO_3$ production, at least at low PP levels, as $CaCO_3$ production cannot happen without organic matter production. This process competes with metabolic-CO_2 driven dissolution in sediments; increasing PP leads to more rain of organic matter to the sea floor, and subsequently to more organic matter oxidation and possibly metabolic $CaCO_3$ dissolution. This is in line with the observation that no significant accumulation of $CaCO_3$ was found in the high production regions of the Southern Ocean, such as Prydz Bay, the western Antarctic Peninsula and the Ross Sea (*Hauck et al.*, 2012). These authors also used

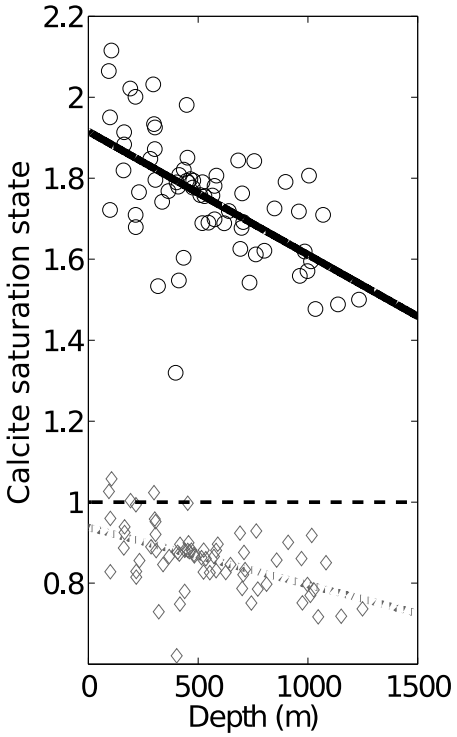

Figure 4.1: The calcite saturation state in the bottom water on the Antarctic shelf (black symbols and line) as calculated from GLODAP and CARINA data (see *Hauck et al.*, 2012, for filtering procedure). The grey symbols and dashed regression line were calculated with a presumed metabolic DIC increase of 100 μmol kg^{-1} in the pore water as estimated from oxygen profiles in the high production regions of the Antarctic shelf (*Sachs et al.*, 2009).

oxygen pore water profiles from *Sachs et al.* (2009) to explain that aragonite cannot be preserved in Antarctic shelf sediments. Here, we add to this by calculating how much the calcite saturation state can change as a result of metabolic-CO_2 production (Figure 4.1). Oxygen profiles from the Antarctic shelf (*Sachs et al.*, 2009) suggest that in the high production regions, dissolved inorganic carbon (DIC) can increase by as much as 100 - 200 μmol kg^{-1} due to oxic remineralization of organic matter in the first centimeter of the sediment. Recalculating the calcite saturation state for the pore waters using a DIC increase of 100 μmol kg^{-1} leads to calcite undersaturation at all depths, and therefore to metabolic-CO_2 driven dissolution of $CaCO_3$.

We made use of the above mentioned concepts and tried to derive a parameterization of sedimentary $CaCO_3$ as a function of satellite-based estimates of PP and water depth. Applying the parameterization, we use PP as a proxy to map the abundance of carbonates in Antarctic shelf sediments. Based on these maps, we calculate a contemporary $CaCO_3$ inventory. The latter amount would be available for dissolution when a reduced bottom water calcite saturation state due to anthropogenic CO_2 uptake would lead to pore water

undersaturation in the regions where $CaCO_3$ is nowadays preserved.

4.2 Data and Fitting Procedure

A set of 390 measurements of the $CaCO_3$ content of surface sediments in continental shelves all around Antarctica was presented in *Hauck et al.* (2012). Their compilation included both newly measured and literature data. In the present analysis, these data were combined with circum-Antarctic calculations of upper ocean PP data based on satellite observations of surface chlorophyll concentrations, sea surface temperature, and sea-ice cover (*Arrigo et al.*, 2008) to estimate large-scale distributions of sediment $CaCO_3$. PP was calculated daily at 4 km horizontal resolution for all Antarctic waters south of 50°S. Daily values at each grid point were integrated over the year to derive annual estimates of PP. The chlorophyll and PP algorithms were validated against a vast amount of field data, including extensive data sets of shelf and coastal areas. The uncertainty of this method was estimated to be less than 10% with respect to chlorophyll and within 25% for PP (*Arrigo et al.*, 2008). Both the sediment $CaCO_3$ and PP data sets were projected onto the bathymetric grid provided by *Timmermann et al.* (2010).

As expected from the competing effects of PP on $CaCO_3$ production and dissolution (see Introduction), there is an optimum value of surface ocean PP where $CaCO_3$ content is maximal; this is elaborated in Figure 4.2. At PP levels below the optimum, $CaCO_3$ content decreases due to nutrient or food limitation of planktonic and benthic carbonate producers. Sediment $CaCO_3$ content is maximal at pelagic PP levels of 5-20 g C m^{-2} yr^{-1}. When PP exceeds the optimum value, $CaCO_3$ content decreases most probably due to carbonate dissolution in the sediments driven by oxic respiration and CO_2 production.

In a first approach, all $CaCO_3$ data were fitted to a Gaussian distribution plus constant background value with upper ocean PP as an independent variable:

$$CaCO_3\ (\%) = A_i \cdot \exp[-\frac{(\mathrm{PP}\ (\mathrm{g\ m^{-2}\ yr^{-1}}) - \mu_i)^2}{2 \cdot \sigma_i^2}] + B_i \qquad (4.1)$$

where $CaCO_3$ (%) is the weight percentage of $CaCO_3$ in the dried sediment, and the parameters A_i (magnitude), μ_i (mean), σ_i (variance), and B_i (background value) were estimated using least-squares regression.

In a second approach, we took into account the water depth dependence of $CaCO_3$ content, as found in *Hauck et al.* (2012), and calculated individual fits for four water depth ranges: 0 - 250 m, 250 - 600 m, 600 - 900 m and 900 - 1000 m. All fits were in the form of a Gaussian distribution plus a constant, as in Eq. 4.1. The estimated parameters A_i, B_i, μ_i and σ_i and their confidence intervals are listed in Table 4.1 and the resulting

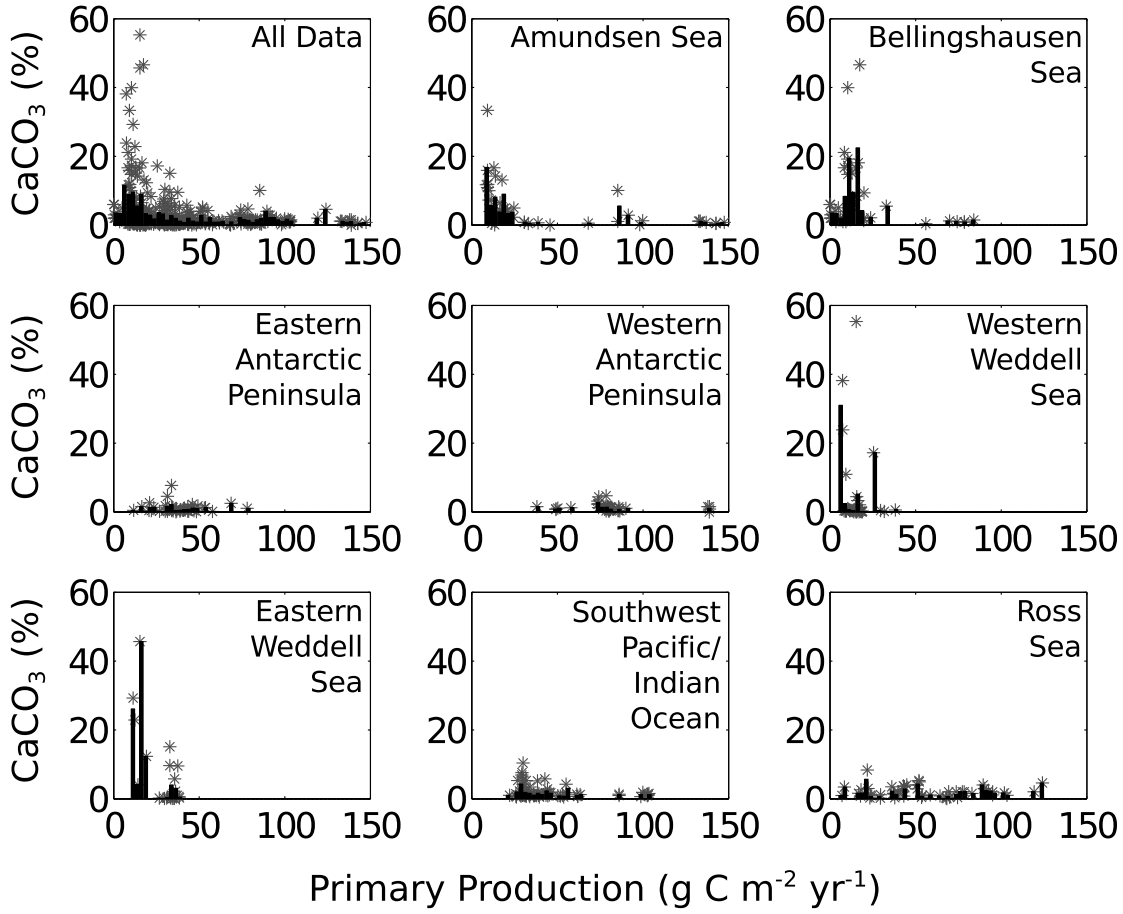

Figure 4.2: $CaCO_3$ versus primary production data for all shelf regions together (upper left) and the different shelf regions separately (name of region indicated in the diagram). Grey asterisks are original data, bars show means within 2.5 g C m^{-2} yr^{-1} bins.

fits are shown in Figures 4.3 and 4.4.

An ensemble of quantitative metrics (Table 4.2) was used to describe the goodness-of-fit, as recommended by *Stow et al.* (2009). The correlation coefficient (r) describes to which extent model and observations vary together. A value close to one indicates that they show the same pattern of variation, and a negative value indicates inverse correlation. The root mean squared error (RMSE), average error (AE) and average absolute error (AAE) are all measures of the misfit, or in other words, of how far the predictions are away from the observations in the variable space. While the AE considers the sign of the discrepancy, and positive and negative discrepancies can average out, RMSE and AAE rather evaluate the magnitude of the offsets. Ideally, they would all be close to zero. The reliability index (RI)

$$\mathrm{RI} = \exp \sqrt{\frac{1}{n} \sum_{i=1}^{n} \left(\log \frac{O_i}{P_i} \right)^2}, \tag{4.2}$$

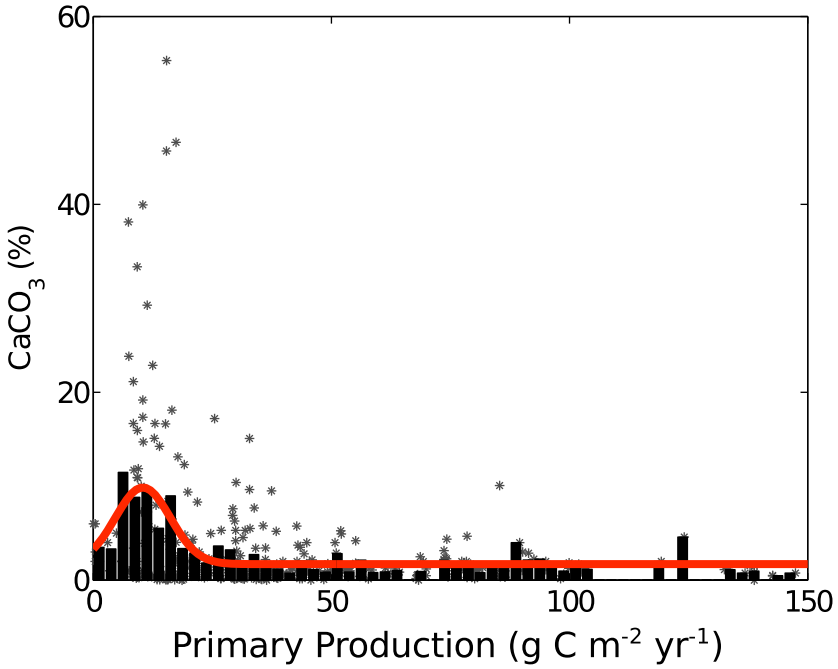

Figure 4.3: Fit to all data. Grey asterisks are original data, bars show means within 2.5 g C m^{-2} yr^{-1} bins. Red line shows fit to a Gaussian distribution plus constant background (Equation 4.1 and Table 4.1).

with O_i being the observations, P_i the predictions and n the number of data points, gives a multiplicative measure of the discrepancies between predictions and observations. A reliability index close to one would be ideal, RI = 2 indicates that the observations and predictions are on average a factor of two different. The modeling efficiency (MEF)

$$\mathrm{MEF} = \frac{\left(\sum_{i=1}^{n}(O_i - \bar{O})^2 - \sum_{i=1}^{n}(P_i - \bar{P})^2\right)}{\sum_{i=1}^{n}(O_i - \bar{O})^2}, \tag{4.3}$$

is a measure of how much better or worse the predictions are compared to the mean of the observations. A MEF of zero indicates that the model is only as good as the average of the observations; at a MEF<0, the model predictions are worse than the average of the observations and at a MEF of one, the model would exactly predict the observations (*Stow et al.*, 2009).

In the following section, where we compare observations to predictions, the observation is the mean $CaCO_3$ content grouped within a 2.5 g C m^{-2} yr^{-1} PP bin as in Figures 4.3 and 4.4. The statistical measures (Table 4.2) describing the discrepancies between observations and predictions (AAE and RMSE) for the depth-independent fit are at the lower end of those for the depth-dependent ones. The quantities describing the goodness-of-fit,

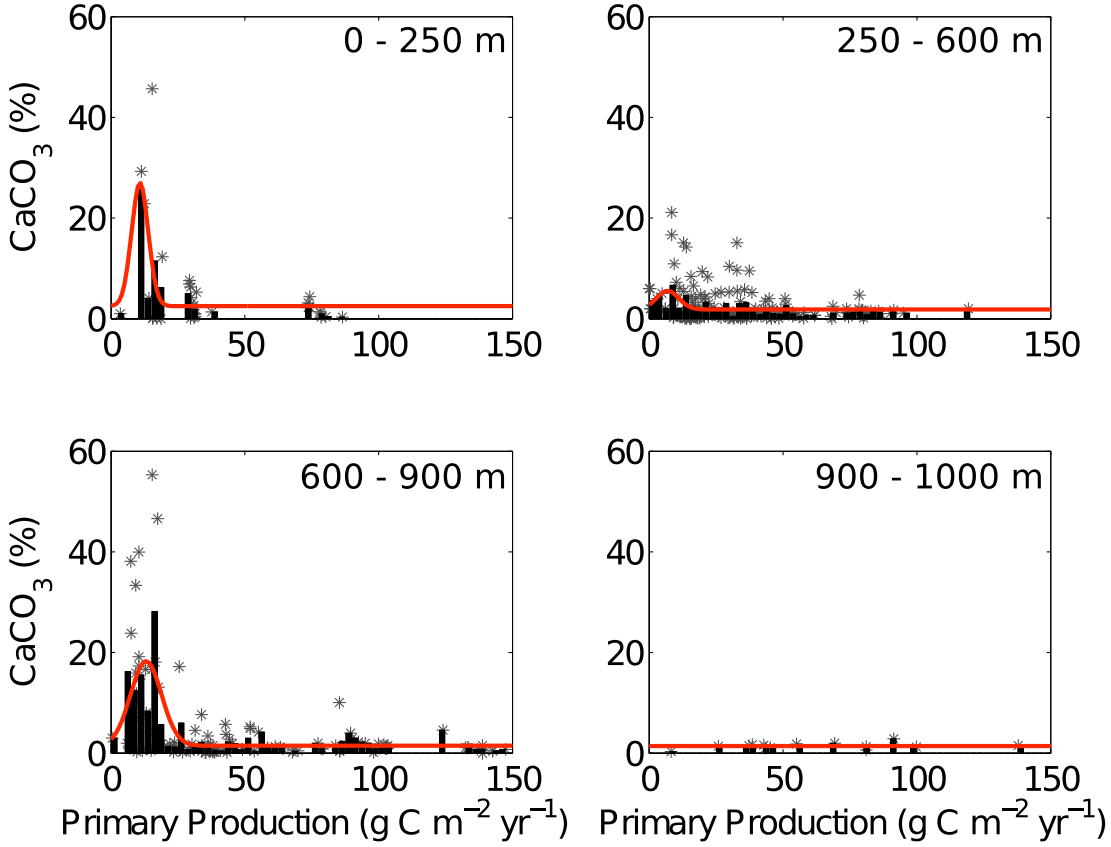

Figure 4.4: Fit within different depth ranges as indicated within the diagrams (0 - 250 m, 250 - 600 m, 600 - 900 m, 900 - 1000 m). Grey asterisks are original data, bars show means within 2.5 g C $m^{-2}yr^{-1}$ bins. Red line shows fit to a Gaussian distribution plus constant background (Equation 4.1 and Table 4.1).

including the correlation coefficient and modeling efficiency, are accordingly higher for the depth-independent fit than for any of the depth-dependent fits. The modeling efficiency for the depth-dependent fit of the depth range 900 - 1000 m is zero, as the model is basically the observation average. The depth-independent fit predicts the observations within a factor of 1.68 (RI), which is as reliable as the depth-dependent fit for the 900 - 1000 m depth range (RI = 1.64) and more reliable than for the 0 - 250 m, 250 - 600 m and 600 - 900 m depth ranges. All univariate goodness-of-fit statistics show that the depth-independent fit is a better predictor of $CaCO_3$ content as a function of PP.

There are two caveats of the depth-dependent parameterization; one is that the number of data points available for the fit is strongly reduced by splitting the data set into four depth compartments, which negatively affects the quality of the fits. The second source of error is the uncertainty associated with the topography product of *Timmermann et al.* (2010). While this is a high-quality product with errors as low as 2% of the water depth close to ship tracks, the error is higher where data were extrapolated, with an upper

Table 4.1: Estimated parameters, their 95% confidence intervals and number of observations (n) derived to describe $CaCO_3$ as a function of primary production (see Eq. 1) using a depth-independent fit and using four fits for four depth compartments: 0 - 250 m; 250 - 600 m; 600 - 900 m; 900 - 1000 m.

Depth range (m)	A_i	μ_i	σ_i	B_i	n
depth-independent fit					
0 - 1000	8.16 ± 2.00	10.41 ± 2.24	5.77 ± 2.37	1.71 ± 0.78	358
depth-dependent fits					
0 - 250	24.52 ± 17.58	10.79 ± 5.07	3.10 ± 3.04	2.52 ±3.07	35
250 - 600	3.70 ± 2.19	6.88 ± 2.86	4.17 ± 2.64	1.84 ± 0.54	184
600 - 900	16.79 ± 4.59	13.07 ± 1.88	5.78 ± 2.55	1.48 ±1.57	125
900 - 1000	-	-	-	1.43 ± 0.35	14

limit being defined as 250 m. At the boundary between depth compartments, errors arise when locations are grouped into the wrong depth compartment where $CaCO_3$ content predictions differ. However, the fits for the depth ranges where high $CaCO_3$ contents were found (0 - 250 m and 600 - 900 m) are only slightly inferior in terms of correlation coefficient and modeling efficiency. It is therefore reasonable to further evaluate both fitting procedures.

The $CaCO_3$ distributions in the different shelf regions all peak at similar PP values (Figure 4.2), so that no bias is expected when applying a single fit to the entire circum-Antarctic data set.

One drawback of both parameterizations is that the sharp increase of $CaCO_3$ at PP levels of 5 g C m^{-2} yr^{-1} is not well reproduced by the Gaussian fit (Figures 4.3 and 4.4). For the depth-independent parameterization, $CaCO_3$ levels are overestimated for PP levels of 0 - 5 g C m^{-2} yr^{-1} and underestimated at 5 - 7.5 g C m^{-2} yr^{-1}. The latter underestimation is also observed in the depth-dependent parameterization for the 600 - 900 m range.

The depth-independent parameterization does not allow $CaCO_3$ content >10%; however, these high values are sparse in the observations and averaging the $CaCO_3$ content over PP ranges of 2.5 g C m^{-2} yr^{-1} yields no mean $CaCO_3$ of >12%.

Two circum-Antarctic maps of $CaCO_3$ (weight %) were produced by applying Eq. 4.1 to all PP data at water depths shallower than 1000 m and south of 60°S with either the depth-independent or depth-dependent sets of parameters. $CaCO_3$ was calculated at a latitudinal and longitudinal resolution of 0.25° x 0.25°. To account for the fact

Table 4.2: Statistics for fits: Correlation coefficient (r); root mean squared error (RMSE); average error or bias (AE); average absolute error (AAE); reliability index (RI) and modeling efficiency (MEF). See *Stow et al.* (2009) and text for further explanation.

Depth range (m)	r	RMSE	AE	AAE	RI	MEF
depth-independent fit						
0 - 1000	0.86	1.3	-0.82	0.93	1.68	0.74
depth-dependent fits						
0 - 250	0.84	3.90	-0.54	3.09	3.14	0.69
250 - 600	0.58	1.13	-0.25	0.91	1.85	0.28
600 - 900	0.81	3.12	-0.03	1.82	2.02	0.65
900 - 1000	-	0.59	0.05	0.42	1.64	-0.01

that organic material and carbonate components produced by organisms feeding on the phytoplankton do not always sink to the sea floor at the exact position where they were produced because of advection by currents, we use the mean PP in a 0.5° x 0.5° box around each position as input PP in Eq. (4.1). Averaging the PP data from a 4 km resolution onto a coarser scale also further reduces its uncertainty.

4.3 Results and Discussion

4.3.1 Evaluation of $CaCO_3$ maps

The predicted $CaCO_3$ distributions for both the depth-dependent and depth-independent parameterizations are presented in Figure 4.5. As prescribed by the parameterization, $CaCO_3$ sediments do not appear in the high-production regions around the western Antarctic Peninsula, in the Ross Sea and in Prydz Bay. High $CaCO_3$ content appears at the outer Amundsen and Bellingshausen and southwestern Weddell Seas and on the narrow shelves of the eastern Weddell Sea and the southwest Pacific and Indian Ocean sectors of the Southern Ocean.

The two parameterizations differ in the magnitude of $CaCO_3$ accumulations at those places where significant amounts are predicted, e.g., in the Amundsen and Bellingshausen Seas, the southwestern Weddell Sea and the southeastern Antarctic Peninsula. The depth-independent parameterization produces more regions with values between 7% and the maximum value of 10%. The map generated using the depth-dependent parameterization

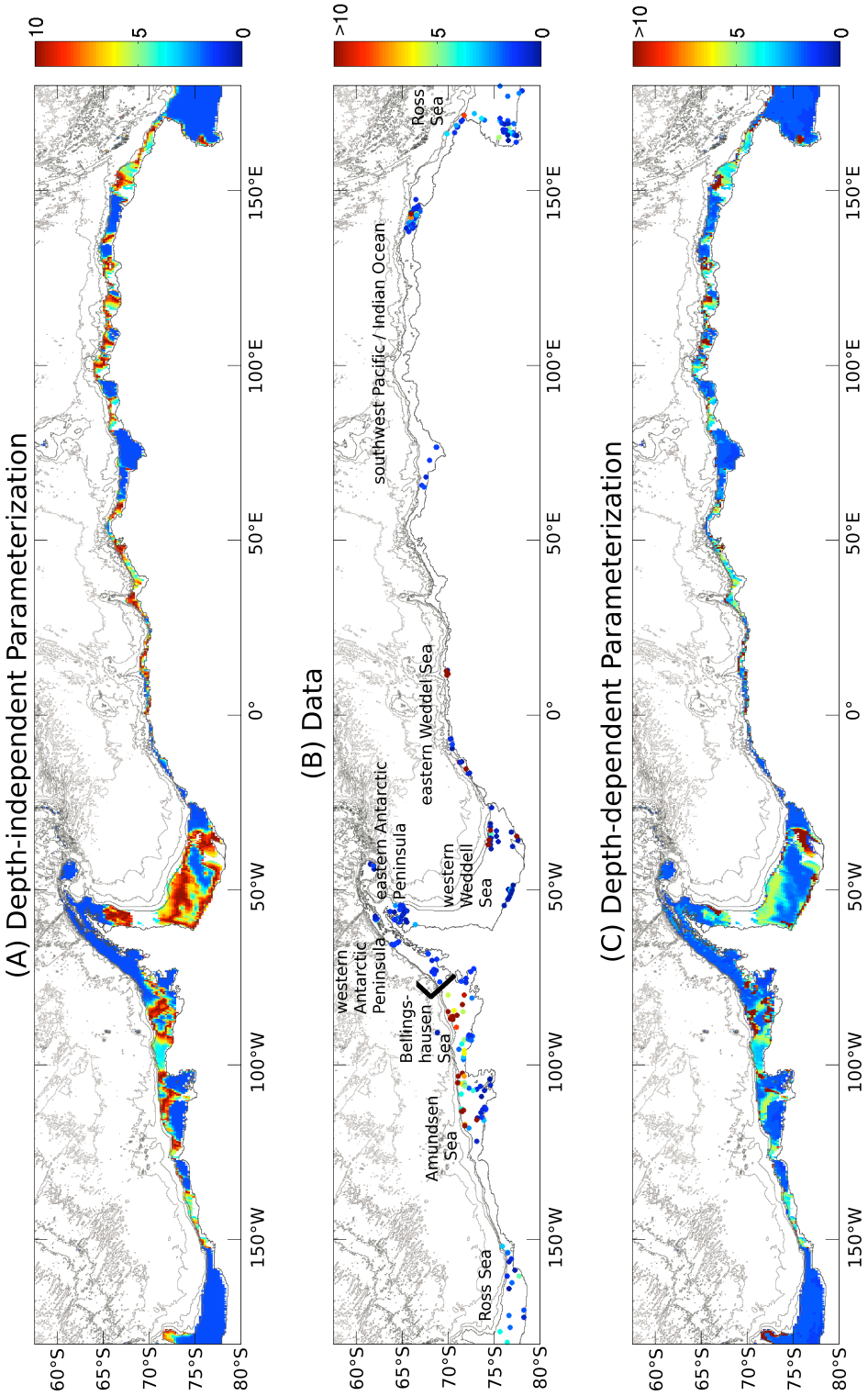

Figure 4.5: $CaCO_3$ (% dry weight) maps produced with PP - $CaCO_3$ - parameterization (a) map of predicted $CaCO_3$ (%) data with depth-independent parameterization, (b) $CaCO_3$ (%) data from *Hauck et al.* (2012), (c) map of predicted $CaCO_3$ (%) data with depth-dependent parameterization. Note that panels (b) and (c) do not show the full range, but are cut off at 10% for better comparability with panel (a).

displays only few locations with more than 7% $CaCO_3$, but peak values go up to 27% (Figure 4.4).

The depth-independent parameterization produces large areas with the maximum $CaCO_3$ content on the southeastern Antarctic Peninsula and southwestern Weddell Sea shelves. Like in the Bellingshausen and Amundsen Seas, the depth-dependent parameterization shows a similar pattern as the depth-independent, but generally with lower values. The environmental setting in the southwestern Weddell Sea is very similar to the one in the Amundsen and Bellingshausen Seas where the broad and deep shelves are covered with sea ice for most of the year. High sedimentary $CaCO_3$ content in the Amundsen and Bellingshausen Seas was explained by high numbers of the planktonic foraminifera *Neogloboquadrina pachyderma* from the water column and the sea ice which may also be concentrated by winnowing of silt and clay (*Hillenbrand et al.*, 2003; *Hauck et al.*, 2012). While only parts of the western Weddell Sea were covered by the data compilation of *Hauck et al.* (2012), a high number of planktonic calcareous foraminifera was found on the outer shelf and slope of the southwestern Weddell Sea and eastern Antarctic Peninsula south of 65°S by *Anderson* (1975). Assuming that a high ratio of calcareous to arenaceous foraminifera, as found by *Anderson* (1975), corresponds to high $CaCO_3$ content, the calculation of high $CaCO_3$ content on the outer shelves of the southeastern Antarctic Peninsula and southwestern Weddell Sea appears to be reasonable. The band of high values on the inner shelf along the coast of the southwestern Weddell Sea does not correspond with observations (compare Figure 4.5b) and is probably spurious. Within the period considered (1997 - 2006), the polynya on the inner southwestern Weddell Sea shelf was open for only two years. The time-series is probably too short to capture the true mean PP in this area.

To complete the evaluation, we compare predicted to observed $CaCO_3$ content at each sample location. As the $CaCO_3$ distribution is very patchy, we calculate the mean $CaCO_3$ in a 100 km radius around each measured or modeled data point. We compare these smoothed data sets and also the average measured and modeled $CaCO_3$ concentration in the different regions (Figure 4.6). While these averaging or smoothing procedures are needed, they also have caveats. The mean of the measurements can only be calculated where data for averaging is available and is biased by the clustering of data points in certain regions and by the sparseness of data in others. Therefore it is hard to judge the skill of the model based on this comparison and we refer to the above discussion of the produced maps. Clearly, the modeled $CaCO_3$ content in the southwest Pacific and Indian Ocean (swP/IO), eastern Antarctic Peninsula and western Weddell Sea regions is higher than observed, due to the fact that areas with high values were calculated for former data gaps. This is more pronounced in the depth-independent parameterization.

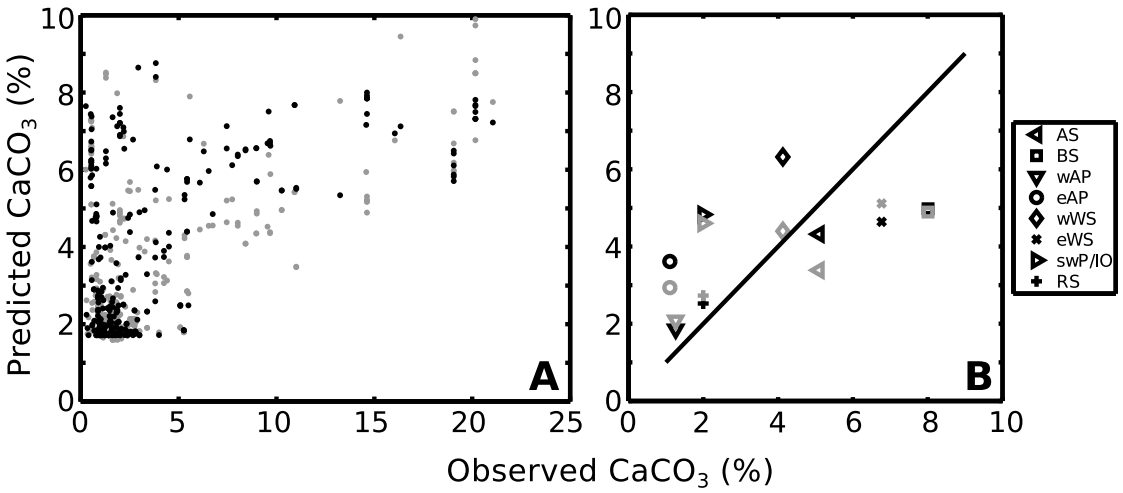

Figure 4.6: Comparison of observed versus predicted $CaCO_3$ (% dry weight) for the depth-independent (black) and depth-dependent (grey) parameterizations. (a) Observations and predictions were smoothed by averaging over a 100 km radius around each measured or predicted data point, (b) regional averages were calculated for the data and predictions for the Amundsen Sea (AS), Bellingshausen Sea (BS), western Antarctic Peninsula (wAP), eastern Antarctic Peninsula (eAP), western Weddell Sea (wWS), eastern Weddell Sea (eWS), southwest Pacific/Indian Ocean (swP/IO) and Ross Sea (RS) regions. The black line shows the one-to-one line.

In contrast, the model suggests that areas with high $CaCO_3$ content were over-represented in the Amundsen Sea, Bellingshausen Sea and eastern Weddell Sea regions.

The mapping procedure fills in situ data gaps in the swP/IO sectors of the Antarctic shelves. As most swP/IO data from *Hauck et al.* (2012) were from locations with relatively high PP levels (Figure 4.2), the mapping procedure reveals possible $CaCO_3$ accumulation sites. It is now possible to split the swP/IO region into the highly productive Prydz Bay (*Arrigo et al.*, 2008) and the remainder of the region. In Prydz Bay, oxic remineralization of organic material drives dissolution of carbonates in the sediments. The remainder of the area has a similar setting as the eastern Weddell Sea, with shallow shelves and limited sea-ice cover. We may therefore expect that carbonates are preserved at shallow depths and that both planktonic and benthic organisms contribute to the $CaCO_3$ production. The swP/IO remains a possible accumulation site for pteropods, as hypothesized by *Hauck et al.* (2012), since it fulfills the requirements for $CaCO_3$ preservation (shallow shelf, average primary production, high pteropod density reported by *Hunt et al.* (2008)). The identification of possible $CaCO_3$ accumulation sites in the swP/IO region suggests that this hypothesis may be valid. However, observations are needed to prove or disprove the hypothesis.

4.3.2 $CaCO_3$ reservoir

One of the main aims is to quantify the total inventory of $CaCO_3$ on Antarctic continental shelves. Quantification is based on the charts with predicted $CaCO_3$ content (Figure 4.5). Further, we follow the procedure of *Archer* (1996). Here we assume that the inventory of $CaCO_3$, which is capable of buffering anthropogenic carbon, is formed by the upper 10 cm of the sediments. First, $CaCO_3$ (%) data were converted to the $CaCO_3$ content in the 10 cm surface layer (g km^{-2}) using the equation:

$$CaCO_3 \text{ (g km}^{-2}) = \frac{CaCO_3(\%)}{100} \cdot \rho \cdot (1 - \phi) \cdot \text{ d} \cdot \text{f} \tag{4.4}$$

where the average porosity (ϕ) of the top 10 cm of the sediment is based on the percentage of $CaCO_3$ (*Archer*, 1996; *DeMenocal et al.*, 1993). Calculated porosities range from 0.845 to 0.860 with a mean of 0.857 for the depth-independent parameterization and from 0.812 to 0.860 with a mean of 0.858 for the depth-dependent parameterization. We use an average grain density (ρ) of 2.5 g cm^{-3} and assume that the $CaCO_3$ content is constant in the upper 10 cm (d) of the sediment, reflecting the bioturbated layer in which $CaCO_3$ can dissolve (*Archer*, 1996; *Berger and Killingley*, 1982; *Boudreau*, 1994; *Martin and Sayles*, 2003). The factor f = 10^{-10} converts from units of g cm^{-2} to g km^{-2}.

In the second step, $CaCO_3$ (g km^{-2}) was integrated over the area of the entire Antarctic continental shelf (4.4 x 10^6 km^2). The inventory calculated with the depth-independent parameterization amounts to 4.3 Pg $CaCO_3$ or 0.52 Pg C whereas the depth-dependent parameterization yields 4.0 Pg $CaCO_3$ or 0.48 Pg C. The spatial dissimilarities between the two different parameterizations level out when integrating over the whole Antarctic shelf. We consider all uncertainties to be accounted for by applying the two different fitting procedures. A back-of-the-envelope estimate to test whether these numbers are in a reasonable range, can be done by calculating the inventories separately in the different shelf regions, solely based on the means of the observations and the area of the regions (Amundsen Sea, Bellingshausen Sea, western and eastern Antarctic Peninsula, western and eastern Weddell Sea, swP/IO, and Ross Sea). Summing up these independent estimates leads to a total of 4.9 Pg $CaCO_3$ or 0.59 Pg C. This is in the same range as the PP and depth-based estimates and confirms that our method is valid. However, given that the samples were not randomly distributed and large data gaps exist, this simple estimate alone would not be trustworthy. The interpolation procedure we presented fills data gaps based on environmental conditions, it can be used to produce maps and is more appropriate to calculate an inventory, even though it also has drawbacks (see section 4.3.1).

Thus, the total inorganic carbon content able to buffer anthropogenic increases in

CO_2 amounts to 0.5 Pg C or 113 g C m^{-2}. The latter value is more than a factor of 100 smaller than the global average amount of $CaCO_3$ in shallow water sediments (18 x 10^3 g C m^{-2} calculated from an estimate of 517 Pg C over an area of 28.3 x10^6 km^2, *Andersson et al.* (2003)). The dissimilarities between these estimates are mainly due to the different contents of $CaCO_3$ in the sediments. *Andersson et al.* (2003) assume 15% $CaCO_3$ in 95% of the sediment area and 80% $CaCO_3$ in the remaining 5%, which is much more than we found in Antarctic shelf sediments. However, their inventory is overestimated by defining the reactive sediment as a 1 m layer. In contrast, we use a reactive or bioturbated layer of 10 cm, in agreement with previous work (*Archer*, 1996; *Broecker and Takahashi*, 1977; *Peng et al.*, 1977). We do not consider exposure of $CaCO_3$ from underneath the bioturbated layer due to erosion. This is legitimate because with percentages of $CaCO_3$ of 10% or less, dissolution of $CaCO_3$ does not induce a significant mass loss. *Andersson et al.* (2003) could have considered erosion and subsequent entrainment of older $CaCO_3$ from below, but the assumption of a static sediment column thicker than the bioturbated layer was shown to overestimate the $CaCO_3$ inventory by a factor of two to three (*Archer*, 1996; *Sundquist*, 1985, and references therein).

For comparison, the buffering capacity of global deep-sea sediments was estimated to be about 1600 Pg C by *Archer* (1996), which is a factor of three smaller than the estimate by *Broecker and Takahashi* (1977) who used a static sediment column. In order to obtain a truly global estimate for the inventory of erodible $CaCO_3$, a new data compilation would be needed to fill data gaps in shallow-water and polar regions from the *Archer* (1996) estimate.

Although there may be uncertainties associated with the global shallow water reservoir, it is certain that the Antarctic reservoir is comparatively small. This suggests that the Antarctic shelves have a limited capacity for buffering anthropogenic increases in CO_2.

4.3.3 Buffering capacity of Antarctic shelf carbonates

The dissolution of $CaCO_3$ can be expressed by more than one reaction equation (e.g., *Hofmann et al.*, 2010), for instance by

$$CaCO_3 + CO_2 + H_2O \rightarrow Ca^{2+} + 2\ HCO_3^- \tag{4.5}$$

or

$$CaCO_3 \rightarrow Ca^{2+} + CO_3^{2-} \tag{4.6}$$

All formulations have in common that the dissolved inorganic carbon (DIC) pool and the total alkalinity (A_T) pool increase in the molar ratio of one to two, i.e.,

$$\Delta A_T = 2\ \Delta DIC \tag{4.7}$$

This leads to a shift in carbonate equilibria, an increase of carbonate ions and a decrease of CO_2, enhancing the ability of the ocean to take up additional CO_2 from the atmosphere. Approximately 0.8 to 0.9 mole of CO_2 are neutralized by dissolution of one mole of calcium carbonate (the exact factor depends on DIC, A_T, T, and S; for details see *Zeebe and Wolf-Gladrow* (2001)). The total amount of carbon that could be neutralized, i.e., taken up by the ocean without significant changes in pH and calcium carbonate saturation states, by the dissolution of the entire Antarctic shelf inventory is thus 0.4 to 0.45 Pg C. This estimate is of the same order of magnitude as most of the recent estimates for the Southern Ocean CO_2 uptake per year - e.g., 0.41 Pg C yr^{-1} south of 40°S (*Valsala and Maksyutov*, 2010), 0.3 Pg C yr^{-1} south of 44°S (*Gruber et al.*, 2009; *Takahashi et al.*, 2009, as recalculated by *Gruber et al.* (2009)), 0.05 Pg C yr^{-1} south of 50°S (*Takahashi et al.*, 2009), 0.4 Pg C yr^{-1} south of 50°S (*McNeil et al.*, 2007).

In order to compare the buffering capacity of the shelf sediments with observed anthropogenic CO_2 increases over the last few decades, the inventories need to be converted into the concentration of CO_2 that can be buffered per water parcel. This requires taking the volume of the overlying water into consideration. If we were to consider only the volume above the shelves (1.8 x 10^{15} m^3) and instantaneous dissolution of the sediment $CaCO_3$, ∼14 to 18 μmol kg^{-1} CO_2 could be buffered per kg of seawater. This is a significant number, corresponding to the increase in anthropogenic carbon over at least two decades on the Antarctic shelf (*Hauck et al.*, 2010). However, due to the slow rate of dissolution at a saturation state close to one (*Keir*, 1980; *Hales and Emerson*, 1997) and mixing with neighboring water masses, values this high will not be reached. As a second example, we assume that the dissolved carbonate from the shelf would be mixed into adjacent waters soon after release. Hence, converting the $CaCO_3$ inventory to concentrations requires a volume larger than the water column above the shelf to be taken into account. Using the volume of the Southern Ocean south of 60°S (7 x 10^{16} m^3) to calculate a concentration of anthropogenic CO_2 that can be buffered by dissolution of $CaCO_3$, we calculate that only ∼0.5 μmol CO_2 could be buffered per kg of seawater, before all carbonates in the bioturbated layer on the Antarctic shelf have been dissolved. The true value depends on the $CaCO_3$ dissolution rate, which differs by several orders of magnitude between laboratory experiments and field data (*Hales and Emerson*, 1997), the mixing of the overlying water, and will probably be below the detection limit.

4.4 Conclusions

The sedimentary carbonate content of the Antarctic shelf is mainly determined by primary production (PP) in the overlying water column. The $CaCO_3$ content first increases with increasing PP, eventually reaching an optimum value but then decreases with further increasing PP.

The relationship between PP and $CaCO_3$ content can be used to estimate the $CaCO_3$ content in regions where no in situ data are available. The buffering capacity of carbonates in Antarctic shelf sediments is too small to delay ocean acidification. This is a surprising outcome, considering the extent of the global abundance of carbonates in shelf sediments. As acidification proceeds, carbonates in the sediments will likely disappear in the end without significantly enhancing the buffering capacity of the ocean.

As polar surface waters are very sensitive to acidification, our results imply that the situation for those sensitive waters is worse than previously thought. The uptake of anthropogenic CO_2 will in the near future cause undersaturation of aragonite (*Orr et al.*, 2005; *González-Dávila et al.*, 2011; *McNeil and Matear*, 2008), which will hamper the formation of carbonate shells in organisms like pteropods, with possible aggravating impact on the Antarctic ecosystem. The sediments will not be able to function as a buffer to stop or delay this trend.

Acknowledgements

This paper is a contribution to the German project Biological Impacts of Ocean Acidification (BIOACID), funded by the Federal Ministry of Education and Research (BMBF, FKZ 03F0608B).

References

Accornero, A., C. Manno, F. Esposito, and M. C. Gambi (2003), The vertical flux of particulate matter in the polynya of Terra Nova Bay. Part II. Biological components, *Antarctic Science*, *15*, 175–188, doi:10.1017/S0954102003001214.

Anderson, J. B. (1975), Factors controlling $CaCO_3$ dissolution in the Weddell Sea from foraminiferal distribution patterns, *Marine Geology*, *19*, 315–332, doi:10.1016/0025-3227(75)90083-3.

Andersson, A. J., F. T. Mackenzie, and L. M. Ver (2003), Solution of shallow-water carbonates: An insignificant buffer against rising atmospheric CO_2, *Geology*, *31*, 513–516.

Archer, D. (1996), An atlas of the distribution of calcium carbonate in sediments of the deep-sea, *Global Biogeochemical Cycles*, *10*, 159–174, doi:10.1029/95GB03016.

Arrigo, K. R., G. van Dijken, and M. Long (2008a), Coastal Southern Ocean: A strong anthropogenic CO_2 sink, *Geophysical Research Letters*, *35, L21602*, doi:10.1029/2008GL035624.

Arrigo, K. R., G. L. van Dijken, and S. Bushinsky (2008b), Primary production in the Southern Ocean, 1997-2006, *Journal of Geophysical Research-Oceans*, *113, C08004*, doi:10.1029/2007JC004551.

Berger, W. H. (1970), Planktonic Foraminifera: Selective solution and the lysocline, *Marine Geology*, *8*, 111 – 138, doi:10.1016/0025-3227(70)90001-0.

Berger, W. H., and J. S. Killingley (1982), Box cores from the equatorial Pacific: ^{14}C sedimentation rates and benthic mixing, *Marine Geology*, *45*, 93–125, doi:10.1016/0025-3227(82)90182-7.

Boudreau, B. P. (1994), Is burial velocity a master parameter for bioturbation?, *Geochimica et Cosmochimica Acta*, *58*, 1243 – 1249, doi:10.1016/0016-7037(94)90378-6.

Broecker, W. S., and T. Takahashi (1977), Neutralization of fossil fuel CO_2 by marine calcium carbonate, in *The fate of fossil fuel CO_2 in the oceans*, edited by N. R. Anderson and A. Malahoff, pp. 213–241, Plenum, N.Y., USA.

DeMenocal, P. B., W. F. Ruddiman, and E. M. Pokras (1993), Influences of high- and low-latitude processes on African terrestrial climate: Pleistocene eolian records from equatorial Atlantic Ocean Drilling Program site 663, *Paleoceanography*, *8*, 209–242, doi:10.1029/93PA02688.

Friedlingstein, P., R. A. Houghton, G. Marland, J. Hackler, T. A. Boden, T. J. Conway, J. G. Canadell, M. R. Raupach, P. Ciais, and C. Le Quéré (2010), Update on CO_2 emissions, *Nature Geoscience*, *3*, 811–812, doi:10.1038/ngeo1022.

GCP (2010), Global Carbon Project: Carbon budget and trends 2009, released on 21 November 2010 on www.globalcarbonproject.org/carbonbudget.

González-Dávila, M., J. M. Santana-Casiano, R. M. Fine, B. Happell, B. Delille, and S. Speich (2011), Carbonate system buffering in the water masses of the Southwest Atlantic sector of the Southern Ocean during February - March 2008, *Biogeosciences*, *8*, 1401–1413, doi:10.5194/bg-8-1401-2011.

Gruber, N., M. Gloor, S. E. Mikaloff Fletcher, S. C. Doney, S. Dutkiewicz, M. J. Follows, M. Gerber, A. R. Jacobson, F. Joos, K. Lindsay, D. Menemenlis, A. Mouchet, S. A. Müller, J. L. Sarmiento, and T. Takahashi (2009), Oceanic sources, sinks, and transport of atmospheric CO_2, *Global Biogeochemical Cycles*, *23*, GB1005, doi:10.1029/2008GB003349.

Hales, B., and S. Emerson (1997), Evidence in support of first-order dissolution kinetics of calcite in seawater, *Earth and Planetary Science Letters*, *148*, 317 – 327, doi:10.1016/S0012-821X(97)00017-4.

Hauck, J., M. Hoppema, R. G. J. Bellerby, C. Völker, and D. Wolf-Gladrow (2010), Data-based estimation of anthropogenic carbon and acidification in the Weddell Sea on a decadal timescale, *Journal of Geophysical Research-Oceans*, *115, C03004*, doi:10.1029/2009JC005479.

Hauck, J., D. Gerdes, C.-D. Hillenbrand, M. Hoppema, G. Kuhn, G. Nehrke, C. Völker, and D. A. Wolf-Gladrow (2012), Distribution and mineralogy of carbonate sediments on Antarctic shelves, *Journal of Marine Systems*, *90*, 77 – 87, doi:10.1016/j.jmarsys.2011.09.005.

Hillenbrand, C.-D., H. Grobe, B. Diekmann, G. Kuhn, and D. K. Fütterer (2003), Distribution of clay minerals and proxies for productivity in surface sediments of the Bellingshausen and Amundsen seas (West Antarctica) - relation to modern environmental conditions, *Marine Geology*, *193*, 253–271, doi:10.1016/S0025-3227(02)00659-X.

Hofmann, A. F., J. J. Middelburg, K. Soetaert, D. A. Wolf-Gladrow, and F. J. R. Meysman (2010), Proton cycling, buffering, and reaction stoichiometry in natural waters, *Marine Chemistry*, *121*, 246 – 255, doi:10.1016/j.marchem.2010.05.004.

Hunt, B. P. V., E. A. Pakhomov, G. W. Hosie, V. Siegel, P. Ward, and K. Bernard (2008), Pteropods in Southern Ocean ecosystems, *Progress in Oceanography*, *78*, 193–221, doi:10.1016/j.pocean.2008.06.001.

Keir, R. S. (1980), The dissolution kinetics of biogenic calcium carbonates in seawater, *Geochimica et Cosmochimica Acta*, *44*, 241 – 252, doi:10.1016/0016-7037(80)90135-0.

Martin, J. H., G. A. Knauer, D. M. Karl, and W. W. Broenkow (1987), VERTEX: carbon cycling in the northeast Pacific, *Deep Sea Research Part A.*, *34*, 267 – 285, doi:10.1016/0198-0149(87)90086-0.

Martin, W. R., and F. L. Sayles (2003), 7.02 - The recycling of biogenic material at the seafloor, in *Treatise on Geochemistry*, edited by H. D. Holland and K. K. Turekian, pp. 37 – 65, Pergamon, Oxford, UK, doi:10.1016/B0-08-043751-6/07089-4.

McNeil, B. I., and R. J. Matear (2008), Southern Ocean acidification: A tipping point at 450-ppm atmospheric CO_2, *Proceedings of the National Academy of Sciences of the United States of America*, *105*, 18,860–18,864, doi:10.1029/2007GB002991.

McNeil, B. I., N. Metzl, R. M. Key, R. J. Matear, and A. Corbiere (2007), An empirical estimate of the Southern Ocean air-sea CO_2 flux, *Global Biogeochemical Cycles*, *21*, GB3011, doi:10.1029/2007GB002991.

Orr, J. C., V. J. Fabry, O. Aumont, L. Bopp, S. C. Doney, R. A. Feely, A. Gnanadesikan, N. Gruber, A. Ishida, F. Joos, R. M. Key, K. Lindsay, E. Maier-Reimer, R. Matear, P. Monfray, A. Mouchet, R. G. Najjar, G. K. Plattner, K. B. Rodgers, C. L. Sabine, J. L. Sarmiento, R. Schlitzer, R. D. Slater, I. J. Totterdell, M. F. Weirig, Y. Yamanaka, and A. Yool (2005), Anthropogenic ocean acidification over the twenty-first century and its impact on calcifying organisms, *Nature*, *437*, 681–686, doi:10.1038/nature04095.

Peng, T. H., W. S. Broecker, G. Kipphut, and N. Shackleton (1977), Benthic mixing in deep sea cores as determined by ^{14}C dating and its implications regarding climate stratigraphy and the fate of fossil fuel CO_2, in *The fate of fossil fuel CO_2 in the oceans*, edited by N. R. Anderson and A. Malahoff, pp. 355–373, Plenum, N.Y., USA.

Sachs, O., E. J. Sauter, M. Schlüter, M. M. Rutgers van der Loeff, K. Jerosch, and O. Holby (2009), Benthic organic carbon flux and oxygen penetration reflect different plankton provinces in the Southern Ocean, *Deep Sea Research Part I*, *56*, 1319 – 1335, doi:10.1016/j.dsr.2009.02.003.

Steinacher, M., F. Joos, T. L. Fröhlicher, G. K. Plattner, and S. C. Doney (2009), Imminent ocean acidification in the Arctic projected with the NCAR global coupled carbon cycle-climate model, *Biogeosciences*, *6*, 515–533, doi:10.5194/bg-6-515-2009.

Stow, C. A., J. Jolliff, D. J. McGillicuddy, S. C. Doney, J. I. Allen, M. A. M. Friedrichs, K. A. Rose, and P. Wallhead (2009), Skill assessment for coupled biological/physical models of marine systems, *Journal of Marine Systems*, *76*, 4–15, doi:10.1016/j.jmarsys.2008.03.011.

Sundquist, E. T. (1985), Geological perspectives on carbon dioxide and the carbon cycle, in *The carbon cycle and atmospheric CO_2: Natural variations archean to present*, *Geophys. Monogr. Ser.*, vol. 32, edited by E. T. Sundquist and W. S. Broecker, pp. 5–59.

Takahashi, T., S. C. Sutherland, R. Wanninkhof, C. Sweeney, R. A. Feely, D. W. Chipman, B. Hales, G. Friederich, F. Chavez, C. Sabine, A. Watson, D. C. E. Bakker, U. Schuster,

N. Metzl, H. Yoshikawa-Inoue, M. Ishii, T. Midorikawa, Y. Nojiri, A. Körtzinger, T. Steinhoff, M. Hoppema, J. Olafsson, T. S. Arnarson, B. Tilbrook, T. Johannessen, A. Olsen, R. Bellerby, C. S. Wong, B. Delille, N. R. Bates, and H. J. W. de Baar (2009), Climatological mean and decadal change in surface ocean pCO_2, and net sea-air CO_2 flux over the global oceans, *Deep-Sea Research Part II-Topical Studies in Oceanography*, *56*, 554–577, doi: 10.1016/j.dsr2.2008.12.009.

Timmermann, R., A. Le Brocq, T. Deen, E. Domack, P. Dutrieux, B. Galton-Fenzi, H. Hellmer, A. Humbert, D. Jansen, A. Jenkins, A. Lambrecht, K. Makinson, F. Niederjasper, F. Nitsche, O. A. Nøst, L. H. Smedsrud, and W. H. F. Smith (2010), A consistent data set of Antarctic ice sheet topography, cavity geometry, and global bathymetry, *Earth System Science Data*, *2*, 261–273, doi:10.5194/essd-2-261-2010.

Valsala, V., and S. Maksyutov (2010), Simulation and assimilation of global ocean pCO_2 and air-sea CO_2 fluxes using ship observations of surface ocean pCO_2 in a simplified biogeochemical offline model, *Tellus Series B-Chemical and Physical Meteorology*, *62*, 821–840, doi: 10.1111/j.1600-0889.2010.00495.x.

Yamamoto-Kawai, M., F. A. McLaughlin, E. C. Carmack, S. Nishino, and K. Shimada (2009), Aragonite undersaturation in the Arctic Ocean: Effects of ocean acidification and sea ice melt, *Science*, *326*, 1098–1100, doi:10.1126/science.1174190.

Yamanaka, Y., and E. Tajika (1996), The role of the vertical fluxes of particulate organic matter and calcite in the oceanic carbon cycle: Studies using an ocean biogeochemical general circulation model, *Global Biogeochemical Cycles*, *10*, 361–382, doi:10.1029/96GB00634.

Zeebe, R. E., and D. A. Wolf-Gladrow (2001), *CO_2 in seawater: Equilibrium, kinetics, isotopes*, *Elsevier Oceanography Series*, vol. 65, p. 346, Elsevier.

Chapter 5

Inter-annual variability of Southern Ocean organic and inorganic carbon fluxes

Inter-annual variability of Southern Ocean organic and inorganic carbon fluxes

Judith Hauck[1], C. Völker[1], T. Wang[1], M. Hoppema [1], M. Losch[1], and D. A. Wolf-Gladrow[1]

[1] Alfred Wegener Institute for Polar and Marine Research, Postfach 12 01 61, 27515 Bremerhaven, Germany

To be submitted to Global Biogeochemical Cycles in June 2012

Abstract Stratospheric ozone depletion and emission of greenhouse gases lead to a trend of the Southern Annular Mode (SAM) toward its high-index polarity. We use a coupled ecosystem-general circulation model to explore changes in the natural carbon budget of the surface Southern Ocean as response to the SAM. The positive phase of the SAM is characterized by stronger than usual westerly winds that induce changes in the physical carbon transport. South of the Polar Front, upwelling and entrainment are stronger than usual. North of the Polar Front there is more intense downwelling while a stronger northward Ekman transport arises across the entire front. These processes nearly balance each other, hence the residual surface DIC change is small compared to the additional DIC input by vertical advection.

The regions south and north of the Polar Front respond differently to the SAM. In the southern part, the entrainment of nutrient-rich deep water enhances diatom and total phytoplankton production. Consequently, more surface CO_2 is drawn down and more organic carbon than usual sinks out of the surface layer. The effect of the additional carbon export on the perturbed DIC budget is larger than that of additional CO_2 outgassing, underlining the importance of the biological carbon pump. In the northern part, primary production is reduced and outgassing of natural CO_2 is the only carbon sink in the perturbed DIC budget besides downwelling. In total, we calculate an additional outgassing of 0.09 Pg C yr^{-1} south of 30°S per unit increase in the standardized SAM index, in line with previous model studies.

5.1 Introduction

The Southern Ocean is one of the main gateways for anthropogenic CO_2 into the ocean's interior (*Khatiwala et al.*, 2009), and it has a pivotal role in the marine and global carbon cycles (*Marinov et al.*, 2006). Yet, the magnitude of the Southern Ocean CO_2 sink is still poorly constrained (*Louanchi et al.*, 1999; *McNeil et al.*, 2007; *Takahashi et al.*, 2009; *Gruber et al.*, 2009). The spatial distribution of the strength, or even the sign, of the Southern Ocean CO_2 flux differs between various methods. For instance, inversion and surface pCO_2 based methods yield similar total sink estimates of 0.3 Pg C yr^{-1} south of 44°S, but the ocean inversion distributes the uptake equally over the Southern Ocean, whereas the pCO_2 based method divides the Southern Ocean at 58°S into a northern sink and a southern source (*Gruber et al.*, 2009). Sparsity of data is a major issue in the Southern Ocean. Simply by adding more data to the pCO_2 database of *Takahashi et al.* (2002), the Southern Ocean's classification changed from a 'major sink' for atmospheric CO_2 (0.38 Pg C yr^{-1} south of 50°S (*Takahashi et al.*, 2002, as recalculated by *Takahashi et al.* (2009))) to a weak sink of 0.05 Pg C yr^{-1} south of 50°S and a small source of 0.01 Pg C yr^{-1} south of 62°S (*Takahashi et al.*, 2009). A key unknown is the role of sea ice in the high-latitude carbon cycle (e.g., *Miller et al.*, 2011); assumptions about sea-ice also affect the estimate of *Takahashi et al.* (2009). Model and data-based estimates reveal a significant CO_2 sink on the Antarctic shelves (*Arrigo et al.*, 2008; *Hauck et al.*, 2010) that were not apparent in the study of *Takahashi et al.* (2009).

Temporal variability of CO_2 fluxes in the Southern Ocean can be divided into variability on seasonal and inter-annual time scales. In the Southern Ocean, where the seasonal temperature range is small compared to temperate latitudes, solubility driven variability is subordinate to biological drawdown as the main source of seasonal variability of surface pCO_2 (*Takahashi et al.*, 2002; *Bakker et al.*, 2008; *Arrigo et al.*, 2008). During winter, entrainment of carbon rich sub-surface water leads to CO_2 enriched surface water relative to the atmosphere. Outgassing, however, is obstructed by sea-ice coverage. After the onset of sea-ice melting, biological activity rapidly reduces surface pCO_2 and the ocean acts as a CO_2 sink (*Bakker et al.*, 2008).

Inter-annual variability is a response to climate variations. The main feature of the atmospheric circulation in the Southern Hemisphere is a circumpolar jet stream that is generated by the large temperature gradient between the cold Antarctic continent and the warm ocean in the sub-tropics. The jet encircles Antarctica nearly symmetrically, scarcely interrupted by land. The jet also determines atmospheric variability in the Southern Hemisphere. One single ring-like, or annular, pattern dominates the internal atmospheric variability in the Southern Hemisphere; it is thus called the Southern Annu-

lar Mode (SAM) and is also known as Antarctic Oscillation. The SAM index was first defined as the sea level pressure difference between 40°S and 65°S (*Gong and Wang*, 1999; *Marshall*, 2003), motivated by the alternation of atmospheric mass between the mid- and high-latitudes. Alternatively, the SAM index can be calculated as the leading empirical orthogonal function of sea level pressure or geopotential height fields (*Thompson and Wallace*, 2000). A positive SAM index indicates a stronger than usual pressure gradient between the subpolar low and the subtropical high regimes. In such a case, the jet stream is displaced polewards and westerly winds become stronger south of about 45°S (*Hall and Visbeck*, 2002; *Thompson and Wallace*, 2000). In recent decades, there has been a positive trend in the SAM index, or, in other words, a shift towards its positive phase (*Marshall*, 2003), driven by the loss of stratospheric ozone ('ozone hole') and the increase in greenhouse gas concentrations (*Thompson et al.*, 2011)

The ocean's response to the SAM trend is under debate. Coarse resolution and eddy resolving models agree with observations that the initial response of the ocean is a stronger northward Ekman transport and that the ACC has moved southward by 50 to 80 km (*Hall and Visbeck*, 2002; *Oke and England*, 2004; *Sen Gupta and England*, 2006; *Hallberg and Gnanadesikan*, 2006; *Hogg et al.*, 2008; *Screen et al.*, 2009; *Böning et al.*, 2008). While this is the full response as seen by coarse resolution ocean models, eddy resolving models and observations additionally reveal an increase in eddy activity with a lag of two to three years. The southward directed eddy fluxes have the potential to largely compensate the intensified Ekman transport so that the average meridional transport and overturning remain nearly unaltered (*Hallberg and Gnanadesikan*, 2006; *Hogg et al.*, 2008; *Screen et al.*, 2009; *Böning et al.*, 2008; *Marshall and Speer*, 2012).

The inter-annual variation in Southern Ocean circulation patterns enforces variability in biogeochemical cycles. Increased upwelling south of the Polar Front (PF) was shown to bring limiting (micro-) nutrients, such as iron, to the surface and to stimulate phytoplankton growth, as observed in satellite-derived chlorophyll estimates (*Lovenduski and Gruber*, 2005). North of the PF, a positive SAM correlated with reduced chlorophyll levels that *Lovenduski and Gruber* (2005) related to deeper than normal mixed layer depths and light limitation. *Lenton and Matear* (2007) and *Lovenduski et al.* (2007) found a negative correlation between the SAM and the Southern Ocean CO_2 uptake. They hypothesized about a significant decrease of the Southern Ocean CO_2 sink with the predicted ongoing trend to a more positive SAM.

Le Quéré et al. (2007) suggested that the Southern Ocean CO_2 sink had become stagnant already in the 1990s, in spite of increasing atmospheric CO_2 concentrations (see also *Zickfeld et al.*, 2008; *Law et al.*, 2008; *Le Quéré et al.*, 2008). The reduction in CO_2 uptake relative to the atmospheric CO_2 increase was related to the strengthening

of subpolar westerlies and consecutive upwelling of carbon-rich deep water during the positive phase of the SAM. But increased winds might as well strengthen the Southern Ocean sink in the future, once the carbon concentration of the surface layer exceeds that of the deep ocean (*Zickfeld et al.*, 2008). Moreover, transport by the Antarctic Circumpolar Current (ACC) and meridional overturning might not change at all (*Böning et al.*, 2008), suggesting that CO_2 fluxes might remain unaffected.

This study aims to contribute to the understanding of the variability in Southern Ocean CO_2 fluxes and the role of biology and export production. We present our model set-up (section 5.2) and evaluate its mean state with respect to circulation, sea-ice, ecosystem and carbonate chemistry (section 5.3). Further, we investigate the inter-annual variability of the system, driven by variations in the SAM index (section 5.4). The hypothesis of *Lovenduski et al.* (2007) that primary production does not contribute significantly to the variability of CO_2 fluxes was recently challenged (*Wang and Moore*, 2012). Here, we present an attempt to unravel the roles of circulation, phytoplankton functional types and total productivity on controlling CO_2 sea-air exchange variability.

5.2 Model

We use the Massachusetts Institute of Technology general circulation model (MITgcm) (*Marshall et al.*, 1997; *MITgcm Group*, 2012). The model is configured globally, but without the Arctic Ocean, on a 2° x (0.38 to 2)° grid. In the Southern Hemisphere, the nominal latitudinal spacing of 2° is scaled by the cosine of the latitude to better resolve the region of interest, namely the Southern Ocean. In addition, we increase the spacing to about half a degree around the equator to resolve the equatorial undercurrent (*Aumont et al.*, 1999). The thickness of 30 vertical layers increases from 10 m at the surface to 500 m below a depth of 3700 m and the bathymetry product of *Timmermann et al.* (2010) is used. A thermodynamic and dynamic sea-ice model (*Losch et al.*, 2010) is coupled to the ocean model. Parameterizations for effects of mesoscale eddies (*Gent and McWilliams*, 1990) and density-driven down-sloping flows on continental shelves (*Campin and Goosse*, 1999) are applied.

The ecosystem and biogeochemistry model REcoM-2 (Regulated Ecosystem Model, version 2; see supplementary information for a detailed model description and equations) with two phytoplankton classes is coupled to the MITgcm. REcoM-2 is based on the *Geider et al.* (1998) model that allows phytoplankton to adapt their stoichiometry to light and temperature conditions and to nutrient supply. Consequently, the ratios of C:N and C:Chl vary in response to different growth conditions. An earlier version of the model (REcoM), with one phytoplankton class, was developed by *Schartau et al.* (2007)

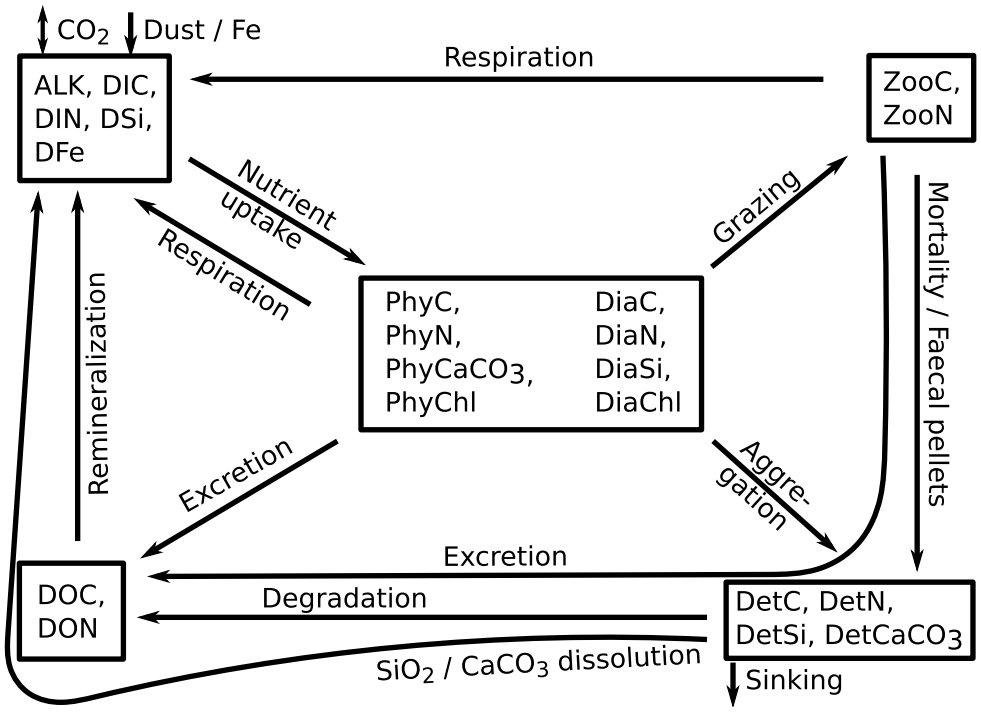

Figure 5.1: Schematic sketch of the ecosystem model REcoM-2. 21 tracers are carried which can be grouped (indicated by boxes) into dissolved nutrients and carbonate system parameters (upper left), phytoplankton (center), zooplankton (upper right), detritus (lower right), and dissolved organic material (lower left). Source and sink terms are depicted by arrows, smaller arrows denote exchange with atmosphere and sediments. Not shown: sediments also release alkalinity, inorganic nutrients and dissolved organic matter.

and extended by *Hohn* (2009). REcoM-2 represents two phytoplankton functional types, namely diatoms (D) and nanophytoplankton (P). Calcium carbonate production in molar units is computed as a function of the gross nanophytoplankton production. The model (Figure 5.1) carries eight phytoplankton tracers (carbon, nitrogen, chlorophyll, calcium carbonate (in P) and silicate (in D) pools). Further tracers are dissolved nutrients (nitrate (DIN), silicate (DSi) and iron (DFe)), dissolved inorganic carbon (DIC) and total alkalinity (TA), detritus with pools of nitrogen, carbon, silicate, iron and calcium carbonate, one type of zooplankton with carbon and nitrogen reservoirs, and dissolved organic nitrogen (DON) and carbon (DOC). Grazing is implemented as a sigmoidal function of prey (*Gentleman et al.*, 2003). The sinking speed for detritus increases vertically (*Kriest and Oschlies*, 2008). REcoM-2 allows for accumulation of sinking material in one single sediment layer. Carbon chemistry and CO_2 fluxes follow the Ocean Carbon Model Intercomparison Project protocols (http://www.ipsl.jussieu.fr/OCMIP/). Gas exchange is parameterized using the *Wanninkhof* (1992) formulation considering chemical enhancement. The effective gas exchange is proportional to the ice-free area in each grid box.

Table 5.1: Overview of performed model runs. Climatological forcing is indicated by *clim* and inter-annually varying forcing by *int*, The letter in brackets denotes daily *(d)* or monthly *(m)* forcing. Forcing with the atmospheric history of CO_2 is marked with *hist*. See section 5.2 for further details.

Acronym	Period	Forcing	Atm CO_2	Dust
Spinup				
S_{ctrl}	1900-1947	CORE (*clim(d)*)	278 ppm	*clim(m)*
S_{var}	1900-1947	CORE (*clim(d)*)	*hist*	*clim(m)*
Experiments				
Ctrl	1948-2010	NCEP (*int(d)*)	278 ppm	*clim(m)* <1978, *int(m)* >1979
Var	1948-2010	NCEP(*int(d)*)	*hist*	*clim(m)* <1978, *int(m)* >1979

The model is initialized with salinity, temperature and nitrate fields from the World Ocean Atlas 2009 (WOA09) (*Locarnini et al.*, 2010; *Antonov et al.*, 2010; *Garcia et al.*, 2010) and with TA and preindustrial DIC fields from GLODAP (*Key et al.*, 2004). The initial field for dissolved iron is from PISCES output (*Aumont et al.*, 2003) with a correction for the Southern Ocean based on observed profiles (*de Baar et al.*, 1999; *Boye et al.*, 2001). Sea surface salinity (SSS) is restored with a time-scale of one year to the Common Ocean-Ice Reference Experiment (CORE) surface salinity field (*Large and Yeager*, 2004).

The model is spun up from 1900 to 1947 (S_{ctrl} and S_{var}, see Table 5.1 for a summary of the different model runs) with climatological forcing from the CORE data set (*Large and Yeager*, 2004). We use daily 10 m winds, 2 m air temperature and humidity, downward long and short wave radiation fields and monthly precipitation, as well as a constant runoff field which we correct for the missing freshwater fluxes from the Arctic by adding 0.08 Sv of runoff evenly spread over the northern boundary of the domain. Wind stress, heat and freshwater fluxes are calculated using bulk formulae (*Large and Yeager*, 2004). The freshwater and salinity balances are maintained globally by a normalization procedure (*Griffies et al.*, 2009).

The period from 1948 to 2010 is simulated (Var and Ctrl) using daily forcing fields from the NCEP/NCAR-R1 data product (*Kalnay et al.*, 1996, updated 2011), except for the runoff field which is kept as in the spin-up. We obtained monthly dust data for 1979 to 2010 from Natalie Mahowald, based on *Mahowald et al.* (2003), but with the bins being reapportioned to match those suggested by Jasper Kok (personal communication to N. Mahowald, 2011), to sustain a closer agreement with observations (e.g., *Wagener et al.*,

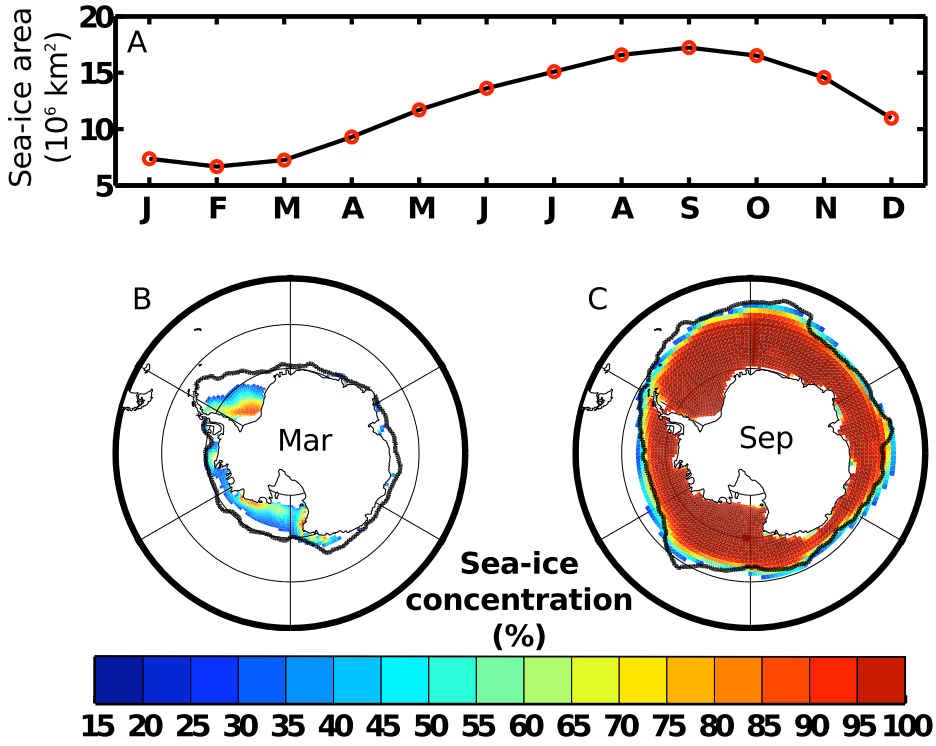

Figure 5.2: Modeled sea-ice extend. (a) Mean seasonal cycle of sea-ice area between 1979 and 2010. Sea-ice concentration (%) in (b) March and in (c) September, at the maximum of sea-ice area. Modeled sea-ice area is shown above 15%, the black solid line marks the corresponding 15% isoline from satellite data for comparison.

2008). Dust is deposited according to the monthly climatology (1979 to 2010) until model year 1978, and on a monthly basis from 1979 onwards.

The spin-up (1900 to 1947, S_{var}) and the inter-annually varying run (1948-2010, Var) are forced with atmospheric CO_2 concentrations from *Enting et al.* (1994) until 1958, and from the Mauna Loa observatory data from 1959 onwards (ftp://ftp.cmdl.noaa.gov/ccg/co2/trends/co2_mm_mlo.txt). A control run, covering the spin-up (S_{ctrl}) and the inter-annually forced periods (Ctrl), is performed with a constant preindustrial atmospheric CO_2 concentration of 278 ppm to differentiate between natural and anthropogenic carbon fluxes.

5.3 Results: mean model state

5.3.1 Southern Ocean circulation and sea-ice dynamics

Sea-ice forms an interface between ocean and atmosphere. A reliable representation of sea ice is important for the study of CO_2 fluxes between ocean and atmosphere. With

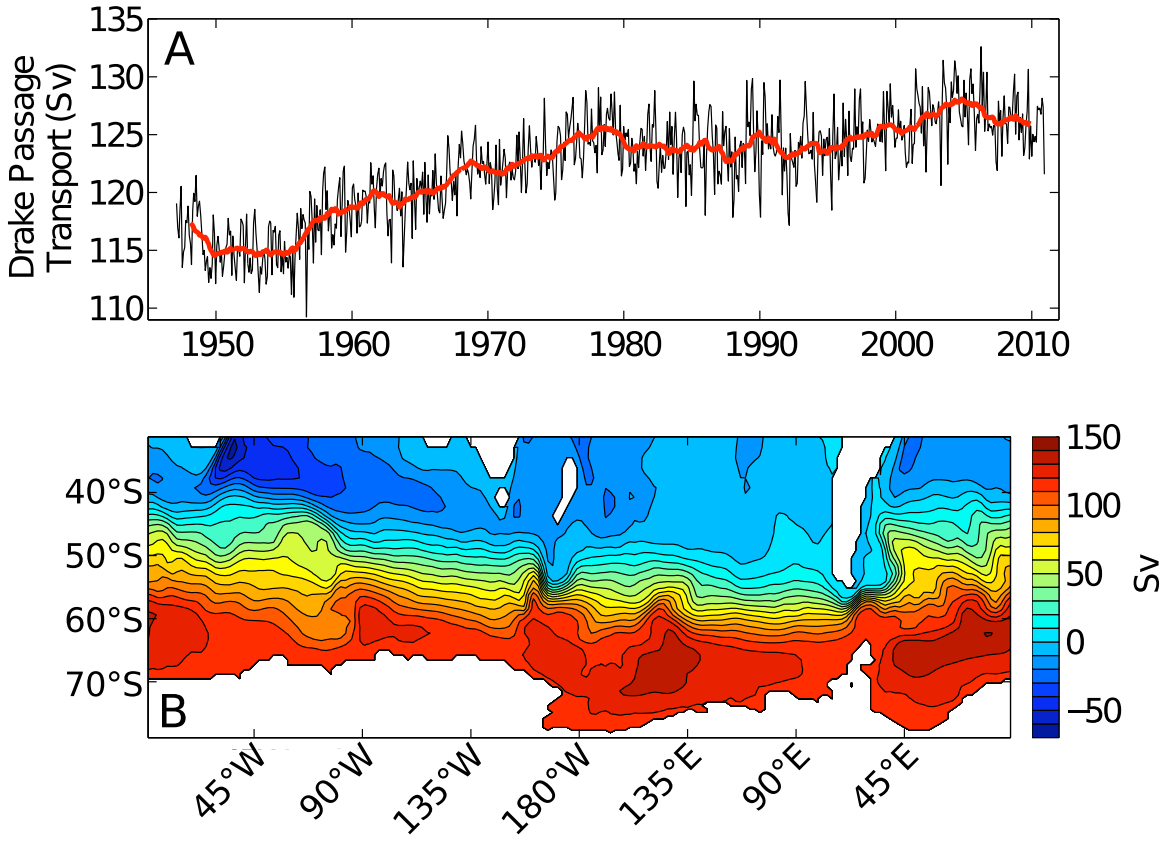

Figure 5.3: Modeled Southern Ocean circulation. (a) Time-series of Drake Passage transport (Sv), black: monthly average, red: running mean over two years, (b) Mean barotropic stream-function (Sv) between 1948 and 2010.

our model set-up we reproduce a reasonable seasonal sea-ice distribution in the Southern Hemisphere (Figure 5.2). The minimum sea-ice extent (averaged over the period 1979 to 2010 to be comparable with observations) occurs in February; the maximum is found in September. Timing and magnitude are in line with passive microwave satellite data (*Cavalieri and Parkinson*, 2008), although the sea-ice extent at its minimum is lower than in observations. Other studies suggest that the realism of the simulated sea-ice fields depends on the resolution of the model grid (e.g., *Losch et al.*, 2010). In our simulation, the annual mean of the total sea-ice area varies between 1.2 and 1.3 x 10^{13} m^2 which compares well to the estimate of about 10^{13} m^2 (*Comiso*, 1999; *Griffies et al.*, 2009) and is similar to the performance of other coarse grid ocean-ice models (*Griffies et al.*, 2009).

In the period with inter-annually varying forcing, the monthly, vertically integrated zonal flow through Drake Passage fluctuates between 109 and 133 Sv which is within the lower part of the range of transport estimated from observations (*Cunningham et al.*, 2003; *Orsi et al.*, 1995; *Whitworth*, 1983; *Whitworth and Peterson*, 1985). In our simulation, the ACC transport shows a weak positive trend between 1955 and 1975, followed by a

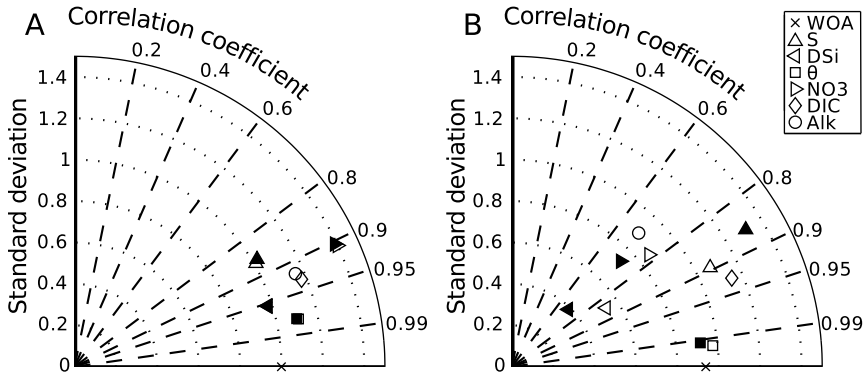

Figure 5.4: Taylor diagrams comparing model salinity, temperature, nitrate and silicate fields to World Ocean Atlas 09 data, and DIC and alkalinity fields to GLODAP. Annual average (open symbols) and mean seasonal cycle (filled symbols) were calculated for the domain south of 30°S and the period 1948 to 2010. The standard deviation is normalized to the standard deviation of the reference data. (a) 3D fields of the entire water column <30°S weighted by volume, (b) 2D surface field <30°S weighted by area.

period of relative stability (Figure 5.3a). Thus, the Drake Passage transport in our model appears to be sufficiently stable and realistic over the study period (1948-2010). The barotropic stream function (Figure 5.3b) with the typical southeastward route from the western Atlantic to the Eastern Pacific and the northward expansion east of the Drake Passage also agrees with other simulations (e.g., *Griffies et al.*, 2009).

The model agreement with WOA09 data is within an expected range for both mean annual and seasonal 3D fields of potential temperature, salinity, nitrate and silicate (south of 30°S, Figure 5.4a). When the total water column is considered, all correlation coefficients are better than 0.86 for both annual average and mean seasonal cycle. The standard deviations of modeled salinity and silicate are close to the standard deviations in WOA09, the standard deviations of potential temperature, alkalinity and DIC are between 10% and 20% and nitrate by about 40% higher than in the observations. A higher standard deviation in the model indicates that gradients are overestimated.

In the surface layer, differences between annual average and seasonal fields become obvious. Potential temperature is very well reproduced because of the atmospheric forcing. Alkalinity, nitrate and silicate have correlation coefficients around 0.8 and normalized standard deviations <1, i.e. gradients are underestimated. Salinity and DIC have correlation coefficients around 0.9 and normalized standard deviations >1. The seasonal signals of silicate and nitrate have lower normalized standard deviations than the annual average, indicating that the seasonal cycle is too weak in the model. The opposite can be observed for salinity, where the standard deviation of the annual average is only 10% higher than in the data; this is in contrast to an overestimation of the variability by 35%

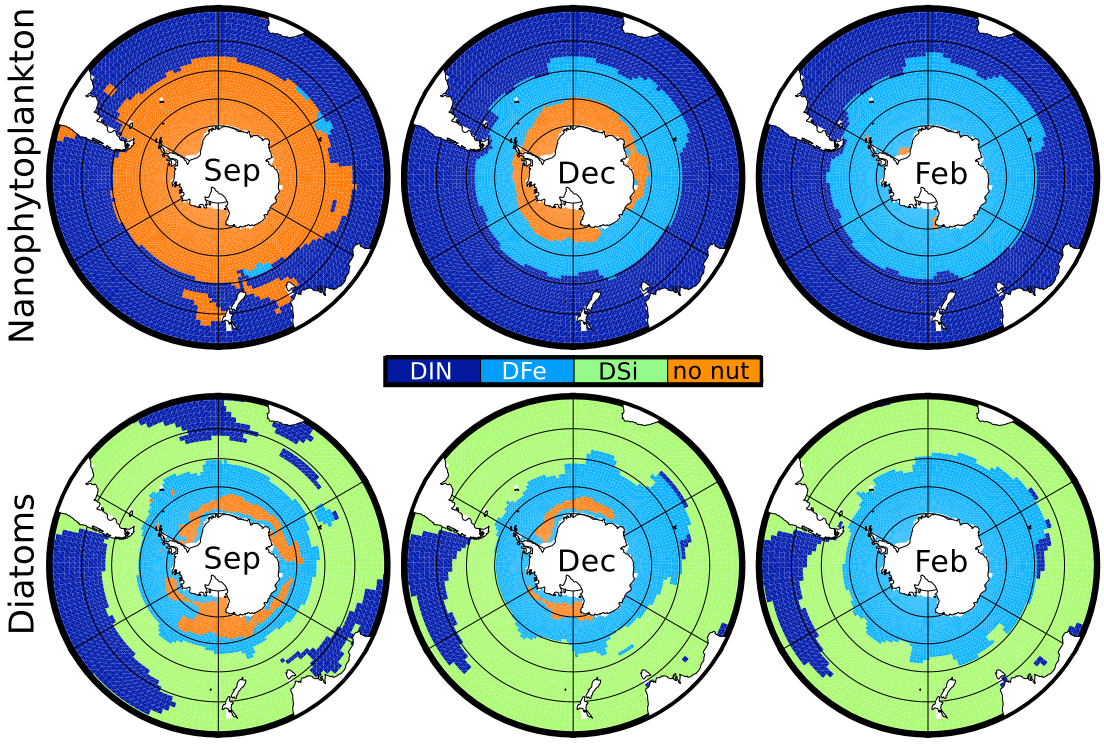

Figure 5.5: Most limiting factors for (top row) nanophytoplankton and (bottom row) diatom growth in (from left to right) spring (September), summer (December) and autumn (February): nitrate (dark blue), iron (light blue), silicate (green), light/temperature/grazing (orange). When no nutrient is limiting with a Michaelis Menten coefficient below 0.7, we assume that light, temperature (and grazing for nanophytoplankton) are limiting (*Schneider et al.*, 2008). See text for further explanation.

in the seasonal cycle. As the model was initialized with fields from this climatology, this demonstrates that the model represents the processes that determine nutrient distribution (i.e., biological production and remineralization) reasonably well, that the model drift is small over the short period considered, and that appropriate boundary conditions for heat and freshwater fluxes are applied.

5.3.2 Phytoplankton growth limitation and distribution

We determine the factors limiting phytoplankton nutrient uptake from the Michaelis-Menten factors (f_i) relating concentration of nutrient i (N_i) to the sum of N_i and the corresponding half saturation constant (K_i): $f_i = N_i/(K_i + N_i)$. The smallest Michaelis-Menten factor f_i indicates the most limiting nutrient. In the case that all nutrients (nitrate, silicate, iron) yield a Michaelis-Menten factor above 0.7, light, temperature or grazing or a combination of those are supposed to control phytoplankton growth or accumulation (*Schneider et al.*, 2008). Small phytoplankton growth north of 50°S is limited by macronu-

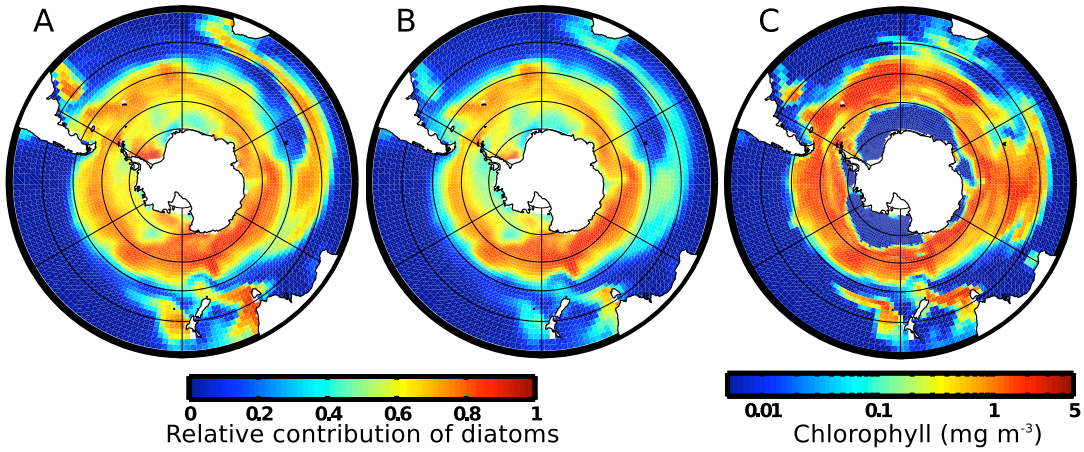

Figure 5.6: Relative contribution (mean of model years 1948 to 2010) of diatoms to surface (a) chlorophyll and (b) phytoplankton carbon (0 = 0%, 1 = 100%). (c) Surface diatom chlorophyll averaged over October and November 2005 to be comparable to *Bracher et al.* (2009).

trients, in our model represented by nitrate, throughout the year (Figure 5.5). South of 50°S, small phytoplankton is not limited by nutrients between May and October; light likely plays an important role during winter. In November, iron limitation sets in as irradiance increases. Diatoms are mostly limited by iron south of 50 to 60°S and by silicate to the north of that. The shift from iron to silicate limitation for diatom growth occurs approximately north of 60°S in the Pacific sector. It takes place further north, between 50 and 60°S in the Indian and Atlantic sectors. Light limitation dominates in few areas between June and December. In the Southern Ocean, which is a high nutrient-low chlorophyll (HNLC) region (*de Baar et al.*, 1990; *Boyd et al.*, 2000), our model reproduces the crucial role of iron limitation. Our simulations indicate silicate limitation for diatoms north of the PF in agreement with observations (*Jacques*, 1983; *Boyd et al.*, 1999).

Diatoms dominate phytoplankton biomass and chlorophyll south of 50 to 60°S (Figure 5.6). Their contribution to standing stocks in terms of carbon and chlorophyll is reduced to less than 20% north of that limit in agreement with observations (*de Baar et al.*, 1999). The Indian sector and the continental margins are exceptions to that rule; here, diatoms can be responsible for up to 50% of the biomass north of 50°S (Figure 5.6b). These exceptional maxima were attributed to intensified iron deposition from dust (*Aumont et al.*, 2003). Diatom chlorophyll (Figure 5.6c) shows the same gradient from low chlorophyll north of about 50°S to high chlorophyll between 50°S and 60°S as in satellite-derived estimates (*Bracher et al.*, 2009).

The zonal averaged vertically integrated net primary production (NPP, Figure 5.7) follows the same pattern as satellite-based estimates (*Behrenfeld and Falkowski*, 1997; *Westberry et al.*, 2008). In the Southern Ocean, there are two peaks. The first peak is

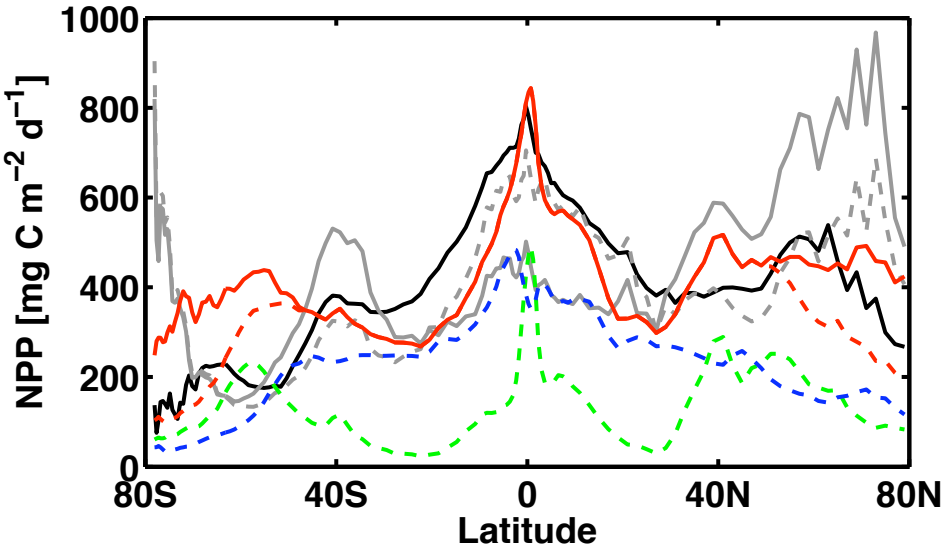

Figure 5.7: Vertically integrated net primary production in mg C m^{-2} d^{-1}. VGPM (gray line) and Eppley (gray dashed line) are chlorophyll-based satellite-derived estimates (*Behrenfeld and Falkowski*, 1997), CBPM (black line) is a chlorophyll and carbon-based satellite-dervied estimate and is considered a significant improvement to VGPM and Eppley (*Westberry et al.*, 2008). The model output (red dashed line) is biased (red line) to cover the same time as the satellite-based estimates. Also shown are the contributions of diatoms (green dashed line) and nanophytoplankton (blue dashed line).

around 40°S, and is dominated by nanophytoplankton in the model. The second peak occurs in the model and in the 'chlorophyll and carbon-based' satellite estimate (CBPM, *Westberry et al.* (2008)) at around 60°S and is dominated by diatoms. It is followed by a decrease further to the south. In the two 'chlorophyll-based' satellite derived estimates (VGPM and Eppley, *Behrenfeld and Falkowski* (1997)), there is just one peak in NPP between about 60°S and the southern end of the domain. The CBPM algorithm to derive net primary production is considered a significant improvement compared to VGPM and Eppley, as it consciously takes account of the decoupling of carbon and chlorophyll and is validated against field data (*Westberry et al.*, 2008). Thus, we argue that the increase towards 80°S represent an overestimation by the VGPM and Eppley products. The model estimate of the diatom belt around 60°S, however, is higher than in all satellite-based estimates and reaches somewhat further north. This might be an artifact of known underestimation of SeaWiFS chlorophyll by 50% in the Southern Ocean (*Szeto et al.*, 2011), but might also indicate a model bias. The model POC export at 100 m south of 30°S is 3.5 Pg C yr^{-1}, in line with the estimate of *Schlitzer* (2002).

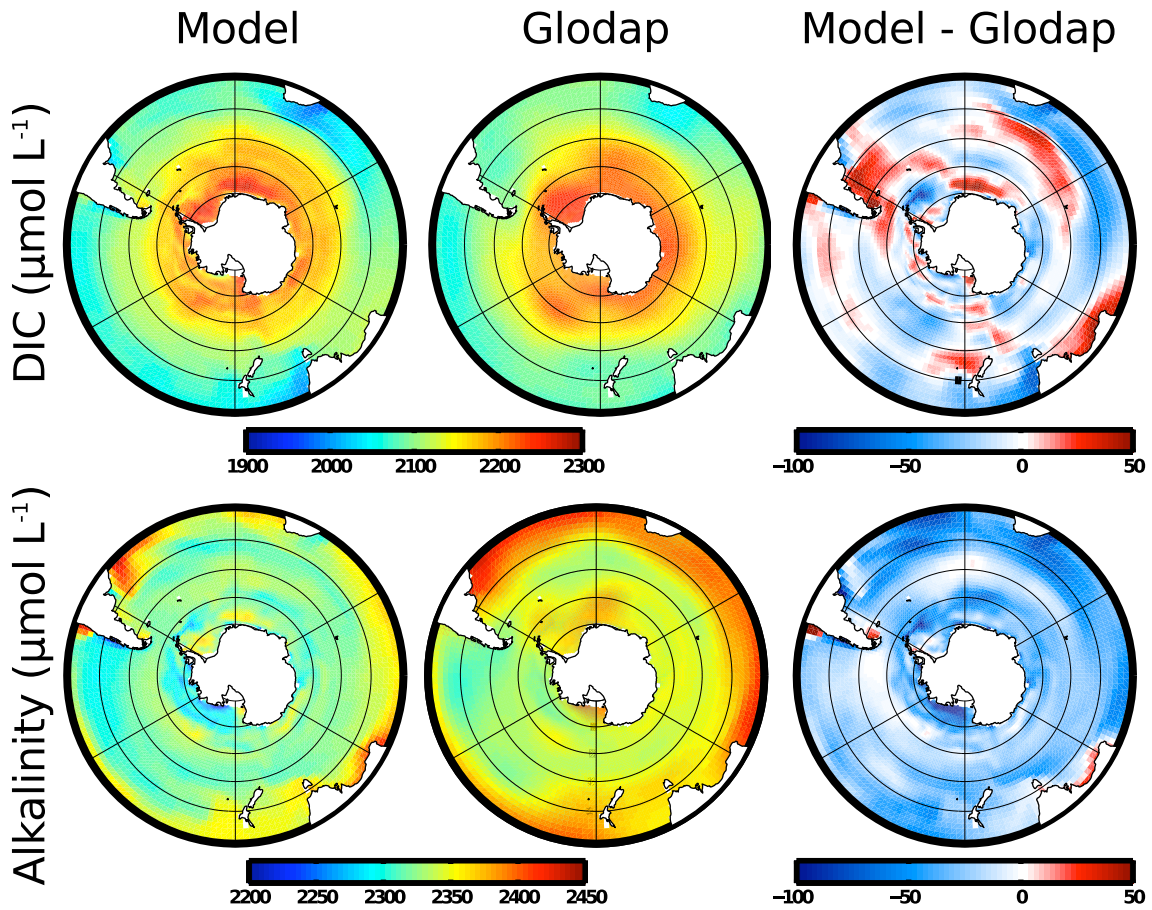

Figure 5.8: Model-data comparison of DIC and alkalinity in the nominal year 2004, all in μmol L^{-1}. Only summer data (January to March and October to December) are used as GLODAP is also biased towards summer. The top row shows DIC, and the bottom row alkalinity. The first column shows model results, the middle column GLODAP and the right column shows the difference (model minus GLODAP).

5.3.3 Contemporary carbonate system

The surface distributions of DIC and TA (Figure 5.8) determine the partial pressure of CO_2 in seawater and by that the CO_2 exchange with the atmosphere. DIC is controlled by advection and diffusion, by sea-air gas exchange, drawdown by primary production, release during respiration and remineralization and by $CaCO_3$ production and dissolution. The reproduction of spatial patterns of DIC compares with GLODAP for the full water column and the surface as seen in the Taylor plots (Figure 5.4). The model captures the DIC gradient from high values close to the continent to lower values further to the north (Figure 5.8), however over- and underestimation occurs regionally. Modeled surface DIC for summer 2004 (GLODAP period) is on average 9.6 μmol L^{-1} too low, which is mostly noise, but might also be biased by the systematic offset of surface TA (as explained

below).

Model surface TA is lower than actually observed in most of the Southern Ocean (Figure 5.8), on average by 30.2 μmol L^{-1} in summer 2004. This can be explained by the loss of alkalinity from the surface layer by calcification (global net calcification is 0.8 Pg C yr^{-1}) and the lack of shallow remineralization. $CaCO_3$ dissolution is computed following a simple approach using a prescribed $CaCO_3$ profile (*Yamanaka and Tajika*, 1996). Moreover, modeled $CaCO_3$ is treated as calcite, but in reality a part is aragonite which dissolves shallower than calcite. In addition, shallow remineralization processes, such as dissolution due to bacterial activity in faecal pellets are not considered in the model as they are still poorly quantified. Therefore, the transport of alkalinity to the deep ocean is too strong, leading to low surface alkalinity in the simulation, especially outside the diatom belt where calcifiers contribute significantly to the total production.

By and large, we present a model set-up that simulates Southern Ocean circulation processes, thermodynamics and core biological processes with satisfactory realism. It is appropriate for the study of carbon fluxes that are controlled by a complex interplay of thermal effects, wind forcing, circulation patterns and biological interaction. The bias in alkalinity is a weakness of the current state of the model; however, we do not draw our conclusions from the mean state of the simulations, but from the changes and shifts in carbon fluxes, for which the alkalinity field is not decisive.

5.4 Inter-annual variability

In the following, the term "natural" CO_2 flux refers to the model run with preindustrial atmospheric CO_2 forcing in contrast to "anthropogenic" CO_2, which is defined as the difference between the model runs with preindustrial and contemporary CO_2 forcing. Yet, the "natural" CO_2 flux is also affected by anthropogenic activities, as the contemporary wind forcing is applied, which has changed since preindustrial times due to the ozone hole and greenhouse gas emissions. The contemporary CO_2 flux variability south of 30°S, determined as one standard deviation in CO_2 flux anomalies (detrended and deseasonalized) is 0.19 Pg C yr^{-1} and is mainly caused by natural CO_2 flux variability (0.17 Pg C yr^{-1}). The magnitude of variability agrees with *Lovenduski et al.* (2007), but is higher than in previous model studies (*Peylin et al.*, 2005; *Wetzel et al.*, 2005). Anthropogenic CO_2 flux variability is smaller (0.07 Pg C yr^{-1}). The patterns of the detrended SAM index show similarities to the natural and contemporary CO_2 flux anomalies (Figure 5.9). In the following, we investigate the influence of the SAM on the inter-annual variability of the Southern Ocean physics, ecosystem and carbon fluxes. We base our analysis on the Ctrl run with inter-annually varying forcing and constant preindustrial atmospheric CO_2 to

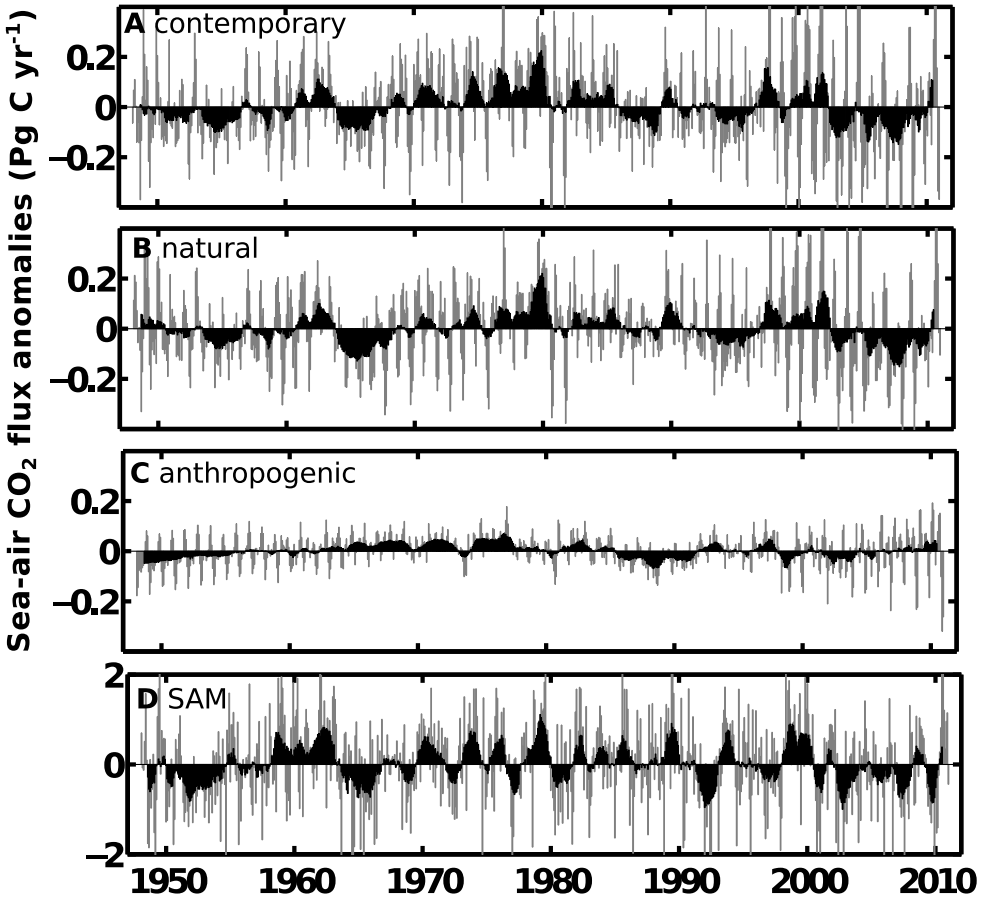

Figure 5.9: Detrended and deseasonalized CO_2 flux anomalies (Pg C yr^{-1}) for (a) contemporary, (b) natural and (c) anthropogenic CO_2 fluxes south of 30°S. Positive anomalies indicate more outgassing or less uptake than in the long-term average. Also shown is (d) the detrended SAM index from the NCEP-NCAR Reanalysis (http://jisao.washington.edu/data/aao/slp).

analyze the inter-annual variability induced by changing climate rather than the trend in anthropogenic CO_2 uptake.

We regress deseasonalized anomalies of state variables and carbon fluxes to the SAM index considering a lag of zero to twelve months. Results are presented at zero lag for physics and with a lag of four months for nutrients, primary production and carbon fluxes. We use the SAM index from 1948 to 2010 based on the leading principal component of sea-level pressure anomalies south of 20°S from the NCEP-NCAR Reanalysis (http://jisao.washington.edu/data/aao/slp). The SAM index is standardized to the period 1979 to 2010 with a mean of zero and a standard deviation of one. We apply a running eight month mean filter to smooth the SAM index.

5.4.1 Response of Southern Ocean physics to SAM

The patterns in sea surface temperature (SST) variability, as depicted by a regression of SST onto the SAM index and corresponding correlation coefficient (Figure 5.10) agree with satellite-based observations (*Lovenduski and Gruber*, 2005). Regions of decreasing temperature are found in the Antarctic and Polar Frontal Zones in the Pacific and Indian Ocean sectors and extend to the Subtropical Zone in the Pacific. In contrast, temperature increases around the Antarctic Peninsula, in parts of the Ross, Weddell and Prydz Bay Gyres and in the entire Subtropical Zone with the single exception of a cold tongue in the Pacific. The temperature response is strongest at zero lag.

The mixed layer depth, calculated using a density criterion (*Kara et al.*, 2000), deepens in a broad band around the Polar Front, and shoals along the Antarctic coast with an increasing SAM index (shown for zero lag in Figure 5.10). An exception is the east Pacific sector, where the mixed layer depth becomes shallower everywhere between the continents and across the Subantarctic Front. The general pattern of mixed layer depth variability is consistent with the inference of increased mixed layer depths north of the PF by *Lovenduski and Gruber* (2005). The boundary line between shoaling and deepening, however, appears further south in the Atlantic and Indian basins in our model.

Changes in upwelling and northward Ekman transport will be discussed in terms of carbon transport in section 5.4.3.

5.4.2 Response of nutrients and biological production to SAM

The response of surface silicate (Figure 5.10) and nitrate (not shown) to a positive SAM event is restricted to the Southern Ocean south of the PF and is largest at a lag of four months. The additional silicate and nitrate seems to be used up before it can be advected further north. The change of silicate concentration as response to the SAM ranges from -9.9 mmol m^{-3} to 12.9 mmol m^{-3}; on average silicate increases by 0.7 mmol m^{-3} south of 50°S. The change in nitrate concentration during positive SAM ranges from -1.1 mmol m^{-3} to 2 mmol m^{-3} and averages 0.7 mmol m^{-3} south of 50°S. The surface iron concentration increases south of the PF, the exceptions being the central Ross and Weddell Gyres and the coastal western Antarctic Peninsula (Figure 5.10). North of the PF, iron increases in the Atlantic sector, in a band south of 40°S in the Indian sector and between the South American continent and 120°W in the Pacific sector. The increase of DFe during positive SAM is between 0 and 0.05 μmol m^{-3} in about 70% of the area. On average, iron increases by 0.009 μmol m^{-3} south of 50°S and by 0.01 μmol m^{-3} south of 30°S. The increase of iron north of the Polar Front might be explained by advective iron loss from south of the Polar Front. The entrainment of iron from deeper water masses into the mixed layer is

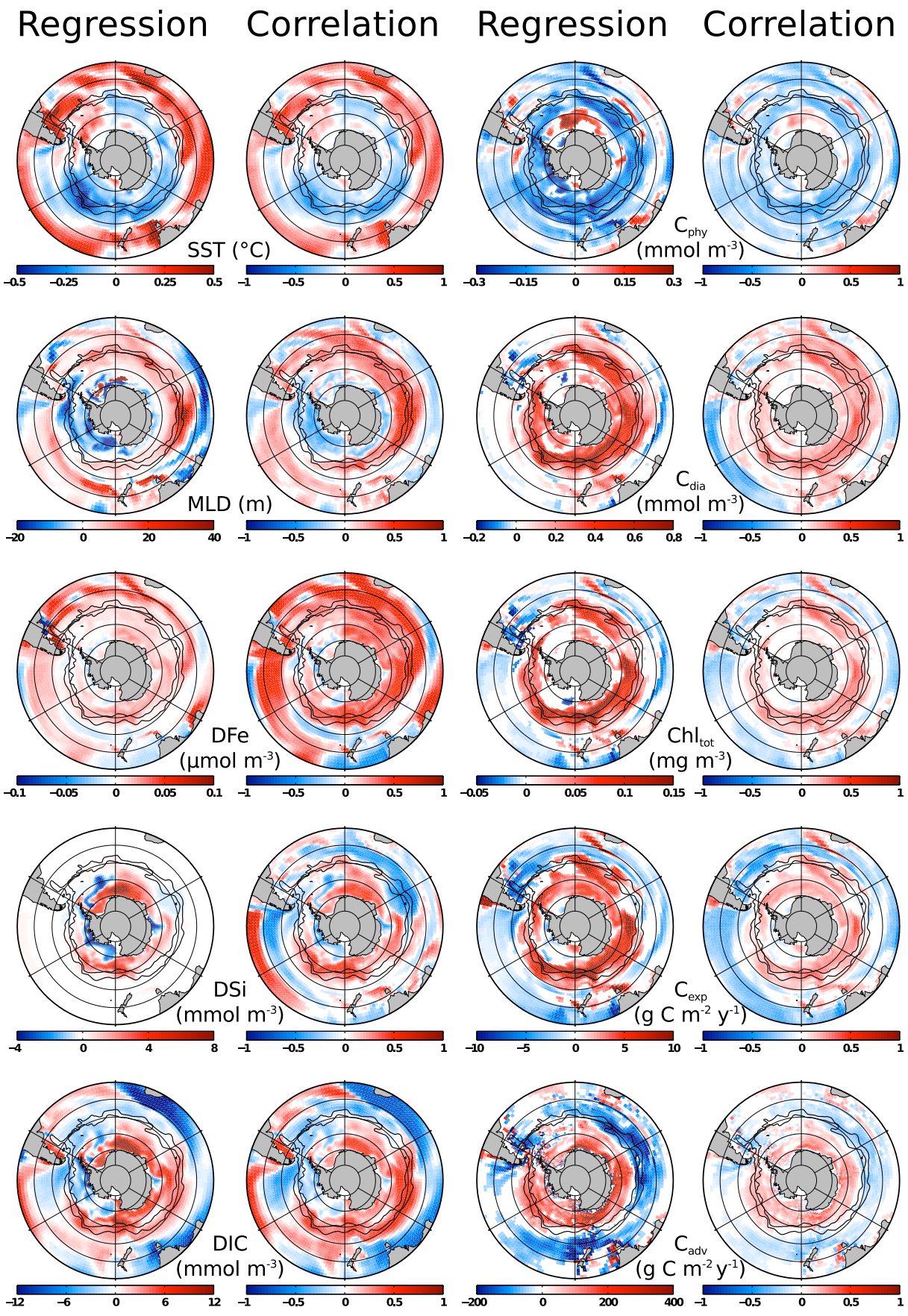
Regression
Correlation
Regression
Correlation
SST (°C)
−0.5 −0.25 0 0.25 0.5
−1 −0.5 0 0.5 1
C_phy (mmol m^-3)
−0.3 −0.15 0 0.15 0.3
−1 −0.5 0 0.5 1
MLD (m)
−20 0 20 40
−1 −0.5 0 0.5 1
C_dia (mmol m^-3)
−0.2 0 0.2 0.4 0.6 0.8
−1 −0.5 0 0.5 1
DFe (µmol m^-3)
−0.1 −0.05 0 0.05 0.1
−1 −0.5 0 0.5 1
Chl_tot (mg m^-3)
−0.05 0 0.05 0.1 0.15
−1 −0.5 0 0.5 1
DSi (mmol m^-3)
−4 0 4 8
−1 −0.5 0 0.5 1
C_exp (g C m^-2 y^-1)
−10 −5 0 5 10
−1 −0.5 0 0.5 1
DIC (mmol m^-3)
−12 −6 0 6 12
−1 −0.5 0 0.5 1
C_adv (g C m^-2 y^-1)
−200 0 200 400
−1 −0.5 0 0.5 1

Figure 5.10: Regression and correlation of state variables and carbon fluxes from the Ctrl run (inter-annual forcing and preindustrial atmospheric CO_2) onto the SAM index. Regression (first and third column) and correlation (second and fourth column) coefficients of variables as indicated in the figures. Shown are regressions of sea surface temperature (SST), mixed layer depth (MLD), dissolved iron (DFe), dissolved silicate (DSi), dissolved inorganic carbon (DIC), small phytoplankton carbon (C_{phy}), diatom carbon (C_{dia}), total chlorophyll (Chl_{tot}), POC export at 100 m (C_{exp}) and upward advection of DIC at 100 m (C_{adv}) onto SAM with no lag for potential temperature and mixed layer depth and with a four months lag for nutrients, phytoplankton and carbon. White areas indicate no trend or no significant correlation at the 95% confidence level. Lines show, from north to south, Subantarctic Front and Polar Front from *Orsi et al.* (1995).

the main source for iron in the Southern Ocean (*Hoppema et al.*, 2003). It mainly occurs in autumn and winter, but at least a quarter of that iron is transported to the north before it can be used up by phytoplankton in spring and summer (*Hoppema et al.*, 2003).

We see a general decrease of nanophytoplankton carbon biomass during positive SAM, with the Weddell Sea as the main exception (Figure 5.10). Diatoms thrive everywhere in and south of the ACC except the central Weddell Gyre. As they dominate the phytoplankton assemblage, this leads to an overall positive response of total chlorophyll; chlorophyll anomalies are positively correlated with SAM anomalies except at some spots of the Weddell and Ross Gyres. The chlorophyll regression to SAM from satellite data (*Lovenduski and Gruber*, 2005) shows a mixed picture. *Lovenduski and Gruber* (2005) conclude that an increase of chlorophyll south of the Polar Front is induced by increased iron supply from below, whereas the reduction of chlorophyll north of the PF is caused by an increased mixed layer depth. In our model, the increase of the mixed layer depth is not restricted to north of the PF, indeed it appears between ca. 60°S and 40°S in the Atlantic, Indian and west Pacific sectors and north of 50°S in the east Pacific sector. We find the same correlation pattern of chlorophyll, but areas of iron increase and MLD deepening overlap. At a first glance, it seems arbitrary to relate the chlorophyll increase south of the PF to additional iron and the chlorophyll decrease north of the PF to a deeper mixed layer as both processes (more iron, deeper mixed layer) occur south and north of the PF. It is evident, though, that iron limitation controls phytoplankton growth only south of the PF in our model (Figure 5.5). Increased iron supply can enhance primary production in this area and seems to play a more important role than the reduced light due to the deepening of the mixed layer. North of the PF, the combined factors of persistent silicate and DIN limitation and deeper mixed layer are likely responsible for the observed reduction of total carbon biomass and chlorophyll (Figure 5.10)

In high nutrient-low chlorophyll regions (HNLC), such as the Southern Ocean south of the Polar Front, the larger diatoms are able to increase their biomass when iron becomes

available (*de Baar et al.*, 2008). This is consistent with the modeled diatoms' response during positive SAM events. In the simulation, this response is caused by higher growth rates when iron limitation is reduced. In reality, the response might be a combination of increased growth rate of diatoms and increased grazing pressure on small phytoplankton.

Other studies explored the future role of diatoms and small phytoplankton in a changing climate and found a reduction of diatom abundance in high latitudes (*Bopp et al.*, 2005; *Marinov et al.*, 2010). This is based on the assumption that the oceans will be more stratified in a warmer climate, which would lead to less nutrient supply. The hypothesis that the oceans will be less mixed in a warmer climate has been challenged (*Russell et al.*, 2006; *Toggweiler and Russell*, 2008) and an intensification of the subpolar westerlies has been observed over the last decades (*Thompson and Solomon*, 2002). It is unclear which level of mixing will be reached under the combined forcing of the warming itself and stronger winds. Nonetheless, our result that less stratification leads to more nutrients and diatom abundance is in line with the arguments of *Bopp et al.* (2005) and *Marinov et al.* (2010) that stronger stratification leads to a decline of nutrients and diatoms. This principle can be applied to better predictions of future mixing when they become available.

5.4.3 Response of carbon fluxes to SAM

The vertical DIC transport anomalies by advection at 100 m are divided into positive anomalies (more upward advection) in the south and negative anomalies (more downward advection) in the northern part of the Southern Ocean (all reported as regressed onto the SAM index with a four months lag in Figure 5.10). On the other hand, the stronger upwelling and entrainment of deep water increases nutrient concentrations and causes elevated diatom and total phytoplankton production south of the Polar Front. As a result, more particulate organic carbon sinks out of the surface layer (Figure 5.10). This drawdown of carbon by raised primary production reduces seawater $p\mathrm{CO}_2$ and counteracts the DIC addition by circulation changes. The change of the CO_2 flux is the residual of circulation and primary production changes.

To assess the importance of the individual carbon fluxes, their effects on the 100 m DIC budget is calculated, similar to *Lovenduski et al.* (2007). The terms J'_{Gasex}, J'_{Bio}, J'_{adv-v} and J'_{adv-h} all describe carbon flux anomalies as regressed onto the SAM index with a four months lag and are integrated over the 100 m surface layer. J'_{bio} accounts for anomalies with respect to the export flux of detritus carbon and detritus CaCO_3 across the 100 m horizon. J'_{Gasex} denotes tendencies in gas-exchange and J'$_{adv-v}$ denotes changes in the vertical advection of DIC across the 100 m horizon. J'_{adv-h} is defined as the divergence of horizontal DIC advection in the 100 m surface layer. The results are

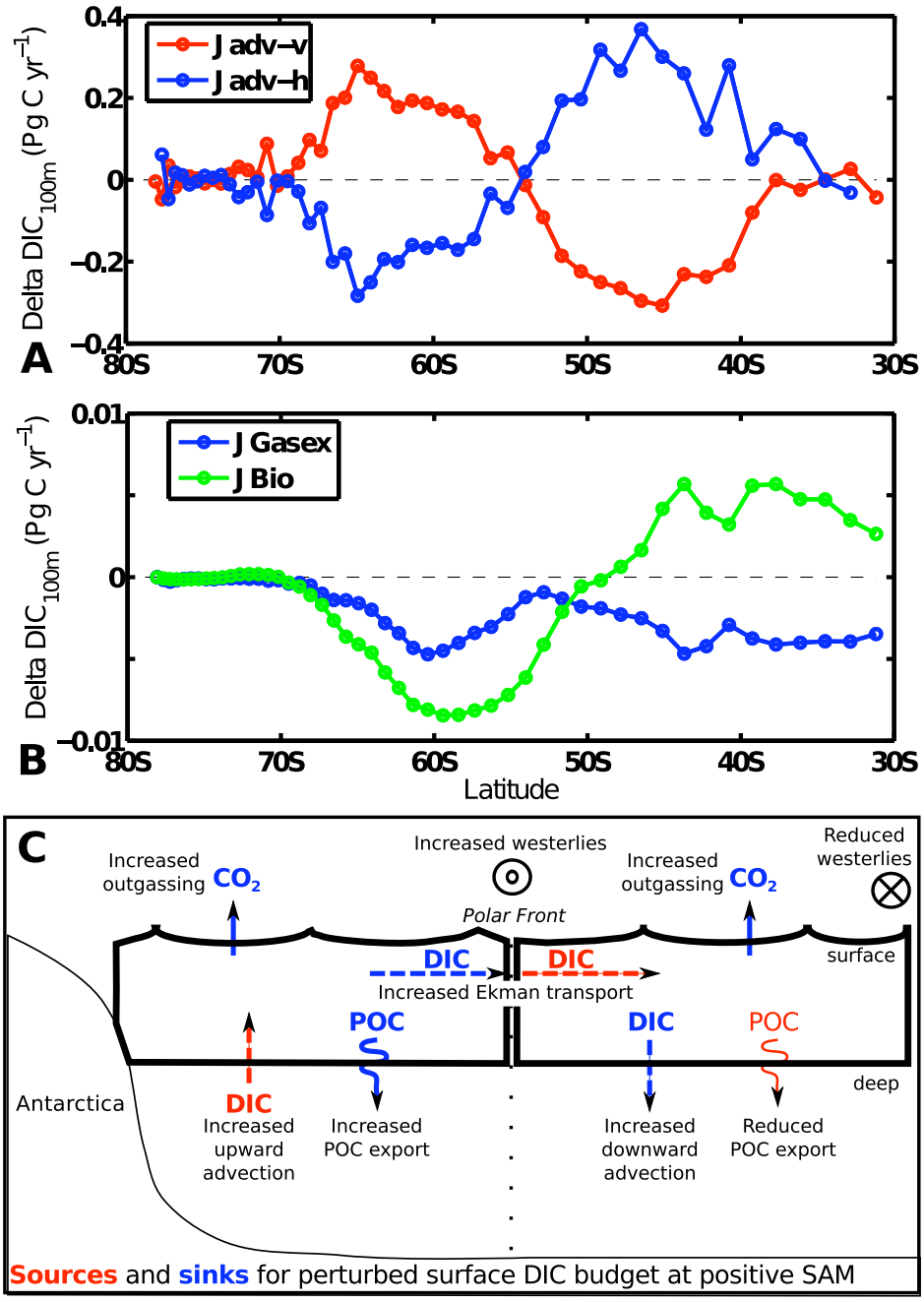

Figure 5.11: Perturbation of natural carbon fluxes in the surface Southern Ocean (100 m) related to an increase of one unit in the standardized SAM index. Negative fluxes indicate a sink for the surface DIC inventory. (a) Contribution of vertical advection (J adv-v) and of divergence of horizontal advection (J adv-h). (b) Contribution of biology (J Bio, green) and sea-air CO_2 exchange (J Gasex, blue, negative = outgassing). (c) Idealized sketch of the perturbed carbon fluxes (red = source, blue = sink for surface DIC inventory).

presented in Figure 5.11a and b as the zonal mean of the tendencies, multiplied by the volume of the 100 m layer at this latitude.

Vertical advection anomalies increase the surface DIC inventory in the south and decrease it north of the Polar Front, so that a similar amount of carbon that is transported into the surface layer in the south is exported to deeper layers in the north. The DIC flux anomalies by horizontal advection nearly balance the vertical advection anomalies (Figure 5.11a), suggesting that stronger Ekman transport links upwelling/entrainment of carbon-rich water in the south and downwelling in the north. The DIC budget of transport anomalies, however, is not closed as the horizontal transport takes time; hence the surface DIC builds up (Figure 5.10) and affects the pCO_2 gradient between ocean and atmosphere.

The DIC changes due to stronger upwelling and entrainment south of the Polar Front and intensified downwelling north of the Polar Front are one order of magnitude larger than the changes in carbon export (Figure 5.10 and 5.11b) and outgassing (Figure 5.11b). The DIC increase by upwelling in the south, however, is nearly balanced by the transport to the north; and north of the Polar Front, the intensified northward DIC transport is nearly balanced by more downwelling. The large additional DIC input by vertical advection south of the PF therefore results in sea-air CO_2 flux changes that might appear to be small. They are, nevertheless, significant and of notable magnitude compared to the annual Southern Ocean CO_2 uptake.

South of ca. 50°S, changes in upwelling/entrainment tend to increase DIC, but are largely offset by stronger northward advection, increased carbon export and outgassing of CO_2. Interestingly, the increase in carbon export, which is attributable to diatoms, has a larger effect than the outgassing of CO_2. North of the Polar Front, export production is reduced and increases the carbon inventory in the surface layer; it is, however, nearly balanced by stronger natural carbon outgassing. Here, the biological carbon pump is weakened and cannot mitigate outgassing, while it clearly reduces potential outgassing south of the Polar Front. We find that biology plays an important role for inter-annually varying carbon fluxes, in contrast to *Lovenduski et al.* (2007), and in agreement with *Wang and Moore* (2012). The total effect of stronger natural carbon outgassing, integrated over the entire Southern Ocean amounts to 0.09 Pg C yr^{-1}, which is the same as found in previous studies (*Lovenduski et al.*, 2007; *Lenton and Matear*, 2007; *Dufour*, 2011). Biology contributes to an additional drawdown of 0.05 Pg C yr^{-1}.

5.5 Concluding remarks

We could reproduce observed patterns in temperature and chlorophyll response to a positive SAM using a 3-dimensional general circulation model and a state-of-the-art ecosystem model. This is the first study, to the best of our knowledge, that simultaneously quantifies changes in the natural carbon budget due to altered carbon transport and primary production. We found that the surface Southern Ocean carbon budget during the positive phase of the SAM is driven by different processes north and south of the PF (Figure 5.11c). In the southern region, the only source to the changed DIC inventory associated with a positive SAM is the stronger upwelling and entrainment of DIC. Intensification of northward Ekman transport, POC export and outgassing of natural CO_2 act as DIC sinks for that region. In the northern part, the DIC inventory is enriched by more surface inflow of carbon-rich water from the south and by reduced POC export. More natural CO_2 outgassing and downwelling act as sinks for the perturbed DIC budget.

We showed that the biological carbon pump plays an important role in the response to the SAM; more carbon is lost from the surface inventory by export of organic carbon than by natural CO_2 outgassing south of the Polar Front.

Lenton et al. (2009) hypothesized that iron supply during positive SAM induces changes in the C:Chl ratio that could explain the increase in chlorophyll (*Lovenduski and Gruber*, 2005) and argued for a weak response by primary production. Our model allows for acclimation of cellular stoichiometry (N:C:Chl:Si for diatoms and N:C:Chl for non-diatoms) to light and nutrient conditions and we could show that both carbon and chlorophyll increase during positive SAM in contrast to the hypothesis by *Lenton et al.* (2009).

Our model has the caveat that it does not resolve eddies that were suggested to counteract the stronger northward Ekman transport (*Böning et al.*, 2008). The respone of eddies, however, is delayed by two to three years, whereas the SAM oscillates between its high and low polarity on time-scales of weeks to months (*Thompson et al.*, 2011). The system cannot reach equilibrium and this raises the question whether the full response by eddies can be completely developed. A first eddy-permitting study (*Dufour*, 2011) calculates the same amount as our coarse model for the additional outgassing of natural CO_2 (0.09 Pg C yr^{-1}) as response to the positive SAM. This provides confidence in our results, but eddy-resolving models are needed to assess the full response of the Southern Ocean carbon cycle to the positive SAM.

References

Antonov, J. I., D. Seidov, T. P. Boyer, R. A. Locarnini, A. V. Mishonov, H. E. Garcia, O. K. Baranova, M. M. Zweng, and D. R. Johnson (2010), World Ocean Atlas 2009, Volume 2: Salinity, in *NOAA Atlas NESDIS 69*, edited by S. Levitus, p. 184, U.S. Government Printing Office, Washington, D.C.

Arrigo, K. R., G. van Dijken, and M. Long (2008), Coastal Southern Ocean: A strong anthropogenic CO_2 sink, *Geophysical Research Letters*, *35, L21602*, doi:10.1029/2008GL035624.

Aumont, O., J. C. Orr, P. Monfray, G. Madec, and E. Maier-Reimer (1999), Nutrient trapping in the equatorial Pacific: The ocean circulation solution, *Global Biogeochemical Cycles*, *13*, 351–369, doi:10.1029/1998GB900012.

Aumont, O., E. Maier-Reimer, S. Blain, and P. Monfray (2003), An ecosystem model of the global ocean including Fe, Si, P colimitations, *Global Biogeochemical Cycles*, *17*, 1060, doi:10.1029/2001GB001745.

Bakker, D. C. E., M. Hoppema, M. Schröder, W. Geibert, and H. J. W. De Baar (2008), A rapid transition from ice covered CO_2–rich waters to a biologically mediated CO_2 sink in the eastern Weddell Gyre, *Biogeosciences*, *5*, 1373–1386, doi:10.5194/bg-5-1373-2008.

Behrenfeld, M. J., and P. G. Falkowski (1997), Photosynthetic rates derived from satellite-based chlorophyll concentration, *Limnology and Oceanography*, *42*, 1–20, doi:10.4319/lo.1997.42.1.0001.

Böning, C. W., A. Dispert, M. Visbeck, S. R. Rintoul, and F. U. Schwarzkopf (2008), The response of the Antarctic Circumpolar Current to recent climate change, *Nature Geoscience*, *1*, 864–869, doi:10.1038/ngeo362.

Bopp, L., O. Aumont, P. Cadule, S. Alvain, and M. Gehlen (2005), Response of diatoms distribution to global warming and potential implications: A global model study, *Geophysical Research Letters*, *32, L19606*, doi:10.1029/2005GL023653.

Boyd, P., J. LaRoche, M. Gall, R. Frew, and R. M. L. McKay (1999), Role of iron, light, and silicate in controlling algal biomass in subantarctic waters SE of New Zealand, *Journal of Geophysical Research*, *104*, 13,395–13,408, doi:10.1029/1999JC900009.

Boyd, P. W., A. J. Watson, C. S. Law, E. R. Abraham, T. Trull, R. Murdoch, D. C. E. Bakker, A. R. Bowie, K. O. Buesseler, H. Chang, M. Charette, P. Croot, K. Downing, R. Frew, M. Gall, M. Hadfield, J. Hall, M. Harvey, G. Jameson, J. LaRoche, M. Liddicoat, R. Ling, M. T. Maldonado, R. M. McKay, S. Nodder, S. Pickmere, R. Pridmore, S. Rintoul, K. Safi, P. Sutton, R. Strzepek, K. Tanneberger, S. Turner, A. Waite, and J. Zeldis (2000), A mesoscale phytoplankton bloom in the polar Southern Ocean stimulated by iron fertilization, *Nature*, *407*, 695–702, doi:10.1038/35037500.

Boye, M., C. M. G. van den Berg, J. T. M. de Jong, H. Leach, P. Croot, and H. J. W. de Baar (2001), Organic complexation of iron in the Southern Ocean, *Deep-Sea Research I*, *48*, 1477–1497, doi:10.1016/S0967-0637(00)00099-6.

Bracher, A., M. Vountas, T. Dinter, J. P. Burrows, R. Röttgers, and I. Peeken (2009), Quantitative observation of cyanobacteria and diatoms from space using PhytoDOAS on SCIAMACHY data, *Biogeosciences*, *6*, 751–764, doi:10.5194/bg-6-751-2009.

Campin, J.-M., and H. Goosse (1999), Parameterization of density-driven downsloping flow for a coarse-resolution ocean model in z-coordinate, *Tellus A*, *51*, 412–430, doi:10.1034/j.1600-0870.1999.t01-3-00006.x.

Cavalieri, D. J., and C. L. Parkinson (2008), Antarctic sea ice variability and trends, 1979-2006, *Journal of Geophysical Research*, *113, C07004*, doi:10.1029/2007JC004564.

Comiso, J. (1999), Bootstrap sea ice concentrations for NIMBUS-7 SMMR and DMSP SSM/I, June to September 2001. National Snow and Ice Data Center Digital Media, *19*.

Cunningham, S. A., S. G. Alderson, B. A. King, and M. A. Brandon (2003), Transport and variability of the Antarctic Circumpolar Current in Drake Passage, *Journal of Geophysical Research*, *108*, 8084, doi:10.1029/2001JC001147.

de Baar, H. J. W., A. G. J. Buma, R. F. Nolting, G. C. Cadée, G. Jacques, and P. J. Tréguer (1990), On iron limitation of the Southern Ocean: experimental observations in the Weddell and Scotia Seas, *Marine Ecology-Progress Series*, *65*, 105–122, doi:10.3354/meps065105.

de Baar, H. J. W., J. T. M. de Jong, R. F. Nolting, K. R. Timmermans, M. A. van Leeuwe, U. Bathmann, M. Rutgers van der Loeff, and J. Sildam (1999), Low dissolved Fe and the absence of diatom blooms in remote Pacific waters of the Southern Ocean, *Marine Chemistry*, *66*, 1–34, doi:10.1016/S0304-4203(99)00022-5.

de Baar, H. J. W., L. J. A. Gerringa, P. Laan, and K. R. Timmermans (2008), Efficiency of carbon removal per added iron in ocean iron fertilization, *Marine Ecology Progress Series*, *364*, 269–282, doi:10.3354/meps07548.

Dufour, C. (2011), Rôle des tourbillons océaniques dans la variabilité récente des flux air-mer de CO_2 dans l'océan Austral, *PhD Thesis, Université de Grenoble*.

Enting, I. E., T. M. L. Wigley, and M. Heimann (1994), Future emissions and concentrations of carbon dioxide: Key ocean/atmosphere/land analyses, *CSIRO Division of Atmospheric Research Technical Paper*, *31*.

Garcia, H. E., R. A. Locarnini, T. P. Boyer, J. I. Antonov, M. M. Zweng, O. K. Baranova, and D. R. Johnson (2010), World Ocean Atlas 2009, Volume 4: Nutrients (phosphate, nitrate, and silicate), in *NOAA Atlas NESDIS 71*, edited by S. Levitus, p. 398, U.S. Government Printing Office, Washington, D.C.

Geider, R. J., H. L. MacIntyre, and T. M. Kana (1998), A dynamic regulatory model of phytoplankton acclimation to light, nutrients, and temperature, *Limnology and Oceanography*, *43*, 679–694, doi:10.4319/lo.1998.43.4.0679.

Gent, P. R., and J. C. McWilliams (1990), Isopycnal mixing in ocean circulation models, *Journal of Physical Oceanography*, *20*, 150–155.

Gentleman, W., A. Leising, B. Frost, S. Strom, and J. Murray (2003), Functional responses for zooplankton feeding on multiple resources: a review of assumptions and biological dynamics, *Deep-Sea Research Part II-Topical Studies in Oceanography*, *50*, 2847–2875, doi:10.1016/j.dsr2.2003.07.001.

Gong, D., and S. Wang (1999), Definition of Antarctic Oscillation index, *Geophysical Research Letters*, *26*, 459, doi:10.1029/1999GL900003.

Griffies, S., A. Biastoch, C. Böning, F. Bryan, G. Danabasoglu, E. Chassignet, M. England, R. Gerdes, H. Haak, R. Hallberg, W. Hazeleger, J. Jungclaus, W. G. Lagre, G. Madec, A. Pirani, B. L. Samuels, M. Scheinert, A. Sen Gupta, C. A. Severijns, H. L. Simmons, A. M. Treguier, M. Winton, S. Yeager, and J. Yin (2009), Coordinated Ocean-Ice Reference Experiments (COREs), *Ocean Modelling*, *26*, 1–46, doi:10.1016/j.ocemod.2008.08.007.

Gruber, N., M. Gloor, S. E. Mikaloff Fletcher, S. C. Doney, S. Dutkiewicz, M. J. Follows, M. Gerber, A. R. Jacobson, F. Joos, K. Lindsay, D. Menemenlis, A. Mouchet, S. A. Müller, J. L. Sarmiento, and T. Takahashi (2009), Oceanic sources, sinks, and transport of atmospheric CO_2, *Global Biogeochemical Cycles*, *23, GB1005*, doi:10.1029/2008GB003349.

Hall, A., and M. Visbeck (2002), Synchronous variability in the southern hemisphere atmosphere, sea ice, and ocean resulting from the annular mode, *Journal of Climate*, *15*, 3043–3057.

Hallberg, R., and A. Gnanadesikan (2006), The role of eddies in determining the structure and response of the wind-driven Southern Hemisphere overturning: Results from the modeling eddies in the Southern Ocean (MESO) project, *Journal of Physical Oceanography*, *36*, 2232–2252, doi:10.1175/JPO2980.1.

Hauck, J., M. Hoppema, R. G. J. Bellerby, C. Völker, and D. Wolf-Gladrow (2010), Data-based estimation of anthropogenic carbon and acidification in the Weddell Sea on a decadal timescale, *Journal of Geophysical Research*, *115, C03004*, doi:10.1029/2009JC005479.

Hogg, A. M., M. P. Meredith, J. R. Blundell, and C. Wilson (2008), Eddy heat flux in the Southern Ocean: Response to variable wind forcing, *Journal of Climate*, *21*, 608–620, doi:10.1175/2007JCLI1925.1.

Hohn, S. (2009), Coupling and decoupling of biogeochemical cycles in marine ecosystems, *PhD Thesis, Universität Bremen*, http://elib.suub.uni-bremen.de/diss/docs/00011278.pdf.

Hoppema, M., H. J. W. de Baar, E. Fahrbach, H. H. Hellmer, and B. Klein (2003), Substantial advective iron loss diminishes phytoplankton production in the Antarctic Zone, *Global Biogeochemical Cycles*, *17, 1025*, doi:10.1029/2002GB001957.

Jacques, G. (1983), Some ecophysiological aspects of the Antarctic phytoplankton, *Polar Biology*, *2*, 27–33, doi:10.1007/BF00258282.

Kalnay, E., M. Kanamitsu, R. Kistler, W. Collins, D. Deaven, L. Gandin, M. Iredell, S. Saha, G. White, J. Woollen, Y. Zhu, M. Chelliah, W. Ebisuzaki, W. Higgins, J. Janowiak, K. C. Mo, C. Ropelewski, J. Wang, A. Leetmaa, R. Reynolds, R. Jenne, and D. Joseph (1996), The NCEP/NCAR 40-year reanalysis project, *Bulletin of the American Meteorological Society*, *77*, 437–471.

Kara, A. B., P. A. Rochford, and H. E. Hurlburt (2000), An optimal definition for ocean mixed layer depth, *Journal of Geophysical Research*, *105*, 16,803–16,821, doi:10.1029/2000JC900072.

Key, R. M., A. Kozyr, C. L. Sabine, K. Lee, R. Wanninkhof, J. L. Bullister, R. A. Feely, F. J. Millero, C. Mordy, and T.-H. Peng (2004), A global ocean carbon climatology: Results from Global Data Analysis Project (GLODAP), *Global Biogeochemical Cycles*, *18, GB4031*, doi:10.1029/2004GB002247.

Khatiwala, S., F. Primeau, and T. Hall (2009), Reconstruction of the history of anthropogenic CO_2 concentrations in the ocean, *Nature*, *462*, 346–349, doi:10.1038/nature08526.

Kriest, I., and A. Oschlies (2008), On the treatment of particulate organic matter sinking in large-scale models of marine biogeochemical cycles, *Biogeosciences*, *5*, 55–72, doi:10.5194/bg-5-55-2008.

Large, W. G., and S. G. Yeager (2004), Diurnal to decadal global forcing for ocean and sea-ice models: The data sets and flux climatologies, *NCAR Technical Note*.

Law, R. M., R. J. Matear, and R. J. Francey (2008), Comment on: "Saturation of the Southern Ocean CO_2 sink due to recent climate change", *Science*, *319*, 570a, doi:10.1126/science.1149077.

Le Quéré, C., C. Rödenbeck, E. T. Buitenhuis, T. J. Conway, R. Langenfelds, A. Gomez, C. Labuschagne, M. Ramonet, T. Nakazawa, N. Metzl, N. P. Gillett, and M. Heimann (2007), Saturation of the Southern Ocean CO_2 sink due to recent climate change, *Science*, *316*, 1735–1738, doi:10.1126/science.1136188.

Le Quéré, C., C. Rödenbeck, E. T. Buitenhuis, T. J. Conway, R. Langenfelds, A. Gomez, C. Labuschagne, M. Ramonet, T. Nakazawa, N. Metzl, N. P. Gillett, and M. Heimann (2008), Response to Comments on "Saturation of the Southern Ocean CO_2 sink due to recent climate change", *Science*, *319*, 570c, doi:10.1126/science.1147315.

Lenton, A., and R. J. Matear (2007), Role of the Southern Annular Mode (SAM) in Southern Ocean CO_2 uptake, *Global Biogeochemical Cycles*, *21, GB2016*, doi:10.1029/2006GB002714.

Lenton, A., F. Codron, L. Bopp, N. Metzl, P. Cadule, A. Tagliabue, and J. Le Sommer (2009), Stratospheric ozone depletion reduces ocean carbon uptake and enhances ocean acidification, *Geophysical Research Letters*, *36, L12606*, doi:10.1029/2009GL038227.

Locarnini, R. A., A. V. Mishonov, J. I. Antonov, T. P. Boyer, H. E. Garcia, O. K. Baranova, M. M. Zweng, and D. R. Johnson (2010), World Ocean Atlas 2009, Volume 1: Temperature, in *NOAA Atlas NESDIS 68*, edited by S. Levitus, p. 184, U.S. Government Printing Office, Washington, D.C.

Losch, M., D. Menemenlis, J.-M. Campin, P. Heimbach, and C. Hill (2010), On the formulation of sea-ice models. Part 1: Effects of different solver implementations and parameterizations, *Ocean Modelling*, *33*, 129–144, doi:10.1016/j.ocemod.2009.12.008.

Louanchi, F., M. Hoppema, and D. C. E. Bakker (1999), Modelled and observed sea surface fCO_2 in the Southern Ocean: a comparative study, *Tellus B*, *51B*, 541–559, doi:10.1034/j.1600-0889.1999.00029.x.

Lovenduski, N. S., and N. Gruber (2005), Impact of the Southern Annular Mode on Southern Ocean circulation and biology, *Geophysical Research Letters*, *32, L11603*, doi:10.1029/2005GL022727.

Lovenduski, N. S., N. Gruber, S. C. Doney, and I. D. Lima (2007), Enhanced CO_2 outgassing in the Southern Ocean from a positive phase of the Southern Annular Mode, *Global Biogeochemical Cycles*, *21, GB2026*, doi:10.1029/2006GB002900.

Mahowald, N., C. Luo, J. del Corral, Zender, and S. C (2003), Interannual variability in atmospheric mineral aerosols from a 22-year model simulation and observational data, *Journal of Geophysical Research*, *108*, 4352, doi:10.1029/2002JD002821.

Marinov, I., A. Gnanadesikan, J. R. Toggweiler, and J. L. Sarmiento (2006), The Southern Ocean biogeochemical divide, *Nature*, *441*, 964–967, doi:10.1038/nature04883.

Marinov, I., S. C. Doney, and I. D. Lima (2010), Response of ocean phytoplankton community structure to climate change over the 21st century: partitioning the effects of nutrients, temperature and light, *Biogeosciences*, *7*, 3941–3959, doi:10.5194/bg-7-3941-2010.

Marshall, G. J. (2003), Trends in the Southern Annular Mode from observations and reanalyses, *Journal of Climate*, *16*, 4134–4143.

Marshall, J., and K. Speer (2012), Closure of the meridional overturning circulation through Southern Ocean upwelling, *Nature Geoscience*, *5*, 171–180, doi:10.1038/ngeo1391.

Marshall, J., A. Adcroft, C. Hill, L. Perelman, and C. Heisey (1997), A finite-volume, incompressible Navier Stokes model for studies of the ocean on parallel computers, *Journal of Geophysical Research*, *102*, 5753–5766, doi:10.1029/96JC02775.

McNeil, B. I., N. Metzl, R. M. Key, R. J. Matear, and A. Corbiere (2007), An empirical estimate of the Southern Ocean air-sea CO_2 flux, *Global Biogeochemical Cycles*, *21, GB3011*, doi: 10.1029/2007GB002991.

Miller, L. A., T. N. Papakyriakou, R. E. Collins, J. W. Deming, J. K. Ehn, R. W. Macdonald, A. Mucci, O. Owens, M. Raudsepp, and N. Sutherland (2011), Carbon dynamics in sea ice: A winter flux time series, *Journal of Geophysical Research*, *116, C02028*, doi: 10.1029/2009JC006058.

MITgcm Group (2012), MITgcm User Manual (online documentation), MIT/EAPS, Cambridge, MA, USA, http://mitgcm.org/public/r2_manual/latest/online_documents/manual.html.

Oke, P. R., and M. H. England (2004), Oceanic response to changes in the latitude of the Southern Hemisphere subpolar westerly winds, *Journal of Climate*, *17*, 1040–1054.

Orsi, A. H., T. Whitworth, and Others (1995), On the meridional extent and fronts of the Antarctic Circumpolar Current, *Deep Sea Research Part I: Oceanographic Research Papers*, *42*, 641–673, doi:10.1016/0967-0637(95)00021-W.

Peylin, P., P. Bousquet, C. Le Quéré, S. Sitch, P. Friedlingstein, G. McKinley, N. Gruber, P. Rayner, and P. Ciais (2005), Multiple constraints on regional CO_2 flux variations over land and oceans, *Global Biogeochemical Cycles*, *19, GB1011*, doi:10.1029/2003GB002214.

Russell, J. L., K. W. Dixon, A. Gnanadesikan, R. J. Stouffer, and J. R. Toggweiler (2006), The Southern Hemisphere westerlies in a warming world: Propping open the door to the deep ocean, *Journal of Climate*, *19*, 6382–6390, doi:10.1175/JCLI3984.1.

Schartau, M., A. Engel, J. Schröter, S. Thoms, C. Völker, and D. Wolf-Gladrow (2007), Modelling carbon overconsumption and the formation of extracellular particulate organic carbon, *Biogeosciences*, *4*, 433–454, doi:10.5194/bg-4-433-2007.

Schlitzer, R. (2002), Carbon export fluxes in the Southern Ocean: results from inverse modeling and comparison with satellite-based estimates, *Deep Sea Research Part II*, *49*, 1623–1644, doi:10.1016/S0967-0645(02)00004-8.

Schneider, B., L. Bopp, M. Gehlen, J. Segschneider, T. L. Frölicher, P. Cadule, P. Friedlingstein, S. C. Doney, M. J. Behrenfeld, and F. Joos (2008), Climate-induced interannual variability of marine primary and export production in three global coupled climate carbon cycle models, *Biogeosciences*, *5*, 597–614, doi:10.5194/bg-5-597-2008.

Screen, J. A., N. P. Gillett, D. P. Stevens, G. J. Marshall, and H. K. Roscoe (2009), The role of eddies in the Southern Ocean temperature response to the Southern Annular Mode, *Journal of Climate*, *22*, 806–818, doi:10.1175/2008JCLI2416.1.

Sen Gupta, A., and M. H. England (2006), Coupled ocean-atmosphere-ice response to variations in the Southern Annular Mode, *Journal of Climate*, *19*, 4457–4486, doi:10.1175/JCLI3843.1.

Szeto, M., P. J. Werdell, T. S. Moore, and J. W. Campbell (2011), Are the world's oceans optically different?, *Journal of Geophysical Research*, *116, C00H04*, doi:10.1029/2011JC007230.

Takahashi, T., S. Sutherland, C. Sweeney, A. Poisson, N. Metzl, B. Tilbrook, N. Bates, R. Wanninkhof, R. Feely, and C. Sabine (2002), Global sea-air CO_2 flux based on climatological surface ocean pCO_2, and seasonal biological and temperature effects, *Deep Sea Research Part II: Topical Studies in Oceanography*, *49*, 1601–1622, doi:10.1016/S0967-0645(02)00003-6.

Takahashi, T., S. C. Sutherland, R. Wanninkhof, C. Sweeney, R. A. Feely, D. W. Chipman, B. Hales, G. Friederich, F. Chavez, C. Sabine, A. Watson, D. C. E. Bakker, U. Schuster, N. Metzl, H. Yoshikawa-Inoue, M. Ishii, T. Midorikawa, Y. Nojiri, A. Körtzinger, T. Steinhoff, M. Hoppema, J. Olafsson, T. S. Arnarson, B. Tilbrook, T. Johannessen, A. Olsen, R. Bellerby, C. S. Wong, B. Delille, N. R. Bates, and H. J. W. De Baar (2009), Climatological mean and decadal change in surface ocean pCO_2, and net sea-air CO_2 flux over the global oceans, *Deep Sea Research Part II: Topical Studies in Oceanography*, *56*, 554–577, doi:10.1016/j.dsr2.2008.12.009.

Thompson, D. W. J., and S. Solomon (2002), Interpretation of recent Southern Hemisphere climate change, *Science*, *296*, 895–899, doi:10.1126/science.1069270.

Thompson, D. W. J., and J. M. Wallace (2000), Annular modes in the extratropical circulation. Part I: Month-to-month variability, *Journal of Climate*, *13*, 1000–1016.

Thompson, D. W. J., S. Solomon, P. J. Kushner, M. H. England, K. M. Grise, and D. J. Karoly (2011), Signatures of the Antarctic ozone hole in Southern Hemisphere surface climate change, *Nature Geoscience*, *4*, 741–749, doi:10.1038/ngeo1296.

Timmermann, R., A. Le Brocq, T. Deen, E. Domack, P. Dutrieux, B. Galton-Fenzi, H. Hellmer, A. Humbert, D. Jansen, A. Jenkins, A. Lambrecht, K. Makinson, F. Niederjasper, F. Nitsche, O. A. Nøst, L. H. Smedsrud, and W. H. F. Smith (2010), A consistent data set of Antarctic ice sheet topography, cavity geometry, and global bathymetry, *Earth System Science Data*, *2*, 261–273, doi:10.5194/essd-2-261-2010.

Toggweiler, J. R., and J. L. Russell (2008), Ocean circulation in a warming climate, *Nature*, *451*, 286–288, doi:10.1038/nature06590.

Wagener, T., C. Guieu, R. Losno, S. Bonnet, and N. Mahowald (2008), Revisiting atmospheric dust export to the Southern Hemisphere ocean: Biogeochemical implications, *Global Biogeochemical Cycles*, *22, GB2006*, doi:10.1029/2007GB002984.

Wang, S., and J. K. Moore (2012), Variability of primary production and air-sea CO_2 flux in the Southern Ocean, *Global Biogeochemical Cycles*, *26, GB1008*, doi:10.1029/2010GB003981.

Wanninkhof, R. (1992), Relationship between wind speed and gas exchange over the ocean, *Journal of Geophysical Research*, *97*, 7373–7382, doi:10.1029/92JC00188.

Westberry, T., M. J. Behrenfeld, D. A. Siegel, and E. Boss (2008), Carbon-based primary productivity modeling with vertically resolved photoacclimation, *Global Biogeochemical Cycles*, *22, GB2024*, doi:10.1029/2007GB003078.

Wetzel, P., A. Winguth, and E. Maier-Reimer (2005), Sea-to-air CO_2 flux from 1948 to 2003: A model study, *Global Biogeochemical Cycles*, *19, GB2005*, doi:10.1029/2004GB002339.

Whitworth, T. (1983), Monitoring the transport of the Antarctic Circumpolar Current at Drake Passage, *Journal of Physical Oceanography*, *13*, 2045–2057.

Whitworth, T., and R. G. Peterson (1985), Volume transport of the Antarctic Circumpolar Current from bottom pressure measurements, *Journal of Physical Oceanography*, *15*, 810–816.

Yamanaka, Y., and E. Tajika (1996), The role of the vertical fluxes of particulate organic matter and calcite in the oceanic carbon cycle: Studies using an ocean biogeochemical general circulation model, *Global Biogeochemical Cycles*, *10*, 361–382, doi:10.1029/96GB00634.

Zickfeld, K., J. C. Fyfe, M. Eby, and A. J. Weaver (2008), Comment on "Saturation of the Southern Ocean CO_2 sink due to recent climate change", *Science*, *319*, 570b, doi:10.1126/science.1146886.

Supplementary Information: Model Equations

Regulated Ecosystem Model with two phytoplankton classes REcoM-2

The Regulated Ecosystem Model, version 2, (REcoM-2) describes the biogeochemistry in the ocean with a relatively simple ecological model including two phytoplankton functional types (diatoms and non-diatoms), one zooplankton and one detritus compartment, and inorganic and organic forms of the main nutrients. Some emphasis is put on phytoplankton physiology, which is described in a way that allows for changes in cellular stoichiometry (N:C:Chl:Si for diatoms and N:C:Chl for non-diatoms, respectively). All in all, the model solves mass balance equations for 21 tracers, which are described by equations of the type

$$\frac{\partial A}{\partial t} = -(\mathbf{U}+\mathbf{w})\cdot\nabla A + \nabla\cdot(\kappa\nabla A) + S(A) \quad (1)$$

where A is the volumetric concentration of a tracer, $\mathbf{U}$ is the three-dimensional advection velocity and κ is the diffusivity, both supplied by the physical circulation model. The sinking velocity of particles $\mathbf{w} = (0, 0, w)$ increases linearly with depth for detritus and has a constant value for phytoplankton and diatoms. $S(A)$ are the biogeochemical sources or sinks of the tracer A and are described in detail, for any of the tracers, in the following.

1 Carbonate chemistry

Dissolved inorganic carbon (DIC**)** The balance of DIC is affected by a number of processes; sources for DIC are respiration by nanophytoplankton (*phy*), diatoms (*dia*) and heterotrophs (*het*), remineralization of dissolved organic carbon (DOC) and dissolution of calcitic detritus (*det*). Sinks are carbon fixation by primary producers and the formation of calcium carbonate (Z). In addition, sea-air flux of CO_2 (F_C) leads to an exchange of carbon with the atmosphere, depending on the partial pressure difference of CO_2 between ocean and atmosphere. This exchange is treated separately as boundary condition in

section 7.

$$\begin{aligned} S(\mathrm{DIC}) = &(r_{phy} - p_{phy}) \cdot \mathrm{C}_{phy} + (r_{dia} - p_{dia}) \cdot \mathrm{C}_{dia} \\ &+ r_{het} \cdot \mathrm{C}_{het} + \rho_{\mathrm{DOC}} \cdot f_T \cdot \mathrm{DOC} \\ &+ \lambda \cdot \mathrm{CaCO}_{3\,det} - Z \end{aligned} \tag{2}$$

See section 3 for details on photosynthesis (p) and phytoplankton respiration (r) rates. C_{phy}, C_{dia} and C_{het} refer to carbon biomass of nanophytoplankton, diatoms and heterotrophs, respectively. See section 4 for the formulation of the heterotrophic respiration rate (r_{het}) and section 6 for the DOC remineralization term ($\rho_{\mathrm{DOC}} \cdot f_T \cdot \mathrm{DOC}$). The calcite dissolution rate (λ) is defined in Eq. 50 and the calcification flux (Z) in Eq. 37.

Total Alkalinity (TA**)** The alkalinity balance is determined by processes co-occurring with primary production and remineralization of dissolved organic matter. Alkalinity is increased by nitrogen assimilation and reduced by remineralization of dissolved organic nitrogen (DON). The contribution of phosphate assimilation and remineralization to alkalinity is taken into account by assuming a constant Redfield ratio (16:1) relating DON to dissolved organic phosphorous (DOP). Further, alkalinity is reduced during calcification and increased during dissolution of CaCO_3.

$$\begin{aligned} S(\mathrm{TA}) = &(1 + \frac{1}{16}) \cdot (a^N_{phy} \cdot \mathrm{C}_{phy} + a^N_{dia} \cdot \mathrm{C}_{dia} - \rho_{\mathrm{DON}} \cdot f_T \cdot \mathrm{DON}) \\ &+ 2\ (\lambda \cdot \mathrm{CaCO}_{3\,det} - Z) \end{aligned} \tag{3}$$

See section 3 for details on the nitrogen assimilation rates (a^N_{phy} and a^N_{dia}), and section 6 for the DON remineralization term ($\rho_{\mathrm{DON}} \cdot f_T \cdot \mathrm{DON}$). The calcification flux (Z) is defined in Eq. 37 and the dissolution rate of CaCO_3 (λ) in Eq. 50.

2 Nutrients

Dissolved Inorganic Nitrogen (DIN**)** DIN in the model is the sum of the concentrations of nitrate, nitrite and ammonia. The DIN pool in the water column is reduced when nanophytoplankton and diatoms take up DIN and build it into their cells. Remineralization of DON is a source for DIN.

$$S(\mathrm{DIN}) = -a^N_{phy} \cdot \mathrm{C}_{phy} - a^N_{dia} \cdot \mathrm{C}_{dia} + \rho_{\mathrm{DON}} \cdot f_T \cdot \mathrm{DON} \tag{4}$$

See section 3 for details on the nitrogen assimilation rates (a^N_{phy} and a^N_{dia}) and section 6 for an explanation of the temperature dependent DON remineralization.

Dissolved Silicate (DSi**)** Silicon cycles between dissolved silicic acid, or silicate DSi, and the biogenic silica in diatoms Si_{dia} and detritus (Si_{det}). Silicate in the water column is drawn down by silicate assimilation and returned via degradation of detritus silica.

$$S(\mathrm{DSi}) = -a^{Si}_{dia} \cdot \mathrm{C}_{dia} + \rho^T_{Si} \cdot \mathrm{Si}_{det} \tag{5}$$

See section 3 for the definition of the silicate assimilation rate (a^{Si}_{dia}). The temperature-dependent dissolution rate of silica ρ^T_{Si} is defined in Eq. 48.

Dissolved Iron (DFe**)** Dissolved iron is treated in the model like in *Parekh et al.* (2004), i.e. it is considered the sum of the concentrations of "free" (i.e. inorganically bound) iron Fe$'$ and organically complexed iron FeL. The partitioning into these two types is assumed to be in chemical equilibrium always, and is calculated at each timestep by solving the law of mass action for a reaction $\mathrm{Fe}' + \mathrm{L} \leftrightarrows \mathrm{FeL}$ with L being the free ligand concentration, assuming both a constant conditional stability constant $K_{FeL} = \mathrm{Fe}' \cdot L/FeL$ and total ligand concentration $\mathrm{L}_T = \mathrm{L} + \mathrm{FeL}$.

Dissolved iron is drawn down in concert with photosynthesis by nanophytoplankton and diatoms and by scavenging of free Fe. Iron is released during respiration of phytoplankton and heterotrophs, remineralization of DOC, and excretion of heterotrophs. Degraded iron is directly remineralized to dissolved iron. For all these processes, we assume a constant iron:carbon ratio (q^{Fe}).

$$\begin{aligned} S(\mathrm{DFe}) = q^{Fe} \cdot ((r_{phy} - p_{phy}) \cdot \mathrm{C}_{phy} + (r_{dia} - p_{dia}) \cdot \mathrm{C}_{dia} + (r_{het} + \epsilon^C_{het}) \cdot \mathrm{C}_{het} \\ + \rho_{\mathrm{DOC}} \cdot f_T \cdot \mathrm{DOC}) - \kappa^{scav}_{Fe} \cdot \mathrm{Fe}' \end{aligned} \tag{6}$$

See section 3 for an explanation of phytoplankton photosynthesis (p) and respiration (r) rates and section 4 for the heterotrophic respiration (r_{het}) and carbon excretion rate (ϵ^C_{het}). The DOC remineralization term is described in section 6.

3 Phytoplankton

The equations for the two classes of phytoplankton are based on a slightly modified version of the physiological model by *Geider et al.* (1998) that has been amended by non-physiological mortality terms, namely grazing and aggregation loss to sinking detritus (*Schartau et al.*, 2007). For diatoms an additional equation describing the formation and loss of biogenic silica in the diatom frustule has been added by *Hohn* (2009).

All physiological rates, such as the photosynthesis and assimilation rates depend on cell quota in the formulation of *Geider et al.* (1998). These are defined as the intracellular ratios of N:C, Chl:C and Si:C:

$$q = \frac{\mathrm{N}}{\mathrm{C}}; \quad q^{Si} = \frac{\mathrm{Si}}{\mathrm{C}}; \quad q^{Chl} = \frac{\mathrm{Chl}}{\mathrm{C}}; \tag{7}$$

In addition quota are used to convert biomass in terms of carbon or nitrogen to Fe, Si, Chl or $CaCO_3$:

$$q^{Fe} = \frac{\mathrm{Fe}}{\mathrm{C}} \quad q^{Si:N} = \frac{\mathrm{Si}}{\mathrm{N}}; \quad q^{Chl:N} = \frac{\mathrm{Chl}}{\mathrm{N}}; \quad q^{CaCO_3:N} = \frac{\mathrm{CaCO_3}}{\mathrm{N}}; \tag{8}$$

Nitrogen pool (N_{phy} **and** N_{dia}**)** The nitrogen pool in nanophytoplankton and diatoms is built up by the assimilation of nitrogen, which is assumed proportional to carbon biomass. Metabolic processes lead to excretion of biogenic nitrogen to the DON pool. At high

intracellular N:C ratios (q), we assume that this excretion is downregulated. Aggregation and grazing by zooplankton transfer nitrogen to the detritus and zooplankton pools:

$$S(\mathrm{N}_{phy}) = a^N_{phy} \cdot \mathrm{C}_{phy} - (\epsilon^N_{phy} \cdot f^{lim}_{phy} + g) \cdot \mathrm{N}_{phy} - G_{phy} \tag{9}$$

$$S(\mathrm{N}_{dia}) = a^N_{dia} \cdot \mathrm{C}_{dia} - (\epsilon^N_{dia} \cdot f^{lim}_{dia} + g) \cdot \mathrm{N}_{dia} - G_{dia} \tag{10}$$

See section 4 for a description of the grazing formulation (G_{phy} and G_{dia}). The carbon-specific nitrogen uptake rate depends on the maximum photosynthetic rate (p^{max}_{phy} and p^{max}_{dia}, Eq. 21, Eq. 22), which is converted to nitrogen units by multiplication with an optimal N:C uptake ratio (σ^N_{phy} and σ^N_{dia}). Nitrogen uptake rates are further affected by the intracellular nitrogen status q through f^{lim}_{phy} and f^{lim}_{dia}, (see Eq. 14 and Eq. 15) and by extracellular nitrogen concentrations through an assumed Michaelis-Menten uptake kinetics.

$$a^N_{phy} = p^{max}_{phy} \cdot \sigma^N_{phy} \cdot f^{lim}_{phy} \cdot \left(\frac{\mathrm{DIN}}{\mathrm{DIN} + K^{\mathrm{N}}_{phy}} \right) \tag{11}$$

$$a^N_{dia} = p^{max}_{dia} \cdot \sigma^N_{dia} \cdot f^{lim}_{dia} \cdot \left(\frac{\mathrm{DIN}}{\mathrm{DIN} + K^{\mathrm{N}}_{dia}} \right) \tag{12}$$

As in the model by *Geider et al.* (1998), both the limiting functions (f^{lim}_{phy} and f^{lim}_{dia}) for nitrogen assimilation (a^N) and excretion (ϵ^N) rates are treated as functions of the intracellular nitrogen status (i.e., N:C ratios q).

The mathematical form of how this regulation is described has no specific basis in physiology. In a slight change against the model by *Geider et al.* (1998) we use a uniform general limitation function for all types of quota regulation, which is given by

$$f(q_1, q_2, \theta) = \begin{cases} 1 - \exp(-4\theta(q_1 - q_2)^2) & \text{if} \quad q_1 < q_2 \\ 0 & \text{if} \quad q_1 \geq q_2 \end{cases} \tag{13}$$

This regulation function is close to one for $q_1 << q_2$, but tends to zero for $q_1 \to q_2$; θ is a dimensionless constant that determines how close q_1 and q_2 have to be for a significant decrease of f.

With this function we can now formulate the functions limiting nitrogen assimilation as

$$f^{lim}_{phy} = f(q_{phy}, q_{phy\,max}, \theta_{max}) \tag{14}$$

and

$$f^{lim}_{dia} = f(q_{dia}, q_{dia\,max}, \theta_{max}) \tag{15}$$

The aggregation rate (g) is assumed to be proportional to the abundance of phytoplankton and detritus:

$$g = \phi_{phy} \cdot \mathrm{N}_{phy} + \phi_{phy} \cdot \mathrm{N}_{dia} + \phi_{det} \cdot \mathrm{N}_{det} \tag{16}$$

The constants ϕ_{phy} and ϕ_{det} are specific aggregation rates (i.e. per unit biomass per unit time) of phytoplankton and detritus, respectively, which reflect the roles of phytoplankton and detritus in the aggregation processes.

Carbon pool (C_{phy} and C_{dia}) The carbon biomass of nanophytoplankton and diatoms increases as a result of carbon assimilation during photosynthesis. Loss terms include excretion (ϵ) of DOC, which is constrained as in the nitrogen pool, respiration (r), aggregation (g), and grazing (G).

$$S(\mathrm{C}_{phy}) = (p_{phy} - \epsilon^{C}_{phy} \cdot f^{lim}_{phy} - r_{phy} - g) \cdot \mathrm{C}_{phy} - \frac{1}{q_{phy}} \cdot G_{phy} \tag{17}$$

$$S(\mathrm{C}_{dia}) = (p_{dia} - \epsilon^{C}_{dia} \cdot f^{lim}_{dia} - r_{dia} - g) \cdot \mathrm{C}_{dia} - \frac{1}{q_{dia}} \cdot G_{dia} \tag{18}$$

Grazing (G) is calculated on the basis of nitrogen biomass and converted to carbon using the intracellular N:C ratio (q_{phy}, q_{dia}). See section 4 for the grazing formulation, Eq. 16 for the aggregation rate g and Eq. 14 and Eq. 15 for the limiter functions for the carbon excretion rates ϵ^{C}_{phy} and ϵ^{C}_{dia}.

The photosynthetic rate (p_{phy} and p_{dia}) is a saturating function of the photosynthetically active radiation (PAR). The saturating light level is affected by the internal chlorophyll status of the cells. The initial slope of the photosynthesis-irradiance-curve is obtained by multiplication of the light harvesting efficiency per chlorophyll (α) with the intracellular chlorophyll to carbon ratio (q^{Chl}).

$$p_{phy} = p^{max}_{phy} \cdot \left(1 - \exp\left(-\alpha_{phy} \cdot q^{Chl}_{phy} \cdot PAR / p^{max}_{phy}\right)\right) \tag{19}$$

$$p_{dia} = p^{max}_{dia} \cdot \left(1 - \exp\left(-\alpha_{dia} \cdot q^{Chl}_{dia} \cdot PAR / p^{max}_{dia}\right)\right) \tag{20}$$

The apparent maximum photosynthetic rates (p^{max}_{phy} and p^{max}_{dia}) are based on the true constant maximum photosynthetic rates μ^{max}_{phy} and μ^{max}_{dia}, but vary with the metabolic state of the cell, external dissolved Fe concentration and temperature:

$$p^{max}_{phy} = \mu^{max}_{phy} \cdot f_T \cdot \min(l^{Fe}_{phy}, l^{N}_{min}) \tag{21}$$

$$p^{max}_{dia} = \mu^{max}_{dia} \cdot f_T \cdot \min(l^{Fe}_{dia}, l^{N}_{min}, l^{Si}_{min}) \tag{22}$$

Growth, as most metabolic processes is faster at higher temperatures. We parameterize this by multiplication of the maximum growth rate with an Arrhenius function f_T of the local temperature (T in Kelvin), relative to a reference temperature T_{ref}:

$$f_T = \exp\left(-4500 \cdot \left(\frac{1}{T} - \frac{1}{T_{ref}}\right)\right) \tag{23}$$

Growth-limitation by iron is represented by a Michaelis-Menten term

$$l^{Fe}_{phy} = \frac{\mathrm{DFe}}{\mathrm{DFe} + K^{Fe}_{phy}}, \quad l^{Fe}_{dia} = \frac{\mathrm{DFe}}{\mathrm{DFe} + K^{Fe}_{dia}} \tag{24}$$

while nitrogen limitation of nanophytoplankton and diatoms is modeled as a function of the intracellular nitrogen quota q, with growth ceasing completely at a minimum quota q_{min}

$$l^N_{min} = f(q_{min}, q, \theta_{min}) \tag{25}$$

For diatoms, photosynthesis is also downregulated if the cellular Si:C ratio (q^{Si}) approaches a minimum ratio q^{Si}_{min}

$$l^{Si}_{min} = f(q^{Si}_{min}, q^{Si}, \theta^{Si}_{min}) \tag{26}$$

θ_{min} and θ^{Si}_{min} are dimensionless constants which regulate the steepness of the quota-growth relation (see Eq. 13).

The respiration rates (r_{phy} and r_{dia}) represent the sum of maintenance metabolic losses and the costs of biosynthesis, which are proportional to the rates of nutrient assimilation:

$$r_{phy} = \eta_{phy} \cdot f^{lim}_{phy} + \zeta^N \cdot a^N_{phy} \tag{27}$$

$$r_{dia} = \eta_{dia} \cdot f^{lim}_{dia} + \zeta^N \cdot a^N_{dia} + \zeta^{Si} \cdot a^{Si}_{dia} \tag{28}$$

See Eq. 14 and Eq. 15 for the limiting functions f^{lim} of the constant maintenance respiration rates η_{phy} and η_{dia}. ζ denotes the cost for nutrient uptake and synthesis of cellular machinery in mol carbon per mol of nitrogen and silicon, respectively. See Eq. 11, Eq. 12 and Eq. 34 for details of the nutrient assimilation rates.

Chlorophyll (Chl_{phy} and Chl_{dia}) Chlorophyll synthesis is modeled as a function of irradiance and of nitrogen assimilation. Chlorophyll is degraded with a fixed rate (d^{Chl}), and lost via aggregation (g) and grazing (G).

$$S(\mathrm{Chl}_{phy}) = s_{phy} \cdot \mathrm{C}_{phy} - (d^{Chl}_{phy} + g) \cdot \mathrm{Chl}_{phy} - G_{phy} \cdot q^{Chl:N}_{phy} \tag{29}$$

$$S(\mathrm{Chl}_{dia}) = s_{dia} \cdot \mathrm{C}_{dia} - (d^{Chl}_{dia} + g) \cdot \mathrm{Chl}_{dia} - G_{dia} \cdot q^{Chl:N}_{dia} \tag{30}$$

See Eq. 16 for the aggregation rate (g). The grazing flux G in terms of nitrogen biomass is converted to chlorophyll using the intracellular Chl:N ratio ($q^{Chl:N}$).

The chlorophyll synthesis rate s is assumed to be proportional to the nitrogen assimilation rate, as nitrogen is required for the synthesis of chlorophyll, for light harvesting and in the photosynthetic apparatus:

$$s_{phy} = a^N_{phy} \cdot q^{Chl:N}_{phy\,max} \cdot \min\left(1, \frac{p_{phy}}{\alpha_{phy} \cdot q^{Chl}_{phy} \cdot PAR}\right) \tag{31}$$

$$s_{dia} = a^N_{dia} \cdot q^{Chl:N}_{dia\,max} \cdot \min\left(1, \frac{p_{dia}}{\alpha_{dia} \cdot q^{Chl}_{dia} \cdot PAR}\right) \tag{32}$$

The carbon-specific nitrogen assimilation rates (a^N_{phy} and a^N_{dia}, see Eq. 11 and 12) are converted to chlorophyll units by multiplication with a constant maximum Chl:N ratio

($q^{Chl:N}_{phy\,max}$) and $q^{Chl:N}_{dia\,max}$). The regulation term $\min(1, p_{phy}/(\alpha_{phy} \cdot q^{Chl}_{phy} \cdot PAR))$ reflects the ratio of enery assimilated to energy absorbed; it increases under low irradiance and declines as photosynthesis becomes light saturated and/or nutrient limited. See Eq. 19 and Eq. 20 for the descriptions of photosynthesis rate p_{phy} and p_{dia}.

Diatom silica pool (Si_{dia}) The silica frustule of diatoms is built through silicate assimilation. Any term that leads to a decrease in N-biomass through excretion, grazing or aggregation, on the other hand, leads to a corresponding transfer of silica to the detritus silica pool.

$$S(\mathrm{Si}_{dia}) = a^{Si}_{dia} \cdot \mathrm{C}_{dia} - (\epsilon^{N}_{dia} \cdot f^{lim}_{dia} + g) \cdot \mathrm{Si}_{dia} - G_{dia} \cdot q^{Si:N}_{dia} \tag{33}$$

The intracellular Si:N ratio $q^{Si:N}_{dia}$ is used to convert the grazing flux G_{dia} (Eq. 42) to the corresponding loss in biogenic silica. See Eq. 16 for the aggregation rate (g) and Eq. 15 for the function (f^{lim}_{dia}) limiting the excretion rate (ϵ^{N}_{dia}).

Silicate assimilation is treated as a relatively independent metabolic pathway. Here, silicon uptake is formulated as Michaelis-Menten kinetics. The maximum silicon uptake rate is calculated from the constant maximum photosynthesis rate (μ^{max}_{dia}) by multiplying it with a constant maximum Si:C uptake ratio (σ^{Si}_{dia}), and is regulated by intracellular N:C and Si:C ratios (f^{lim}_{dia} and f^{Si}_{dia}) and temperature (f_T). Silicon uptake is reduced when cellular Si:C ratios (q^{Si}) approach the maximum Si:C ratio (q^{Si}_{max}). θ^{Si}_{max} is a dimensionless constant which is used to regulate the slope.

$$a^{Si}_{dia} = \mu^{max}_{dia} \cdot \sigma^{Si}_{dia} \cdot f_T \cdot f^{lim}_{dia} \cdot f^{Si}_{dia} \cdot \left(\frac{\mathrm{DSi}}{\mathrm{DSi} + K^{\mathrm{Si}}_{dia}}\right) \tag{34}$$

$$f^{Si}_{dia} = f(q^{Si}, q^{Si}_{max}, \theta^{Si}_{max}) \tag{35}$$

Iron limitation shows an indirect influence on silicate assimilation via variable intracellular Si:N:C ratios by affecting the assimilation of nitrogen and carbon. See Eq. 15 for the description of the limiting function f^{lim}_{dia} and Eq. 23 for the definition of the temperature dependence f_T.

Calcite pool ($\mathrm{CaCO}_{3\,phy}$) In REcoM-2, the formation of biogenic calcium carbonate is limited to calcifying phytoplankton (i.e. coccolithophorids) which are assumed to form a constant fraction of the non-diatom phytoplankton. Formation of CaCO_3 by heterotrophs, such as foraminifera or pteropods is neglected. Biogenic CaCO_3 is transformed into detritus CaCO_3 along with organic matter excretion, respiration, aggregation and grazing.

$$S(\mathrm{CaCO}_{3\,phy}) = Z - (\epsilon^{C}_{phy} \cdot f^{lim}_{phy} + r_{phy} + g) \cdot \mathrm{CaCO}_{3\,phy} - G_{phy} \cdot q^{CaCO_3:N}_{phy} \tag{36}$$

Calcification (Z) is proportional to gross carbon fixation by nanophytoplankton:

$$Z = \psi \cdot p_{phy} \cdot \mathrm{C}_{phy} \tag{37}$$

ψ is the calcite production ratio that incorporates the ratio of calcium carbonate producers to total nanophytoplankton and the CaCO_3:POC ratio in coccolithophorids. The latter

is assumed to be 1.

See Eq. 14 for the function f_{phy}^{lim} limiting the excretion rate ϵ_{phy}^{C}. Nanophytoplankton photosynthesis (p_{phy}) respiration (r_{phy}) and aggregation (g) rates are defined in Eq. 19, Eq. 27 and Eq. 16, respectively. The grazing flux G_{phy} (Eq. 41) is calculated in units of nitrogen biomass and converted to $CaCO_3$ using the intracellular $CaCO_3$:N ratio ($q_{phy}^{CaCO_3:N}$).

4 Heterotrophs

Nitrogen pool (N_{het}) Heterotrophic zooplankton increase their nitrogen pool via grazing, and loose nitrogen through excretion of DON and a quadratic mortality term:

$$S(\mathrm{N}_{het}) = G \cdot \gamma - m_{het} \cdot \mathrm{N}_{het}^2 - \epsilon_{het}^{N} \cdot \mathrm{N}_{het} \tag{38}$$

A quadratic term is used for the mortality of heterotrophs ($m_{het} \cdot \mathrm{N}_{het}^2$), and the excretion rate ϵ_{het}^{N} transfers heterotrophic nitrogen directly to the DON pool. The grazing efficiency γ determines how much of the grazed phytoplankton is built into heterotrophic biomass. We assume that sloppy feeding and the formation of feces transfer the remainder of the grazed phytoplankton directly to detritus.

The grazing on nanophytoplankton and diatoms is defined as:

$$G = \xi \cdot \frac{(\mathrm{N}_{phy} + \mathrm{N}_{dia}^{'})^2}{\varphi_1 + (\mathrm{N}_{phy} + \mathrm{N}_{dia}^{'})^2} \cdot f_T \cdot \mathrm{N}_{het} \tag{39}$$

The grazing rate is calculated from a constant maximum grazing rate (ξ) by multiplication with a sigmoidal dependency of nutritional intake to resource density with half-saturation constant φ_1. It depends on temperature following the same relationship as for phytoplankton growth (f_T). $\mathrm{N}_{dia}^{'}$ encompasses a preference term for grazing on diatoms, relative to that on nanophytoplankton:

$$\mathrm{N}_{dia}^{'} = \tau \cdot \frac{\mathrm{N}_{dia}^2}{\varphi_2 + \mathrm{N}_{dia}^2} \cdot \mathrm{N}_{dia} \tag{40}$$

Here, τ is the maximum diatom preference and is smaller than one, which implies that zooplankton grazes preferably on nanophytoplankton; the effective grazing preference is allowed to vary with diatom biomass, with φ_2 being the half saturation parameters for grazing preference of diatoms. $\varphi_2 = 0$ implies a constant preference.

The relative contributions of grazing on nanophytoplankton and on diatoms to the total grazing flux are calculated by their respective proportion to the total zooplankton food resource.

$$G_{phy} = G \cdot \frac{\mathrm{N}_{phy}}{\mathrm{N}_{phy} + \mathrm{N}_{dia}^{'}} \tag{41}$$

$$G_{dia} = G \cdot \frac{\mathrm{N}_{dia}^{'}}{\mathrm{N}_{phy} + \mathrm{N}_{dia}^{'}} \tag{42}$$

Carbon pool (C_{het}) The heterotrophic carbon biomass is a balance between carbon uptake via grazing and carbon loss via mortality, carbon excretion and respiration.

$$\begin{aligned} S(\mathrm{C}_{het}) = & \left(\frac{1}{q_{phy}} \cdot G_{phy} + \frac{1}{q_{dia}} \cdot G_{dia}\right) \cdot \gamma - \frac{1}{q_{het}} \cdot m_{het} \cdot \mathrm{N}_{het}^2 \\ & - \epsilon_{het}^{C} \cdot \mathrm{C}_{het} - r_{het} \cdot \mathrm{C}_{het} \end{aligned} \tag{43}$$

The grazing flux in terms of nitrogen biomass is converted to carbon biomass using the respective intracellular N:C ratios (q_{phy} and q_{dia}). Sloppy feeding causes some of the grazed phytoplankton to be transferred directly to the detritus pool, as determined by the grazing efficiency γ. The remainder is built into heterotropic biomass. The quadratic mortality flux ($m_{het} \cdot \mathrm{N}_{het}^2$), which causes carbon to be lost to the detritus compartment, is converted to carbon using the intracellular heterotrophic N:C ratio (q_{het}). When the C:N ratio in heterotrophs ($q_{het}^{C:N} = 1/q_{het}$) exceeds the Redfield ratio, heterotrophic respiration is assumed to drive the ratio back towards Redfield, with a time-scale κ_{het}:

$$r_{het} = \begin{cases} f_T \cdot (q_{het}^{C:N} - q_{Redfield}^{C:N})/\kappa_{het} & \text{if} \quad q_{het}^{C:N} > q_{Redfield}^{C:N} \\ 0 & \text{if} \quad q_{het}^{C:N} \leq q_{Redfield}^{C:N} \end{cases} \tag{44}$$

5 Detritus

Nitrogen pool (N_{det}) Losses of phytoplankton nitrogen due to aggregation, mortality and sloppy feeding have to pass the N_{det} compartment before being degraded to DON, which is the only loss term for detrital nitrogen.

$$S(\mathrm{N}_{det}) = G \cdot (1-\gamma) + g \cdot (\mathrm{N}_{phy} + \mathrm{N}_{dia}) + m_{het} \cdot \mathrm{N}_{het}^2 - \rho_{PON} \cdot f_T \cdot \mathrm{N}_{det} \tag{45}$$

See section 4 for a definition of the grazing flux G, the grazing efficiency γ and the zooplankton mortality flux ($m_{het} \cdot \mathrm{N}_{het}^2$). The aggregation rate g is defined in Eq. 16. Degradation of N_{det} to DON is based on a constant degradation rate (ρ_{PON}) and a temperature dependency (f_T, Eq. 23).

Carbon pool (C_{det}) The C_{det} compartment is balanced by carbon sources associated with sloppy feeding, aggregation of phytoplankton, mortality of heterotrophs and degradation of C_{det} to DOC as the only loss term.

$$\begin{aligned} S(\mathrm{C}_{det}) = & \left(\frac{1}{q_{phy}} \cdot G_{phy} + \frac{1}{q_{dia}} \cdot G_{dia}\right) \cdot (1-\gamma) + g \cdot (\mathrm{C}_{phy} + \mathrm{C}_{dia}) \\ & + \frac{1}{q_{het}} \cdot m_{het} \cdot \mathrm{N}_{het}^2 - \rho_{POC} \cdot f_T \cdot \mathrm{C}_{det} \end{aligned} \tag{46}$$

The grazing and the quadratic mortality flux (see section 4), which are calculated in terms of N biomass, are converted to carbon biomass via the respective intracellular N:C ratios (q_{phy}, q_{dia} and q_{het}). The sloppy feeding part of the grazing flux is transfered to the C_{det} compartment, while the main grazing flux is built into heterotrophic biomass,

as determined by the grazing efficiency γ. The degradation term consists of a constant degradation rate ρ_{POC} and takes into account a temperature dependency f_T (see Eq. 23).

Silica pool (Si_{det}) The detrital silica budget consists of aggregation, grazing and excretion fluxes from diatoms to detritus and silica dissolution, which shifts silicon from Si_{det} to dissolved silicate.

$$S(\mathrm{Si}_{det}) = (g + \epsilon^N_{dia} \cdot f^{lim}_{dia}) \cdot \mathrm{Si}_{dia} + G_{dia} \cdot q^{Si:N}_{dia} - \rho^T_{Si} \cdot \mathrm{Si}_{det} \tag{47}$$

See section 3 for definitions of the aggregation (g) and excretion (ϵ) fluxes and section 4 for the grazing fluxes (G).

The silica dissolution rate ρ^T_{Si} follows the temperature dependence of *Kamatani* (1982), until it exceeds the maximum dissolution rate ρ_{Si}

$$\rho^T_{Si} = min(1.32 \cdot 10^{16} \cdot \exp(\frac{-11200}{T}), \rho_{Si}) \tag{48}$$

Calcium carbonate pool ($\mathrm{CaCO}_{3\,det}$) Nanophytoplankton loses CaCO_3 to the detrital CaCO_3 compartment via excretion, respiration, aggregation and grazing. Dissolution of CaCO_3 leads to an increase in DIC and alkalinity (see section 1).

$$\begin{aligned} S(\mathrm{CaCO}_{3\,det}) = (&\epsilon^C_{phy} \cdot f^{lim}_{phy} + r_{phy} + g + G_{phy} \cdot q^{CaCO_3:N}_{phy}) \cdot \mathrm{CaCO}_{3\,phy} \\ &- \lambda \cdot \mathrm{CaCO}_{3\,det} \end{aligned} \tag{49}$$

The nanophytoplankton excretion term (ϵ^C_{phy}) is regulated by intracellular quota as defined in Eq. 14. Refer to section 3 for a definition of the respiration (r_{phy}) and the aggregation (g) rates. The grazing flux is calculated in terms of nitrogen biomass (Eq. 41) and is converted to $\mathrm{CaCO}_{3\,det}$ by multiplication with the intracellular CaCO_3:N ratio ($q^{CaCO_3:N}_{phy}$).

Detrital calcite decreases exponentially with water depth with a vertical length scale of 3500 m according to *Yamanaka and Tajika* (1996). The dissolution rate λ [d^{-1}] depends on the sinking speed of detritus, so that

$$\lambda = \frac{w_{det}}{3500\ m} \tag{50}$$

where w_{det} increases with depth according to

$$w_{det} = 20\ m\ s^{-1} + 0.0288\ s^{-1} \cdot\ depth\ (m) \tag{51}$$

6 Dissolved Organic Matter (DOM)

Dissolved Organic Nitrogen (DON) DON is produced via N excretion by nanophytoplankton, diatoms and heterotrophs, and by degradation of detrital N. It is turned into

DIN by remineralization.

$$S(\mathrm{DON}) = \epsilon^N_{phy} \cdot f^{lim}_{phy} \cdot \mathrm{N}_{phy} + \epsilon^N_{dia} \cdot f^{lim}_{dia} \cdot \mathrm{N}_{dia} + \epsilon^N_{het} \cdot \mathrm{N}_{het} + \rho_{PON} \cdot f_T \cdot \mathrm{N}_{det} - \rho_{\mathrm{DON}} \cdot f_T \cdot \mathrm{DON} \tag{52}$$

The constant excretion rates of phytoplankton (ϵ^N_{phy} and ϵ^N_{dia}) are reduced if the N:C ratio is larger than a threshold (see Eq. 14 and Eq. 15). Heterotrophic nitrogen excretion ($\epsilon^N_{het} \cdot \mathrm{N}_{het}$) depends only on the heterotrophic biomass. Degradation of N_{det} to DON and remineralization from DON to DIN is temperature dependent, so that the constant degradation (ρ_{PON}) and remineralization (ρ_{DON}) rates are multiplied with the Arrhenius function (f_T, see Eq. 23).

Dissolved Organic Carbon (DOC**)** DOC sources are carbon excretion by nanophytoplankton, diatoms and heterotrophs, and degradation of C_{det}. Remineralization of DOC leads to a transfer of carbon from DOC to DIC.

$$S(\mathrm{DOC}) = \epsilon^C_{phy} \cdot f^{lim}_{phy} \cdot \mathrm{C}_{phy} + \epsilon^C_{dia} \cdot f^{lim}_{dia} \cdot \mathrm{C}_{dia} + \epsilon^C_{het} \cdot \mathrm{C}_{het} + \rho_{POC} \cdot f_T \cdot \mathrm{C}_{det} - \rho_{\mathrm{DOC}} \cdot f_T \cdot \mathrm{DOC} \tag{53}$$

Metabolic excretion of organic matter by phytoplankton is determined by a constant excretion rate (ϵ^C_{phy} and ϵ^C_{dia}) and cell quota (see section 3). The heterotrophic excretion rate per heterotrophic biomass is constant (ϵ^C_{het}). The constant degradation (ρ_{POC}) and remineralization (ρ_{DOC}) rates that determine the fluxes from C_{det} to DOC and from DOC to DIC are altered following the Arrhenius function (f_T, Eq. 23).

7 Boundary conditions and early diagenesis

In its present version, REcoM-2 considers neither riverine input of nutrients, carbon and alkalinity, nor permanent burial of organic matter, calcium carbonate and silica in the sediment. At the sea surface, we assume no normal flux of tracers, except for DIC that can exchange with the atmospheric reservoir of CO_2. This surface boundary condition can be written as

$$\kappa \frac{\partial A}{\partial z}\bigg|_{z=\eta} = \begin{cases} 0 & \text{for} \quad A \neq \mathrm{DIC} \\ F_{\mathrm{C}} & \text{for} \quad A = \mathrm{DIC} \end{cases} \tag{54}$$

where η is the sea surface elevation, and the air-sea flux of carbon F_{C} (positive for flux out of the ocean) is calculated from DIC, TA, atmospheric $p\mathrm{CO}_2$, temperature, salinity and wind speed, follwing OCMIP protocols. Likewise, we assume no horizontal flux of tracers at lateral boundaries.

At the bottom of the ocean, the sinking flux of particulates (nanophytoplankton, diatoms and detritus) is directed into a homogeneous sediment layer, where POC and PON are degraded and instantaneously remineralized and calcium carbonate and silica are dis-

solved with fixed rates. The corresponding equations are

$$\begin{aligned}
\frac{\partial \mathrm{POC}_{sed}}{\partial t} &= w_{det} \cdot \mathrm{C}_{det} - d^{C} \cdot \mathrm{POC}_{sed} \\
\frac{\partial \mathrm{PON}_{sed}}{\partial t} &= w_{det} \cdot \mathrm{N}_{det} - d^{N} \cdot \mathrm{PON}_{sed} \\
\frac{\partial \mathrm{Si}_{sed}}{\partial t} &= w_{det} \cdot \mathrm{Si}_{det} - d^{Si} \cdot \mathrm{Si}_{sed} \\
\frac{\partial \mathrm{CaCO_3}_{sed}}{\partial t} &= w_{det} \cdot \mathrm{CaCO_3}_{det} - d^{CaCO_3} \cdot \mathrm{CaCO_3}_{sed}
\end{aligned} \tag{55}$$

where POC_{sed}, POC_{sed}, Si_{sed}, and $\mathrm{CaCO_3}_{sed}$ are vertically integrated concentrations in the sediment layer, i.e. they have the unit mol m^{-2}. d^{C}, d^{N}, d^{Si}, and d^{CaCO_3} are the degradation or dissolution rates for POC, PON, Si and $\mathrm{CaCO_3}$, respectively.

The nutrients and alkalinity released during the degradation/remineralization and dissolution are directly returned into the water as a flux, i.e. the boundary condition at the ocean bottom is

$$\kappa \frac{\partial A}{\partial z}\bigg|_{z=-H} = \begin{cases}
d^{C} \cdot \mathrm{POC}_{sed} + d^{CaCO_3} \cdot \mathrm{CaCO_3}_{sed} & \text{for} \quad A = \mathrm{DIC} \\
d^{N} \cdot \mathrm{PON}_{sed} & \text{for} \quad A = \mathrm{DIN} \\
(1 + 1/16) \cdot d^{N} \cdot \mathrm{PON}_{sed} + 2 d^{CaCO_3} \cdot \mathrm{CaCO_3}_{sed} & \text{for} \quad A = \mathrm{TA} \\
d^{Si} \cdot \mathrm{Si}_{sed} & \text{for} \quad A = \mathrm{DSi} \\
q^{Fe} \cdot d^{C} \cdot \mathrm{POC}_{sed} & \text{for} \quad A = \mathrm{DFe} \\
0 & \text{for} \quad \text{all other tracers}
\end{cases} \tag{56}$$

References

Geider, R. J., H. L. MacIntyre, and T. M. Kana (1998), A dynamic regulatory model of phytoplanktonic acclimation to light, nutrients, and temperature, *Limnology and Oceanography*, *43*, 679–694, doi:10.4319/lo.1998.43.4.0679.

Hohn, S. (2009), Coupling and decoupling of biogeochemical cycles in marine ecosystems, *PhD Thesis, Universität Bremen*, http://elib.suub.uni-bremen.de/diss/docs/00011278.pdf.

Kamatani, A. (1982), Dissolution rates of silica from diatoms decomposing at various temperatures, *Marine Biology*, *68*, 91–96.

Parekh, P., M. J. Follows, and E. Boyle (2004), Modeling the global ocean iron cycle, *Global Biogeochemical Cycles*, *18, GB1002*, doi:10.1029/2003GB002061.

Schartau, M., A. Engel, J. Schröter, S. Thoms, C. Völker, and D. Wolf-Gladrow (2007), Modelling carbon overconsumption and the formation of extracellular particulate organic carbon, *Biogeosciences*, *4*, 433–454, doi:10.5194/bg-4-433-2007.

Yamanaka, Y., and E. Tajika (1996), The role of the vertical fluxes of particulate organic matter and calcite in the oceanic carbon cycle: Studies using an ocean biogeochemical general circulation model, *Global Biogeochemical Cycles*, *10*, 361–382, doi:10.1029/96GB00634.

Table 1: Model coefficients and their standard values

Symbol	Value	Unit	Parameter
T_{ref}	288.15	K	reference temperature
ψ	0.02	dimensionless	calcite production ratio
q^{Fe}	0.005	μmol Fe (mmol C)$^{-1}$	Fe:C ratio
κ_{Fe}^{scav}	0.001	d^{-1}	Fe scavenging rate
α_{phy}	0.19	mmol C (mg Chl)$^{-1}$ (W m^{-2} d)$^{-1}$	initial slope of P-I curve
α_{dia}	0.26	mmol C (mg Chl)$^{-1}$ (W m^{-2} d)$^{-1}$	diatom initial slope of P-I curve
μ_{phy}^{max}	3.0	d^{-1}	maximum photosynthesis rate
μ_{dia}^{max}	3.0	d^{-1}	diatom maximum photosynthesis rate
ϵ_{phy}^{N}	0.05	d^{-1}	excretion rate of nitrogen
ϵ_{dia}^{N}	0.05	d^{-1}	diatom excretion rate of nitrogen
ϵ_{phy}^{C}	0.10	d^{-1}	excretion rate of carbon
ϵ_{dia}^{C}	0.10	d^{-1}	diatom excretion rate of carbon
σ_{phy}^{N}	0.20	mol N (mol C)$^{-1}$	N:C uptake ratio
σ_{dia}^{N}	0.20	mol N (mol C)$^{-1}$	diatom N:C uptake ratio
σ_{dia}^{Si}	0.20	mol Si (mol C)$^{-1}$	diatom Si:C uptake ratio
K_{phy}^{N}	0.55	mmol N m^{-3}	half-saturation constant N uptake
K_{dia}^{N}	1.0	mmol N m^{-3}	diatom half-saturation constant N uptake
K_{phy}^{Fe}	0.02	μmol Fe m^{-3}	half-saturation constant Fe uptake
K_{dia}^{Fe}	0.12	μmol Fe m^{-3}	diatom half-saturation constant Fe uptake
K_{dia}^{Si}	4.0	mmol Si m^{-3}	diatom half-saturation constant Si uptake
$q_{phy\,max}$	0.20	mol N (mol C)$^{-1}$	maximum N:C ratio
$q_{dia\,max}$	0.20	mol N (mol C)$^{-1}$	diatom maximum N:C ratio
q_{max}^{Si}	0.80	mol Si (mol C)$^{-1}$	diatom maximum Si:C ratio
q_{min}	0.04	mol N (mol C)$^{-1}$	minimum N:C ratio
q_{min}^{Si}	0.04	mol Si (mol C)$^{-1}$	minimum Si:C ratio
$q_{phy\,max}^{Chl:N}$	4.2	mg Chl (mmol N)$^{-1}$	nanophytoplankton maximum Chl:N ratio
$q_{dia\,max}^{Chl:N}$	5.6	mg Chl (mmol N)$^{-1}$	diatom maximum Chl:N ratio
θ_{max}	1000	dimensionless	regulation slope
θ_{min}	50	dimensionless	regulation slope
θ_{min}^{Si}	1000	dimensionless	regulation slope
θ_{max}^{Si}	1000	dimensionless	regulation slope
ζ^{N}	2.33	mol C (mol N)$^{-1}$	C cost of N assimilation
ζ^{Si}	0	mol C (mol Si)$^{-1}$	C cost of Si assimilation
ϕ_{phy}	0.02	(mmol N m^{-3})$^{-1}$ d^{-1}	phytoplankton specific aggregation rate
ϕ_{det}	0.22	(mmol N m^{-3})$^{-1}$ d^{-1}	detrius specific aggregation rate
η_{phy}	0.01	d^{-1}	maintenance respiration rate
η_{dia}	0.01	d^{-1}	diatom maintenance respiration rate
d_{phy}^{Chl}	0.3	d^{-1}	chlorophyll degradation rate
d_{dia}^{Chl}	0.3	d^{-1}	diatom chlorophyll degradation rate
γ	0.3	dimensionless	grazing efficiency

Table 2: Model coefficients and their standard values

Symbol	Value	Unit	Parameter
m_{het}	0.05	(mmol N m^{-3})$^{-1}$ d^{-1}	quadratic mortality rate
ϵ^N_{het}	0.1	d^{-1}	zooplankton N excretion rate
ϵ^C_{het}	0.1	d^{-1}	zooplankton C excretion rate
φ_1	0.35	(mmol N m^{-3})^2	half-saturation constant for grazing
φ_2	0	(mmol N m^{-3})^2	half-saturation constant for diatom grazing preference
ξ	2.4	mmol N m^{-3} d^{-1}	maximum grazing rate
τ	0.5	dimensionless	maximum preference for grazing on diatoms
$q^{C:N}_{Redfield}$	6.625	mol C (mol N)$^{-1}$	Redfield ratio of C:N
κ_{het}	0.01	d	time-scale for restoring towards Redfield
ρ_{PON}	0.165	d^{-1}	PON degradation rate
ρ_{POC}	0.15	d^{-1}	POC degradation rate
ρ_{DON}	0.11	d^{-1}	DON remineralisation rate
ρ_{DOC}	0.1	d^{-1}	DOC remineralisation rate
ρ_{Si}	0.02	d^{-1}	Si dissolution rate
L_T	1	μmol m^{-3}	total ligand concentration
K_{FeL}	100	m^3 μmol^{-1}	ligand stability constant
d^{C}	0.005	d^{-1}	POC degradation rate in sediment
d^{N}	0.005	d^{-1}	PON degradation rate in sediment
d^{Si}	0.005	d^{-1}	Si degradation rate in sediment
$d^{\mathrm{CaCO_3}}$	0.005	d^{-1}	$CaCO_3$ degradation rate in sediment

Chapter 6

Synthesis

6.1 Current and Future Changes in the Southern Ocean Carbon Cycle

The Southern Ocean is and will continue to experience various changes in a high-CO_2 world, which affect carbon cycling and thereby feed back on the atmospheric CO_2 concentration and climate. For instance, global warming is competing with regional cooling in the Southern Ocean, which is related to the continuing positive trend in the Southern Annular Mode (SAM) index. Both processes are a result of the anthropogenic changes of the atmospheric composition and they have opposite implications for ocean mixing. On the one hand, global warming leads to more stratification; on the other hand, the high-index polarity of the SAM induces stronger westerly winds, which leads to more mixing (see chapter 2.5). Any circulation change will feed back on carbon and nutrient cycling and might start a chain of consequences. These indirect effects of CO_2 emissions are overlain by the direct effect of higher partial pressure of CO_2 (pCO_2) in the atmosphere. The latter amplifies the pCO_2 gradient between ocean and atmosphere, which forces the ocean to take up more CO_2. As a consequence, carbonate equilibria shift and the ocean becomes more acidic.

The main focus of this thesis is to examine two processes in the changing Southern Ocean carbon cycle:

1. The dissolution of carbonate sediments from Antarctic shelves as a repercussion of ocean acidification (chapters 3 and 4) and

2. the consequences of changes and variability of atmospheric forcing for upper ocean carbon fluxes (chapter 5).

The two different process studies will first be discussed separately here, followed by a general discussion of the implications for the conceptual picture of the future Southern Ocean carbon cycle.

6.2 Dissolution of carbonate sediments

Due to the higher pCO_2 in the atmosphere, the Southern Ocean has turned from a preindustrial source to a contemporary sink for CO_2 (*Hoppema*, 2004b). The uptake of anthropogenic carbon simultaneously decreases the pH of the surface water and the saturation states of calcite and aragonite. The present day calcite and aragonite saturation states in the Southern Ocean are low in comparison to other regions and the changes are largest at the surface due to anthropogenic CO_2 uptake from the atmosphere. In combination,

this suggests that carbonate undersaturation might occur at the surface before the entire underlying water column will be undersaturated (*Hauck et al.*, 2010). The effects on Southern Ocean calcifiers and ecosystems are mostly unclear, though there is increasing evidence that acidification impairs calcification by various organisms (*Orr et al.*, 2005; *Moy et al.*, 2009; *Beaufort et al.*, 2011). It is clear, on the other hand, that carbonate sediments will start to dissolve when exposed to a carbonate undersaturated water column (e.g. *Keir*, 1980).

In a previous study, *Andersson et al.* (2003) applied a box model to conclude that there are insufficient amounts of $CaCO_3$ to buffer acidification globally. These authors define a buffer effect as a process, which restores pH to its original value after a small perturbation. This is mainly attributed to the fact that the dissolution is slow and the alkalinity signal will subsequently be diluted by mixing processes. As the shallow-water dissolution signal is only released along the continental margins and anthropogenic CO_2 uptake occurs globally, the shallow carbonates cannot maintain a global surface pH of 8.2 as in preindustrial times. Nevertheless, alkalinity accumulation can occur on smaller spatial scale (*Andersson et al.*, 2007), and the results of the global box model might not be applicable to all oceanic regions individually. This alkalinity accumulation could locally or regionally mitigate ocean acidification or enhance the ocean's CO_2 uptake capacity compared to a scenario without shallow $CaCO_3$ dissolution. A negative feedback of any magnitude is relevant for future acidification scenarios. Therefore, in the following, the term *buffering* refers to a process of alkalinity release, which increases pH, but does not necessarily restore it to its original value.

In order to assess the role of carbonate sediments for future pH changes, several critical questions need to be answered: How much carbonate is available in the next decades or centuries for dissolution as a response to calcite and aragonite undersaturation? Will the sediments release a significant alkalinity signal that can mitigate or retard acidification and enhance the ocean's capability to take up CO_2 from the atmosphere?

The size of the carbonate reservoir and factors that affect sediment $CaCO_3$ content and mineralogy were addressed in chapter 3, and the results can be summarized as follows:

- The bottom water over the Antarctic shelves all around the continent is oversaturated with respect to calcite. High-Salinity Shelf Water and Ice-Shelf Water are oversaturated with respect to calcite and aragonite and cannot be responsible for dissolution of $CaCO_3$ in contrast to the hypothesis by *Anderson* (1975). Aragonite undersaturation at shallow depths (300 – 700 m) occurs where Circumpolar Deep Water comes close to the shelf break, such as along the western Antarctic Peninsula or in parts of the southwest Pacific and Indian Ocean (*Orsi et al.*, 1995).

- High $CaCO_3$ contents (>15% mass of sediment) were found at shallow depths (150 – 200 m) and between 600 and 900 m water depth on the broad shelves of the Amundsen, Bellingshausen and western Weddell Seas. The latter coincides with the outer shelf regions, where winnowing by currents likely plays a role.

- Insignificant (<2%) amounts of $CaCO_3$ were found in the regions with high primary production levels, such as the western Antarctic Peninsula, the Ross Sea and Prydz Bay, likely due to the metabolic-CO_2 release during oxic remineralization of organic matter in the sediments.

- Aragonite was not found in the sediment. The aragonite saturation horizon is currently at about 1000 m depth, but small amounts of metabolic CO_2 can further acidify the pore water and shift the "apparent" aragonite saturation horizon as experienced by the pore waters to shallow depths. Hence, aragonite probably dissolves in the sediments.

These results provided the foundation for the estimate of the total inventory of $CaCO_3$ on all Antarctic shelves (chapter 4). As $CaCO_3$ was distributed very patchily on a sub-regional scale, a simple spatial interpolation would not be appropriate to integrate the $CaCO_3$ content all around the Antarctic. A quantitative parameterization for $CaCO_3$ was developed based on the relationship between $CaCO_3$, primary production and water depth. Dissolution of $CaCO_3$ by metabolic CO_2 at high primary production levels is the most important factor in the relationship between $CaCO_3$ and primary production. In regions with high primary production, more organic carbon is deposited on the sea floor where it is remineralized. Oxic remineralization produces CO_2, acidifies the pore water, and subsequently causes dissolution of $CaCO_3$. At low primary production levels, however, the $CaCO_3$ rain to the sea floor has to increase with increasing primary production, as biogenic $CaCO_3$ production cannot occur without organic matter production. Either $CaCO_3$ is directly formed by primary producers along with organic matter, or by heterotrophic calcifiers, such as foraminifera or pteropods, given that sufficient food is supplied by primary producers. These processes suggest a relation as drawn in Figure 6.1: At low primary production levels, $CaCO_3$ increases with increasing primary production, until it reaches an optimum. Past that threshold a further increase of primary production is followed by metabolic-CO_2 release which decreases $CaCO_3$ concentration in the sediment.

In reality, a number of other factors are also important for the relative amount of $CaCO_3$ in the sediments, such as the rain of opal and terrigenous material that can dilute the carbonate content. The empirical parameterization was developed to interpolate the $CaCO_3$ data set. It does not allow to deduce a stoichiometric relationship of $CaCO_3$ and organic matter production in the euphotic zone, $CaCO_3$ dissolution and decay of organic

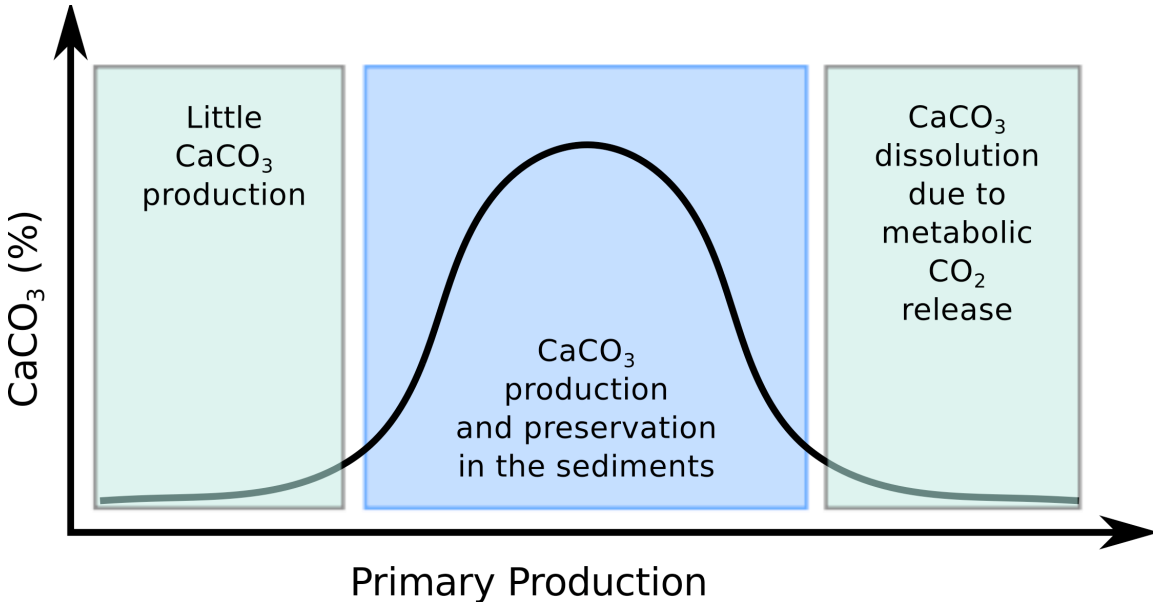

Figure 6.1: Idealized relation between primary production in the water column and $CaCO_3$ content in the sediments. $CaCO_3$ can only be produced when either primary producers form calcium carbonate along with organic matter or when food supply is sufficient to allow for heterotrophic calcification. Large organic matter deposits to the sediments can elevate the metabolic-CO_2 production, which in turn results in $CaCO_3$ undersaturation and dissolution.

matter during sinking, and $CaCO_3$ dissolution and remineralization of organic matter in the sediments. Nevertheless, $CaCO_3$ production and dissolution in the sediments are the two main processes for $CaCO_3$ accumulation and preservation in the sediments and both are dependent on organic matter production. It is thus highly likely that they determine the relationship between primary production and $CaCO_3$ (Figure 6.1).

The relationship between primary production and carbonate sediments can be used together with satellite-derived primary production estimates to chart $CaCO_3$ all around the Antarctic shelves. The total amount of $CaCO_3$ that would be available to dissolve in the next decades or centuries is 0.5 Pg C, which is comparable to the annual Southern Ocean CO_2 uptake. It is obvious from this comparison, that dissolution of $CaCO_3$ will not delay acidification considerably. Time-dependent rates, such as the CO_2 uptake rate, the $CaCO_3$ dissolution rate, the bioturbation rate, and the mixing rate of the water masses will determine when the carbonate reservoirs will be depleted. Given the small amount of total $CaCO_3$, these rates and processes were not quantified. Yet, it is clear that not all $CaCO_3$ will dissolve instantaneously, so that the alkalinity signal to be released will most probably be too small to be detectable.

Further conclusions can be drawn from the evidence gathered in this study. The dissolution of $CaCO_3$ from the Antarctic shelves will neither buffer acidification nor enhance

the CO_2 uptake capacity of the Southern Ocean significantly. The Antarctic ecosystem will be continuously subjected to acidification with all its potential implications for flora and fauna. Thus, perhaps unfortunately, humans' effort to reduce atmospheric CO_2 concentration or growth rate cannot rely on shallow carbonate dissolution from the Antarctic shelves.

Perspectives for future research

The $CaCO_3$ distribution patterns (chapter 3) were based on a data set that made use of available samples and did not cover all regions equally well. The interpolation technique (chapter 4) filled data gaps and made the inventory estimate possible. Yet, more research and samples would be of great use to produce a complete data compilation and test some of the proposed hypotheses. For example, the hypothesis whether the southwest Pacific and Indian Ocean sectors of the Antarctic shelves could be a possible accumulation site for pteropods can only be addressed with improved data. In addition, very shallow depth regions were undersampled, partly because they do not represent a large part of the Antarctic shelves, but mainly because they are hard to access by ships. These data would facilitate a more detailed analysis of the depth horizon above which aragonite can be preserved, if existent.

As hypothesised in chapter 3 large cyclonical gyre systems, such as the Weddell and Ross gyres, keep naturally more corrosive (modified) Circumpolar Deep Water away from the shelves. This hypothesis should be addressed in a follow-up study with more water column carbonate chemistry data to investigate any pattern in the calcite and aragonite saturation states on the Antarctic shelves and the role of the gyres. It is unclear if the gyres will be less severely affected by acidification than other regions or whether this effect of low 'natural acidity' will be balanced or overcompensated by high anthropogenic CO_2 uptake on the shelves.

Chapter 4 revealed the relation between primary production and the relative amount of $CaCO_3$ in the sediments. An empirical relationship between primary production and sediment $CaCO_3$ was derived and an explanation proposed. A sediment model study could be used, for example, to calculate the rain rates of organic and calcareous material to the sea floor that are needed to reproduce the $CaCO_3$ vs. primary production relationship. Such a model could also reveal possible implications for the rain ratio (organic to inorganic particulate carbon rain). Does the rain ratio increase with increasing primary production, i.e., do calcifiers contribute less to the total production at high production levels? If yes, how could this species shift be explained and is it systematic? Could we eventually even learn something on $CaCO_3$ production and how to better parameterize $CaCO_3$ production in models?

Another question would be whether the relationship between primary production and sediment $CaCO_3$ is valid globally or at least in certain regions. Would the optimum level shift due to different bottom water carbonate saturation states? Does it only work where the calcareous rain is relatively low, because otherwise the dissolution would not leave a significant signature?

6.3 Inter-annual variability of carbon fluxes

The ozone hole over Antarctica and the emission of greenhouse gases has led to a stronger thermal contrast at the top of the troposphere (*Shindell and Schmidt*, 2004; *Thompson et al.*, 2011). The stronger temperature gradient causes a stronger than usual pressure gradient, which accordingly accelerates the westerly winds (Figure 6.2). A pressure gradient that is stronger than usual is related to the positive polarity of the Southern Annular Mode, which is responsible for most of the recent climate change in the Southern Hemisphere (e.g. *Hall and Visbeck*, 2002). Hence, the intensification and poleward shift of the westerlies over the last decades is typically attributed to the trend of the SAM toward its positive phase (*Shindell and Schmidt*, 2004; *Thompson and Solomon*, 2002; *Thompson et al.*, 2011). The intensified winds accelerate gas-exchange between ocean and atmosphere, indicating that more CO_2 could be taken up at higher wind speeds. More forceful winds, however, also increase upwelling and entrainment of carbon-rich deep water, thereby reducing the gradient between atmospheric and oceanic pCO_2, which is the main driving factor for gas-exchange. The entrained deep water is also enriched in nutrients, which can stimulate phytoplankton growth and export production. How all these processes interact and what it means for the Southern Ocean carbon cycle in the future is the urgent question that needs to be answered.

A three dimensional model was used to disentangle the different co-occurring processes, such as changing circulation, biological export fluxes and gas-exchange between ocean and atmosphere (chapter 5). The perturbed carbon cycle due to climate change can be described as follows (Figure 6.2). Circulation changes have the largest effect on the surface DIC inventory. South of the Polar Front, a positive SAM induces anomalously increased upwelling and entrainment of carbon-rich deep water into the 100 m surface layer. This DIC increase is nearly balanced by the stronger northward Ekman transport of the surface water, which is now enriched with carbon. The northward advection therefore acts as a DIC sink for the region south of the Polar Front, but as a source to the region north of the Polar Front. In the north, more DIC than usual is advectively transported out of the surface layer and this additional downwelling is of about the same size as the anomalous upwelling in the south. In total, the circulation changes nearly balance in terms of DIC

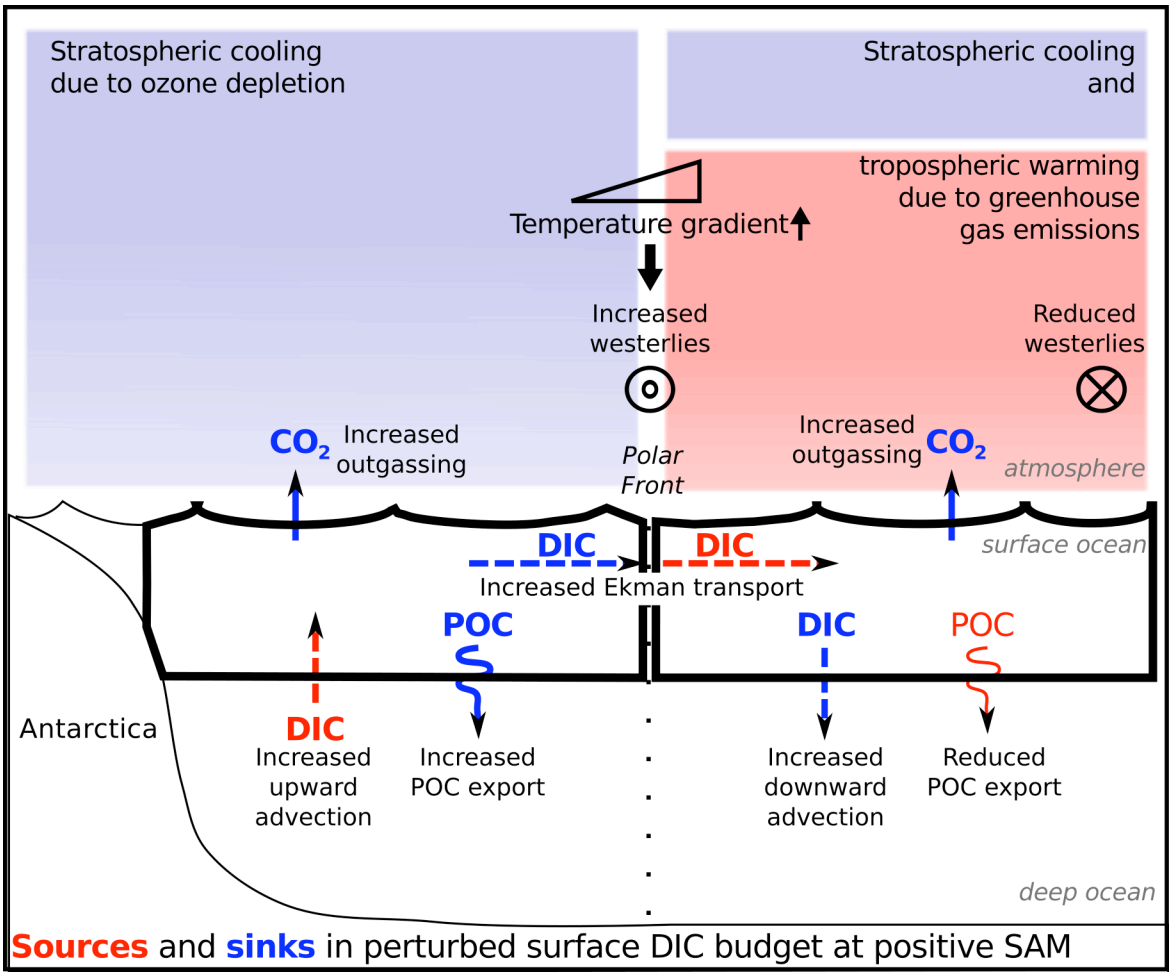

Figure 6.2: At a positive SAM the atmospheric forcing is perturbed by a stronger than usual temperature gradient at the top of the troposphere. Consequently, the westerly winds that drive the Antarctic Circumpolar Current are intensified. This leads to stronger northward Ekman transport and more upwelling and entrainment in the south and more downwelling in the north (Ekman pumping). Carbon flux anomalies that tend to increase the surface DIC inventory are marked in red, and those that decrease the inventory in blue. DIC: dissolved inorganic carbon, POC: particulate organic carbon.

transport. The northward transport, however, takes time, so that the surface DIC is increased shortly after a perturbation towards the high-index polarity of the SAM and affects the pCO_2 difference (ΔpCO_2) between ocean and atmosphere and therefore the sea-air CO_2 flux.

The resulting ΔpCO_2 is the sum of DIC increase by circulation changes and anomalous CO_2 drawdown via the biological carbon pump. The entrained deep water also carries iron and enhances diatom growth and export poduction. South of the Polar Front, more DIC is drawn down by biology than by outgassing. North of the Polar Front, export production is reduced, probably because of persistent macronutrient limitation and a deepening of

the mixed layer. Here, outgassing and downwelling of natural CO_2 are the only sinks for the surface DIC inventory.

The response of the Southern Ocean carbon cycle to the SAM was discussed in the context of natural CO_2. Practically this was done by forcing the model with the preindustrial atmospheric CO_2 concentration but today's climate (e.g. wind field), which is perturbed by humans. The contemporary Southern Ocean CO_2 uptake is the sum of natural and anthropogenic sea-air CO_2 exchange. The anthropogenic CO_2 uptake will increase in the future due to increasing CO_2 content in the atmosphere. Our results suggest that the sea-to-air flux of natural CO_2 will tend to lower the future Southern Ocean CO_2 uptake, in line with previous model studies (*Lovenduski et al.*, 2007; *Lenton and Matear*, 2007; *Le Quéré et al.*, 2007; *Lenton et al.*, 2009).

Böning et al. (2008) challenged the view that increased westerlies lead to intensified meridional overturning and they suggest a counteracting transport by eddies. The coarse resolution model used for the present study does not resolve eddies and therefore uses a parameterization to approximate their effects. This approach probably underestimates the transport by eddies; however, the eddies' response is usually delayed by two to three years. The SAM, on the other hand, oscillates between its high and low polarity on time-scales as short as weeks (*Thompson et al.*, 2011). The system cannot adjust to the new state, and therefore the question arises whether the full response by eddies, which is delayed by a few years, can be completely developed. Thus the direct response to the oscillating SAM might be more important than the delayed increase of the eddy activity. In the future, eddy compensation might become more important if the SAM will more constantly be in its positive phase. It is encouraging that preliminary eddy-permitting simulations (*Dufour*, 2011) yield the same amount of anomalous outgassing of natural CO_2 (ca. 0.1 Pg C yr^{-1}) as coarse resolution studies (chapter 5, *Lovenduski et al.* (2007); *Lenton and Matear* (2007)).

Perspectives for future research

The topic inter-annual variability of upper ocean carbon fluxes and sea-air CO_2 exchange provides many unresolved questions. The most prominent debate is on the role of eddies. Ideally, the model study from chapter 5 should be repeated with an eddy-resolving model; unfortunately, the high-resolution models required to study eddies are still expensive to run for longer time periods like the sixty years required for this study.

In the literature, a number of different methods have been used to analyze the effects of the SAM on the Southern Ocean carbon cycle. A regression analysis was applied in chapter 5; other studies compare a model run with inter-annual forcing to a run with climatological forcing and analyze the differences (e.g., *Le Quéré et al.*, 2010). This method does not

allow for a mechanistic understanding of how much a flux or concentration changes per unit change of the SAM index, but it permits to quantify the bulk contribution of the inter-annual varying forcing to the trend in CO_2 sea-air exchange. A third method is to compare a reference run with climatological forcing to another run with perturbed forcing, i.e., a wind field is created where the westerlies are intensified and shifted poleward like during a positive SAM event (*Dufour*, 2011). The latter can be applied to study the effect of the SAM in an eddy-resolving or permitting model, as it is sufficient to run the model with constant forcing for a few years. The different methods, however, are not necessarily directly comparable. Using the present day inter-annual atmospheric forcing, the system experiences a positive SAM event, but might not reach equilibrium as after few weeks the polarity of the SAM index might have changed (*Thompson et al.*, 2011). This might not mirror what would happen in a future with constant positive SAM. On the other hand, constantly applying a perturbed wind field, might bring the system into an equilibrium that it did not reach in the recent past.

The model itself (chapter 5) can be improved and further developed; especially the model drift in alkalinity needs to be addressed. Currently, subsurface dissolution of $CaCO_3$, for example by dissolution of aragonite or by metabolic CO_2 in marine snow particles, is missing. Subsurface dissolution, however, is needed to prevent the reduction of surface alkalinity and its accumulation in deeper layers. The calcite dissolution rate should also be dependent on the actual calcite saturation state. Once the surface alkalinity is more stable, its role in the SAM-induced changes of sea-air CO_2 exchange can be further explored.

The model does not consider ballasting by $CaCO_3$ or biogenic silica. This process should be included in the model, given the trend towards more diatom production. Would even more carbon be transported to the deep ocean due to faster sinking diatoms?

A larger scale project that is most useful would be a more detailed comparison of a suite of models and their responses to the SAM, which would allow to detect models' strengths and weaknesses and give a range of the system's possible response. More specifically, a comparison with models with different physics and same biology could provide a range of responses to possible circulation changes. Vice versa a comparison with a model with the same physics and different biology would lead to more insights on the response to changes in biology.

An analysis of the trend in CO_2 fluxes and the contributions of natural and anthropogenic CO_2 could be the subject of a follow-up study. Further, using climatological and inter-annual forcing in parallel, the trend in CO_2 exchange due to atmospheric CO_2 increase and changes in atmospheric circulation can be separated. Going a step further, this approach can also be applied to the future by forcing the model with predictions of

future atmospheric changes.

This thesis concentrates on the Southern Ocean carbon cycle. Yet, the export of carbon and nutrients by mode or bottom waters out of the Southern Ocean can determine the amount of biological production and gas-exchange at low latitudes (*Marinov et al.*, 2006). These processes should be considered in future studies.

6.4 Conclusion

The Southern Ocean carbon cycle is a complex system and many open questions remain to be solved. Important conclusions on how the Southern Ocean carbon cycle will evolve in a high-CO_2 world can be drawn from the process studies on carbonate sediments and inter-annual variability.

The atmospheric CO_2 concentration will further increase and force the Southern Ocean to act as a CO_2 sink. Circulation changes and anomalous natural CO_2 outgassing as a response to the SAM may, however, attenuate the growth rate of CO_2 uptake relative to the atmospheric CO_2 increase. Stronger upwelling and entrainment south of the Polar Front supplies (micro-) nutrients, such as iron, to the surface; this fosters diatom growth and export production and thereby a part of the entrained carbon is directly transported back to the subsurface layer. The contrary is true north of the Polar Front. Here, primary production is reduced, most likely due to unaltered (macro-) nutrient limitation and a deepening of the mixed layer; accordingly less carbon sinks out of the surface layer. Diatoms outcompete small phytoplankton when more iron is supplied and this shift in community composition could additionally feed back on the carbon export by ballasting; it is unclear whether this could partly compensate the reduced export production in the northern part of the Southern Ocean.

The role of the biology in the changing Southern Ocean was in previous studies either not addressed (*Le Quéré et al.*, 2007) or found to be insignificant (*Lovenduski et al.*, 2007; *Lenton and Matear*, 2007) until recently (*Wang and Moore*, 2012). This (chapter 5) is the first study that simultaneoulsy quantifies the changes in carbon transport and biological export as a response to the SAM. Future work is required to address the possible compensating role of eddy activity and the effects of changes in the Southern Ocean carbon and nutrient budgets on low latitude CO_2 sea-air exchange and export production (*Marinov et al.*, 2006).

The positive SAM trend of the last decades was mostly driven by the destruction of the stratospheric ozone layer, and to some extent by the rise of greenhouse gas concentrations in the atmosphere. The ozone layer is expected to recover in the next decades; however, the forcing by greenhouse gases will become stronger. As a consequence, the SAM trend

towards its high-index polarity is expected to continue (*Thompson et al.*, 2011). How global warming and its proposed tendency to more stratification will interfere with that will be most critical for the evolution of the Southern Ocean carbon cycle.

As the Southern Ocean continues to sequester CO_2 from the atmosphere, anthropogenic ocean acidification will proceed and might even be amplified by more upwelling of deep water, which is naturally rich in carbon (*Lenton et al.*, 2009). It will not be delayed by early buffering of shallow carbonates. Aragonite, which will reach undersaturation first, is nowadays not preserved in Antarctic shelf sediments and cannot act as a buffer. Calcite undersaturation will be reached later and there is too little calcite available for dissolution to constitute a significant negative feedback to acidification. Calcifying organisms, such as pteropods might disappear from the Antarctic food web (*Orr et al.*, 2005) and it is unknown how this will change food web structures and biogeochemical cycles.

References

Accornero, A., C. Manno, F. Esposito, and M. C. Gambi (2003), The vertical flux of particulate matter in the polynya of Terra Nova Bay. Part II. Biological components, *Antarctic Science*, *15*, 175–188, doi:10.1017/S0954102003001214.

Anderson, J. B. (1975), Factors controlling $CaCO_3$ dissolution in the Weddell Sea from foraminiferal distribution patterns, *Marine Geology*, *19*, 315–332, doi:10.1016/0025-3227(75)90083-3.

Andersson, A. J., F. T. Mackenzie, and L. M. Ver (2003), Solution of shallow-water carbonates: An insignificant buffer against rising atmospheric CO_2, *Geology*, *31*, 513–516.

Andersson, A. J., N. R. Bates, and F. T. Mackenzie (2007), Dissolution of carbonate sediments under rising pCO_2 and ocean acidification: Observations from Devil's Hole, bermuda, *Aquatic Geochemistry*, *13*, 237–264, doi:10.1007/s10498-007-9018-8.

Aoki, S., Y. Sasai, H. Sasaki, H. Mitsudera, and G. D. Williams (2010), The cyclonic circulation in the Australian-Antarctic basin simulated by an eddy-resolving general circulation model, *Ocean Dynamics*, *60*, 743–757, doi:10.1007/s10236-009-0261-y.

Archer, D., H. Kheshgi, and E. Maier-Reimer (1997), Multiple timescales for neutralization of fossil fuel CO_2, *Geophysical Research Letters*, *24*, 405–408, doi:10.1029/97GL00168.

Archer, D., M. Eby, V. Brovkin, A. Ridgwell, L. Cao, U. Mikolajewicz, K. Caldeira, K. Matsumoto, G. Munhoven, A. Montenegro, and K. Tokos (2009), Atmospheric lifetime of fossil fuel carbon dioxide, *Annual Review of Earth and Planetary Sciences*, *37*, 117–134, doi:10.1146/annurev.earth.031208.100206.

Archer, D. A., and R. T. Pierrehumbert (2011), *The Warming Papers: The Scientific Foundation for the Climate Change Forecast*, Wiley-Blackwell, Hoboken, NJ.

Arrigo, K. R., G. van Dijken, and M. Long (2008), Coastal Southern Ocean: A strong anthropogenic CO_2 sink, *Geophysical Research Letters*, *35, L21602*, doi:10.1029/2008GL035624.

Balch, W. M., D. T. Drapeau, B. C. Bowler, E. Lyczskowski, E. S. Booth, and D. Alley (2011), The contribution of coccolithophores to the optical and inorganic carbon budgets during the Southern Ocean Gas Exchange Experiment: New evidence in support of the "Great Calcite Belt" hypothesis, *Journal of Geophysical Research*, *116, C00F06*, doi:10.1029/2011JC006941.

Beaufort, L., I. Probert, T. de Garidel-Thoron, E. M. Bendif, D. Ruiz-Pino, N. Metzl, C. Goyet, N. Buchet, P. Coupel, M. Grelaud, B. Rost, R. E. M. Rickaby, and C. de Vargas (2011), Sensitivity of coccolithophores to carbonate chemistry and ocean acidification, *Nature*, *476*, 80–83, doi:10.1038/nature10295.

Bednaršek, N., G. A. Tarling, S. Fielding, and D. C. E. Bakker (2011), Population dynamics and biogeochemical significance of *Limacina helicina antarctica* in the Scotia Sea (Southern Ocean), *Deep Sea Research Part II: Topical Studies in Oceanography*, *59–60*, 105–116, doi: 10.1016/j.dsr2.2011.08.003.

Berelson, W. M., W. M. Balch, R. Najjar, R. A. Feely, C. Sabine, and K. Lee (2007), Relating estimates of $CaCO_3$ production, export, and dissolution in the water column to measurements of $CaCO_3$ rain into sediment traps and dissolution on the sea floor: A revised global carbonate budget, *Global Biogeochemical Cycles*, *21*, GB1024, doi:10.1029/2006GB002803.

Böning, C. W., A. Dispert, M. Visbeck, S. R. Rintoul, and F. U. Schwarzkopf (2008), The response of the Antarctic Circumpolar Current to recent climate change, *Nature Geoscience*, *1*, 864–869, doi:10.1038/ngeo362.

Broecker, W. S., and A. Sanyal (1998), Does atmospheric CO_2 police the rate of chemical weathering?, *Global Biogeochemical Cycles*, *12*, 403–408, doi:10.1029/98GB01927.

Caldeira, K., and P. B. Duffy (2000), The role of the Southern Ocean in uptake and storage of anthropogenic carbon dioxide, *Science*, *287*, 620–622, doi:10.1126/science.287.5453.620.

Caldeira, K., and M. E. Wickett (2003), Anthropogenic carbon and ocean pH, *Nature*, *425*, 365, doi:10.1038/425365a.

Canadell, J. G., C. Le Quéré, M. R. Raupach, C. B. Field, E. T. Buitenhuis, P. Ciais, T. J. Conway, N. P. Gillett, R. A. Houghton, and G. Marland (2007), Contributions to accelerating atmospheric CO_2 growth from economic activity, carbon intensity, and efficiency of natural sinks, *Proceedings of the National Academy of Sciences of the United States of America*, *104*, 18,866–18,870, doi:10.1073/pnas.0702737104.

Collier, R., J. Dymond, S. Honjo, S. Manganini, R. Francois, and R. Dunbar (2000), The vertical flux of biogenic and lithogenic material in the Ross Sea: moored sediment trap observations 1996-1998, *Deep Sea Research Part II: Topical Studies in Oceanography*, *47*, 3491–3520, doi: 10.1016/S0967-0645(00)00076-X.

Cox, P. M., R. A. Betts, C. D. Jones, S. A. Spall, and I. J. Totterdell (2000), Acceleration of global warming due to carbon-cycle feedbacks in a coupled climate model, *Nature*, *408*, 184–186, doi:10.1038/35041539.

Dessler, A. E., and S. C. Sherwood (2009), A Matter of Humidity, *Science*, *323*, 1020–1021, doi:10.1126/science.1171264.

Dickson, A. G. (1981), An exact definition of total alkalinity and a procedure for the estimation of alkalinity and total inorganic carbon from titration data, *Deep Sea Research Part A*, *28*, 609 – 623, doi:10.1016/0198-0149(81)90121-7.

Dickson, A. G., C. L. Sabine, and J. R. Christian (Eds.) (2007), *Guide to best practices for ocean CO_2 measurements*, 191 pp., PICES Special Publication 3.

Dufour, C. (2011), Rôle des tourbillons océaniques dans la variabilité récente des flux air-mer de CO_2 dans l'océan Austral, *PhD Thesis, Université de Grenoble*.

Fabry, V. J., B. A. Seibel, R. A. Feely, and J. C. Orr (2008), Impacts of ocean acidification on marine fauna and ecosystem processes, *ICES Journal of Marine Science*, *65*, 414–432, doi:10.1093/icesjms/fsn048.

Falkowski, P. (2003), 8.05 - Biogeochemistry of Primary Production in the Sea, in *Treatise on Geochemistry*, edited by W. H. Schlesinger, pp. 185 – 213, Elsevier, doi:10.1016/B0-08-043751-6/08129-9.

Farrell, J. W., and W. L. Prell (1989), Climate change and $CaCO_3$ preservation: An 800,000 year bathymetric reconstruction from the central equatorial Pacific Ocean, *Paleoceanography*, *4*, 447–466, doi:10.1029/PA004i004p00447.

Field, C. B., M. J. Behrenfeld, and J. T. Randerson (1998), Primary production of the biosphere: Integrating terrestrial and oceanic components, *Science*, *281*, 237–240, doi:10.1126/science.281.5374.237.

Foldvik, A. (2004), Ice shelf water overflow and bottom water formation in the southern Weddell Sea, *Journal of Geophysical Research*, *109, C02015*, doi:10.1029/2003JC002008.

Fourier, J.-B. F. (1827), On the temperature of the terrestrial sphere and interplanetary space, *Mémoires de l'Académie Royale des Sciences*, *7*, 569–604.

Fraile, I., M. Schulz, S. Mulitza, and M. Kucera (2008), Predicting the global distribution of planktonic foraminifera using a dynamic ecosystem model, *Biogeosciences*, *5*, 891–911, doi:doi:10.5194/bg-5-891-2008.

Gangstø, R., M. Gehlen, B. Schneider, L. Bopp, O. Aumont, and F. Joos (2008), Modeling the marine aragonite cycle: changes under rising carbon dioxide and its role in shallow water $CaCO_3$ dissolution, *Biogeosciences*, *5*, 1057–1072, doi:10.5194/bg-5-1057-2008.

González-Dávila, M., J. M. Santana-Casiano, R. A. Fine, J. Happell, B. Delille, and S. Speich (2011), Carbonate system in the water masses of the Southeast Atlantic sector of the Southern Ocean during February and March 2008, *Biogeosciences*, *8*, 1401–1413, doi:10.5194/bg-8-1401-2011.

Gordon, A. L., A. H. Orsi, R. Muench, B. A. Huber, E. Zambianchi, and M. Visbeck (2009), Western Ross Sea continental slope gravity currents, *Deep Sea Research Part II: Topical Studies in Oceanography*, *56*, 796–817, doi:10.1016/j.dsr2.2008.10.037.

Gruber, N., M. Gloor, S. E. Mikaloff Fletcher, S. C. Doney, S. Dutkiewicz, M. J. Follows, M. Gerber, A. R. Jacobson, F. Joos, K. Lindsay, D. Menemenlis, A. Mouchet, S. A. Müller, J. L. Sarmiento, and T. Takahashi (2009), Oceanic sources, sinks, and transport of atmospheric CO_2, *Global Biogeochemical Cycles*, *23, GB1005*, doi:10.1029/2008GB003349.

Hall, A., and M. Visbeck (2002), Synchronous variability in the Southern Hemisphere atmosphere, sea ice, and ocean resulting from the annular mode, *Journal of Climate*, *15*, 3043–3057.

Hauck, J., M. Hoppema, R. G. J. Bellerby, C. Völker, and D. Wolf-Gladrow (2010), Data-based estimation of anthropogenic carbon and acidification in the Weddell Sea on a decadal timescale, *Journal of Geophysical Research*, *115, C03004*, doi:10.1029/2009JC005479.

Heinze, C., E. Maier-Reimer, and K. Winn (1991), Glacial pCO_2 reduction by the world ocean: Experiments with the Hamburg Carbon Cycle Model, *Paleoceanography*, *6*, 395–430, doi:10.1029/91PA00489.

Hoppema, M. (2004a), Weddell Sea is a globally significant contributor to deep-sea sequestration of natural carbon dioxide, *Deep-Sea Research I*, *51*, 1169–1177, doi:10.1016/j.dsr.2004.02.011.

Hoppema, M. (2004b), Weddell Sea turned from source to sink for atmospheric CO_2 between pre-industrial time and present, *Global and Planetary Change*, *40*, 219–231, doi:10.1016/j.gloplacha.2003.08.001.

Hoppema, M., E. Fahrbach, and M. Schröder (1997), On the total carbon dioxide and oxygen signature of the circumpolar deep water in the Weddell Gyre, *Oceanologica Acta*, *20*, 783–798.

Huhn, O., H. H. Hellmer, M. Rhein, C. Rodehacke, W. Roether, M. P. Schodlok, and M. Schröder (2008), Evidence of deep- and bottom-water formation in the western Weddell Sea, *Deep Sea Research Part II: Topical Studies in Oceanography*, *55*, 1098–1116, doi:10.1016/j.dsr2.2007.12.015.

Hunt, B. P. V., E. A. Pakhomov, G. W. Hosie, V. Siegel, P. Ward, and K. Bernard (2008), Pteropods in Southern Ocean ecosystems, *Progress In Oceanography*, *78*, 193–221, doi:10.1016/j.pocean.2008.06.001.

Hurrell, J. W., and H. Van Loon (1994), A modulation of the atmospheric annual cycle in the Southern Hemisphere, *Tellus*, *46A*, 325–338.

IPCC (2007), *Climate Change 2007: Synthesis Report. Contribution of Working Groups I, II and III to the Fourth Assessment Report of the Intergovernmental Panel on Climate Change*, 104 pp., IPCC, Geneva, Switzerland, Core Writing Team, and Pachauri, R. K. and Reisinger, A. (Eds.).

Jansen, H., and D. A. Wolf-Gladrow (2001), Carbonate dissolution in copepod guts: a numerical model, *Marine Ecology Progress Series*, *221*, 199–207, doi:10.3354/meps221199.

Jansen, H., R. E. Zeebe, and D. A. Wolf-Gladrow (2002), Modeling the dissolution of settling $CaCO_3$ in the ocean, *Global Biogeochemical Cycles*, *16*, 1027, doi:10.1029/2000GB001279.

Keir, R. S. (1980), The dissolution kinetics of biogenic calcium carbonates in seawater, *Geochimica et Cosmochimica Acta*, *44*, 241 – 252, doi:10.1016/0016-7037(80)90135-0.

Khatiwala, S., F. Primeau, and T. Hall (2009), Reconstruction of the history of anthropogenic CO_2 concentrations in the ocean, *Nature*, *462*, 346–349, doi:10.1038/nature08526.

Lacis, A. A., G. A. Schmidt, D. Rind, and R. A. Ruedy (2010), Atmospheric CO_2: Principal control knob governing Earth's temperature, *Science*, *330*, 356–359, doi:10.1126/science.1190653.

Langer, G., G. Nehrke, and S. Jansen (2007), Dissolution of Calcidiscus leptoporus coccoliths in copepod guts? A morphological study, *Marine Ecology Progress Series*, *331*, 139–146, doi:10.3354/meps331139.

Law, R. M., R. J. Matear, and R. J. Francey (2008), Comment on "Saturation of the Southern Ocean CO_2 sink due to recent climate change", *Science*, *319*, 570a, doi:10.1126/science.1149077.

Le Quéré, C., C. Rödenbeck, E. T. Buitenhuis, T. J. Conway, R. Langenfelds, A. Gomez, C. Labuschagne, M. Ramonet, T. Nakazawa, N. Metzl, N. Gillett, and M. Heimann (2007), Saturation of the Southern Ocean CO_2 sink due to recent climate change, *Science*, *316*, 1735–1738, doi:10.1126/science.1136188.

Le Quéré, C., C. Rödenbeck, E. T. Buitenhuis, T. J. Conway, R. Langenfelds, A. Gomez, C. Labuschagne, M. Ramonet, T. Nakazawa, N. Metzl, N. Gillett, and M. Heimann (2008), Response to Comments on "Saturation of the Southern Ocean CO_2 sink due to recent climate change", *Science*, *319*, 570c, doi:10.1126/science.1147315.

Le Quéré, C., T. Takahashi, E. T. Buitenhuis, C. Rödenbeck, and S. C. Sutherland (2010), Impact of climate change and variability on the global oceanic sink of CO_2, *Global Biogeochemical Cycles*, *24, GB4007*, doi:10.1029/2009GB003599.

Lenton, A., and R. J. Matear (2007), Role of the Southern Annular Mode (SAM) in Southern Ocean CO_2 uptake, *Global Biogeochemical Cycles*, *21, GB2016*, doi:10.1029/2006GB002714.

Lenton, A., F. Codron, L. Bopp, N. Metzl, P. Cadule, A. Tagliabue, and J. Le Sommer (2009), Stratospheric ozone depletion reduces ocean carbon uptake and enhances ocean acidification, *Geophysical Research Letters*, *36, L12606*, doi:10.1029/2009GL038227.

Lipps, J. H., and W. N. Krebs (1974), Planktonic foraminifera associated with Antarctic sea ice, *The Journal of Foraminiferal Research*, *4*, 80–85, doi:10.2113/gsjfr.4.2.80.

Lovenduski, N. S., and N. Gruber (2005), Impact of the Southern Annular Mode on Southern Ocean circulation and biology, *Geophysical Research Letters*, *32, L11603*, doi:10.1029/2005GL022727.

Lovenduski, N. S., N. Gruber, S. C. Doney, and I. D. Lima (2007), Enhanced CO_2 outgassing in the Southern Ocean from a positive phase of the Southern Annular Mode, *Global Biogeochemical Cycles*, *21, GB2026*, doi:10.1029/2006GB002900.

Lozier, M. S. (2010), Deconstructing the conveyor belt, *Science*, *328*, 1507–1151, doi:10.1126/science.1189250.

Maier-Reimer, E., U. Mikolajewicz, and A. Winguth (1996), Future ocean uptake of CO_2: interaction between ocean circulation and biology, *Climate Dynamics*, *12*, 711–721.

Marinov, I., A. Gnanadesikan, J. R. Toggweiler, and J. L. Sarmiento (2006), The Southern Ocean biogeochemical divide, *Nature*, *441*, 964–967, doi:10.1038/nature04883.

Marshall, G. J. (2003), Trends in the Southern Annular Mode from observations and reanalyses, *Journal of Climate*, *16*, 4134–4143.

McNeil, B. I., and R. J. Matear (2008), Southern Ocean acidification: A tipping point at 450-ppm atmospheric CO_2, *Proceedings of the National Academy of Sciences of the United States of America*, *105*, 18,860–18,864, doi:10.1073/pnas.0806318105.

Mikaloff Fletcher, S. E., N. Gruber, A. R. Jacobson, M. Gloor, S. C. Doney, S. Dutkiewicz, M. Gerber, M. Follows, F. Joos, K. Lindsay, D. Menemenlis, A. Mouchet, S. A. Müller, and J. L. Sarmiento (2007), Inverse estimates of the oceanic sources and sinks of natural CO_2 and the implied oceanic carbon transport, *Global Biogeochemical Cycles*, *21, GB1010*, doi:10.1029/2006GB002751.

Millero, F. J. (2007), The Marine Inorganic Carbon Cycle, *Chemical Reviews*, *107*, 308–341, doi:10.1021/cr0503557.

Moy, A. D., W. R. Howard, S. G. Bray, and W. T. Trull (2009), Reduced calcification in modern Southern Ocean planktonic foraminifera, *Nature Geoscience*, *2*, 276–280, doi: 10.1038/NGEO460.

Mucci, A. (1983), The solubility of calcite and aragonite in seawater at various salinities, temperatures, and one atmosphere total pressure, *American Journal of Science*, *289*, 780–799, doi:10.2475/ajs.283.7.780.

Orr, J. C., V. J. Fabry, O. Aumont, L. Bopp, S. C. Doney, R. A. Feely, A. Gnanadesikan, N. Gruber, A. Ishida, F. Joos, R. M. Key, K. Lindsay, E. Maier-Reimer, R. Matear, P. Monfray, A. Mouchet, R. G. Najjar, G.-K. Plattner, K. B. Rodgers, C. L. Sabine, J. L. Sarmiento, R. Schlitzer, R. D. Slater, I. J. Totterdell, M.-F. Weirig, Y. Yamanaka, and A. Yool (2005), Anthropogenic ocean acidification over the twenty-first century and its impact on calcifying organisms, *Nature*, *437*, 681–686, doi:10.1038/nature04095.

Orsi, A. H., T. Whitworth, and W. D. Nowlin (1995), On the meridional extent and fronts of the Antarctic Circumpolar Current, *Deep Sea Research Part I: Oceanographic Research Papers*, *42*, 641–673, doi:10.1016/0967-0637(95)00021-W.

Pierrehumbert, R. T. (2011), Infrared radiation and planetary temperature, *Physics Today*, *64*, 33–38, doi:10.1063/1.3541943.

Pierrehumbert, R. T., H. Brogniez, and R. Roca (2007), On the relative humidity of the atmosphere, in *The global circulation of the atmosphere*, edited by T. Schneider and A. H. Sobel, p. 385, Princeton University Press, Princeton, USA.

Rintoul, S. R. (1998), On the origin and influence of Adélie Land Bottom Water, in *Ocean, Ice and Atmosphere: Interactions at the Antarctic Continental Margin, Antarctic Reserach Series., vol. 75*, edited by S. S. Jacobs and R. F. Weiss, pp. 151–171, AGU, Washington, D.C., doi:10.1029/AR075p0151.

Russell, J. L., K. W. Dixon, A. Gnanadesikan, R. J. Stouffer, and J. R. Toggweiler (2006), The Southern Hemisphere westerlies in a warming world: Propping open the door to the deep ocean, *Journal of Climate*, *19*, 6382–6390, doi:10.1175/JCLI3984.1.

Sarmiento, J. L., T. M. C. Hughes, R. J. Stouffer, and S. Manabe (1998), Simulated response of the ocean carbon cycle to anthropogenic climate warming, *Nature*, *393*, 245–249, doi: 10.1038/30455.

Sarmiento, J. L., J. Dunne, A. Gnanadesikan, R. M. Key, K. Matsumoto, and R. Slater (2002), A new estimate of the $CaCO_3$ to organic carbon export ratio, *Global Biogeochemical Cycles*, *16*, 1107, doi:10.1029/2002GB001919.

Screen, J. A., N. P. Gillett, D. P. Stevens, G. J. Marshall, and H. K. Roscoe (2009), The role of eddies in the Southern Ocean temperature response to the Southern Annular Mode, *Journal of Climate*, *22*, 806–818, doi:10.1175/2008JCLI2416.1.

Shindell, D. T., and G. A. Schmidt (2004), Southern Hemisphere climate response to ozone changes and greenhouse gas increases, *Geophysical Research Letters*, *31, L18209*, doi: 10.1029/2004GL020724.

Siegenthaler, U., T. F. Stocker, E. Monnin, D. Lüthi, J. Schwander, B. Stauffer, D. Raynaud, J.-M. Barnola, H. Fischer, V. Masson-Delmotte, and J. Jouzel (2005), Stable carbon cycle-climate relationship during the Late Pleistocene, *Science*, *310*, 1313–1317, doi: 10.1126/science.1120130.

Sigman, D. M., M. P. Hain, and G. H. Haug (2010), The polar ocean and glacial cycles in atmospheric CO_2 concentration, *Nature*, *466*, 47–55, doi:10.1038/nature09149.

Sokolov, S., and S. R. Rintoul (2007), Multiple jets of the Antarctic Circumpolar Current south of Australia, *Journal of Physical Oceanography*, *37*, 1394–1412, doi:10.1175/JPO3111.1.

Sokolov, S., and S. R. Rintoul (2009), Circumpolar structure and distribution of the Antarctic Circumpolar Current fronts: 1. Mean circumpolar paths, *Journal of Geophysical Research*, *114, C11019*, doi:10.1029/2008JC005108.

Sundquist, E. T. (1993), The global carbon dioxide budget, *Science*, *259*, 934–941.

Takahashi, T., S. C. Sutherland, R. Wanninkhof, C. Sweeney, R. A. Feely, D. W. Chipman, B. Hales, G. Friederich, F. Chavez, C. Sabine, A. Watson, D. C. E. Bakker, U. Schuster, N. Metzl, H. Yoshikawa-Inoue, M. Ishii, T. Midorikawa, Y. Nojiri, A. Körtzinger, T. Steinhoff, M. Hoppema, J. Olafsson, T. S. Arnarson, B. Tilbrook, T. Johannessen, A. Olsen, R. Bellerby, C. S. Wong, B. Delille, N. R. Bates, and H. J. W. de Baar (2009), Climatological mean and decadal change in surface ocean pCO_2, and net sea-air CO_2 flux over the global oceans, *Deep Sea Research Part II: Topical Studies in Oceanography*, *56*, 554–577, doi:10.1016/j.dsr2.2008.12.009.

Thompson, D. W. J., and S. Solomon (2002), Interpretation of recent Southern Hemisphere climate change, *Science*, *296*, 895–899, doi:10.1126/science.1069270.

Thompson, D. W. J., S. Solomon, P. J. Kushner, M. H. England, K. M. Grise, and D. J. Karoly (2011), Signatures of the Antarctic ozone hole in Southern Hemisphere surface climate change, *Nature Geoscience*, *4*, 741–749, doi:10.1038/ngeo1296.

Toggweiler, J. R., and J. L. Russell (2008), Ocean circulation in a warming climate, *Nature*, *451*, 286–288, doi:10.1038/nature06590.

Tortell, P. D., C. D. Payne, Y. Li, S. Trimborn, B. Rost, W. O. Smith, C. Riesselman, R. B. Dunbar, P. Sedwick, and G. R. DiTullio (2008), CO_2 sensitivity of Southern Ocean phytoplankton, *Geophysical Research Letters*, *35, L04605*, doi:10.1029/2007GL032583.

Tyndall, J. (1861), On the absorption and radiation of heat by gases and vapours, and on the physical connexion of radiation, absorption and conduction, *Philosophical Magazine Series 4*, *22*, 169–194, 273–285.

van Heuven, S. M. A. C., M. Hoppema, O. Huhn, H. A. Slagter, and H. J. W. de Baar (2011), Direct observation of increasing CO_2 in the Weddell Gyre along the Prime Meridian during 1973-2008, *Deep Sea Research Part II: Topical Studies in Oceanography*, *58*, 2613–2635, doi: 10.1016/j.dsr2.2011.08.007.

Volk, T., and M. I. Hoffert (1985), Ocean carbon pumps: Analysis of relative strengths and efficiencies in ocean driven atmospheric CO_2 changes, in *The carbon cycle and atmospheric CO_2: natural variations, Archean to present*, edited by E. T. Sundquist and W. S. Broecker, pp. 99–110, Geophysical Monograph 32, American Geophysical Union.

Walker, J. C. G., P. B. Hays, and J. F. Kasting (1981), A negative feedback mechanism for the long-term stabilization of Earth's surface temperature, *Journal of Geophysical Research*, *86*, 9776–9782, doi:10.1029/JC086iC10p09776.

Wang, S., and J. K. Moore (2012), Variability of primary production and air-sea CO_2 flux in the Southern Ocean, *Global Biogeochemical Cycles*, *26, GB1008*, doi:10.1029/2010GB003981.

Whitworth, T. (1983), Monitoring the transport of the Antarctic Circumpolar Current at Drake Passage, *Journal of Physical Oceanography*, *13*, 2045–2057.

Whitworth, T., and W. D. Nowlin (1987), Water masses and currents of the Southern Ocean at the Greenwich Meridian, *Journal of Geophysical Research*, *92*, 6462–6476, doi: 10.1029/JC092iC06p06462.

Whitworth, T., and R. G. Peterson (1985), Volume transport of the Antarctic Circumpolar Current from bottom pressure measurements, *Journal of Physical Oceanography*, *15*, 810–816.

Wunsch, C. (1998), The work done by the wind on the oceanic general circulation, *Journal of Physical Oceanography*, *28*, 2332–2340.

Wunsch, C. (2002), What is the thermohaline circulation?, *Science*, *298*, 1179–1181, doi: 10.1126/science.1079329.

Zeebe, R. E., and D. A. Wolf-Gladrow (2001), *CO_2 in seawater: equilibrium, kinetics, isotopes*, *Elsevier Oceanography Series*, vol. 65, p. 346, Elsevier.

Zickfeld, K., J. C. Fyfe, M. Eby, and A. J. Weaver (2008), Comment on "Saturation of the Southern Ocean CO_2 sink due to recent climate change", *Science*, *319*, 570b, doi: 10.1126/science.1146886.

Universität Bremen

Name: Judith Hauck Ort, Datum: Bremen, 31. Mai 2012

Anschrift: Donaustr. 7, 28199 Bremen

ERKLÄRUNG

Hiermit erkläre ich, dass ich die Doktorarbeit mit dem Titel:

Processes in the Southern Ocean carbon cycle: Dissolution of carbonate sediments and inter-annual variability of carbon fluxes

selbstständig verfasst und geschrieben habe und außer den angegebenen Quellen keine weiteren Hilfsmittel verwendet habe.

Ebenfalls erkläre ich hiermit, dass es sich bei den von mir abgegebenen Arbeiten um 3 identische Exemplare handelt.

.....
(Unterschrift)